




ADVERTIMENT. L'accés als continguts d'aquesta tesi queda condicionat a l'acceptació de les condicions d'ús establertes per la següent llicència Creative Commons:  http://cat.creativecommons.org/?page_id=184

ADVERTENCIA. El acceso a los contenidos de esta tesis queda condicionado a la aceptación de las condiciones de uso establecidas por la siguiente licencia Creative Commons:  <http://es.creativecommons.org/blog/licencias/>

WARNING. The access to the contents of this doctoral thesis it is limited to the acceptance of the use conditions set by the following Creative Commons license:  <https://creativecommons.org/licenses/?lang=en>



**Universitat Autònoma
de Barcelona**

**Peptide functionalized nanoliposomes for
biomolecule intracellular delivery, prepared using
compressed CO₂**

Dolores Bueno López

Tesi doctoral

Programa de Doctorat de Ciència dels Materials

Directores

Dr. Elisabet González Mira

Dr. Nora Ventosa Rull

Tutor Dr. Gonzalo Guirado López

Departament de Química

Facultat de Ciències

2020

La present memòria es presenta per aspirar al Grau de Doctor per:

Dolores Bueno López,

Vist i plau:

Dr. Elisabet González Mira

Dr. Nora Ventosa Rull

Dr. Gonzalo Guirado López

Bellaterra, 31 de gener de 2020



ELISABET GONZÁLEZ MIRA, Postdoctoral Researcher of CIBER-BBN and **NORA VENTOSA RULL** Scientific Researcher, of the Spanish Council of Research at the Materials Science Institute of Barcelona (ICMAB-CSIC)

CERTIFY

That **Dolores Bueno López**, Master in Sustainable Chemistry, has performed, under their management, the research work entitled "**Peptide functionalized nanoliposomes for biomolecule intracellular delivery, prepared using compressed CO₂**". This work has been performed under the mark of the Materials Science Ph.D. program of the Chemistry Department of the Autonomous University of Barcelona.

And in witness whereof this is signed by

Directors

Dr. Elisabet González Mira

Dr. Nora Ventosa Rull

Bellaterra, 31 de gener de 2020



“Temo que esté usted confundiendo la objetividad con la indiferencia. En la base de la investigación no está la indiferencia, está el interés, el amor por la verdad.”

(Jean Guitton)

Agradecimientos

Dice Chesterton que dar la vuelta al mundo es el camino más corto para llegar adonde ya se está. Y yo me siento un poco así: ha sido un largo viaje para llegar hasta donde estoy ahora mismo. Un viaje con un ritmo de montaña rusa, subiendo lentamente grandes cuestas y lanzándome luego en picado cabeza abajo... La verdad es que no ha sido un camino fácil. Como una vez dijo mi médico: *Lo hicimos porque no sabíamos que era imposible.*

Según la OMS, una de cada cuatro personas tendrá un problema de salud mental a lo largo de su vida. Yo prefiero decir que una de cada cuatro personas somos un superhéroe oculto, pero son esas otras tres personas quienes marcan la diferencia y sacan a la luz lo mejor de nosotros. Esta historia más que de mí, va de cómo muchas de esas tres personas consiguieron que yo cumpliera mi sueño de hacer un doctorado en el CSIC. Por eso, estoy convencida de que estos agradecimientos son la parte más importante de la tesis (de hecho, serán las únicas páginas que se lean algunos), unas páginas que tendrían sentido, aunque finalmente no hubiera habido tesis como en tantos momentos ha estado a punto de pasar. Mi vuelta al mundo chestertoniana empezó en enero de 2013 y en el momento de escribir estas líneas estamos en enero de 2020. Son un puñado de años y de personas que los han llenado. Disculpadme si me dejo a alguien: no están todos los que son, pero sí son todos los que están.

Esta gran aventura dio comienzo gracias al Prof. Jaume Veciana y a la Prof. Concepció Rovira que me dieron la oportunidad de formar parte de su grupo de investigación y además hicieron que me sintiera parte de él desde la primera entrevista. Como guías de viaje he contado con la Dra. Nora Ventosa y la Dr. Elisabet González. Nora Ventosa a lo largo de todo este tiempo ha sido mucho más que una directora de tesis excelente: no solo he contado con su supervisión y orientación profesionales durante todo el camino sino, más importante, con su calidad humana, comprensión y ánimos que han hecho que todo este esfuerzo haya desembocado en una tesis. De ella es el mérito de que yo retomara el trabajo tras un año de baja, y que, poco a poco, siguiera este “entrenamiento” hasta el final. Muchas gracias por creer en mí cuando yo no era capaz

de hacerlo. La Dr. Elisabet González se incorporó después como codirectora, aportando una visión enriquecedora y también mucho soporte, ánimos y amistad.

Agradezco al ya extinto Ministerio de Economía y Competitividad la beca predoctoral que me concedieron, así como la ayuda económica para la realización de dos meses de estancia en el grupo del Prof. Wolfgang Parak del AG Biophotonik, en la Philipps-Universität de Marburg. Finalmente, el trabajo de esos meses no se ha incluido en esta memoria de tesis. But I want to thank him for the opportunity to learn more things of cell culture, confocal microscopy and flow cytometry. Gracias a la Dr. Neus Feliu que me orientó en todo el diseño de experimentos y la realización de los mismos. Gracias al equipo de españoles (Uri, Dani, Isa) que me hizo sentir como en casa nada más llegar. Thank you to all my friends and partners from the group, I really learned a lot from your professionalism. We also enjoyed our spare time.

Gracias a la Dr. Pilar Rivera por las primeras nociones en el cultivo celular y en la microscopía confocal. Gracias también a Ruixue Xu por sus imágenes de confocal del capítulo 5. Gracias al Dr. Andreu Cabot por proporcionarnos las nanopartículas metálicas para funcionalizar mis liposomas. Gracias a Paula Zamora por su simpatía y su buen hacer. Tampoco se ha recogido en esta tesis todo el trabajo de sincrotrón pero no por ello dejo de estar agradecida a la Dr. Eva Pereiro que corrigió, sugirió y orientó desde el primer momento y a la Dr. Ana J. Pérez por toda su paciencia y formación.

En el proyecto NanoFabry, continuado por Lipocell y Terarmet, he conocido y colaborado con muchos grandes profesionales a los que me gustaría dar especialmente las gracias. Gracias a la Dr. Miriam Royo por acogerme en su grupo para enseñarme las bases del HPLC de la mano del siempre dispuesto Dr. Daniel Pulido. ¡Todavía os debo un pastel! Gracias al Dr. Pepe Corchero por su proteína GLA y sus Western-blot. Gracias a la Dr. Ibane Abasolo y Natalia García Aranda por toda la parte in vitro e in vivo de esta tesis. Gracias a la Dr. Johanna Scheper por su gestión. Gracias a todos vosotros por las conversaciones científicas y no tan científicas en las largas reuniones de proyecto.

A lo largo de estos años he contado con el apoyo técnico de muchas personas a las que también estoy muy agradecida. Gracias al Dr. Pablo Castro y a Martí de Cabo por las

sesiones de cryo-TEM. Gracias Dr. Lidia Ferrer y Dr. Evelyn Moreno por las noches de sincrotrón. I would like to expand my gratitude to Prof. Jan Skov Pedersen, from Aarhus University in Denmark, for the conducted analysis of the SAXS data of liposomes, and Prof. Dganit Danino from CryoEM Laboratory of Soft Matter, Technion, in Israel for the cryo-TEM images. Gracias a la Dr. Judit Morlà por la ayuda con el ultravioleta y el DiD. Gracias a la Dr. Alba Eustaquio por su valioso conocimiento de HPLC y su ayuda en el desarrollo del método para analizar liposomas. Gracias a Ramón González por todas las medidas de HPLC, repeticiones, cambios de agenda, y por sus pacientes explicaciones. Gracias al Dr. Jordi Faraudo por las simulaciones teóricas. Gracias a todo el personal del ICMAB, incluido el administrativo dentro del cual me gustaría dar las gracias especialmente a Carme Gimeno y Pietat Sierra.

En esta vuelta al mundo no he estado nunca sola: gracias muy especiales a todos los integrantes del grupo Nanomol. Cuando llegué aquí reinaban las supercríticas, que en seguida me acogieron en sus filas (gracias Ingrid, Eve, Elena, María, Eva, Elisa, Lidia, Antonio). Cuando me reincorporé al grupo después de mi baja habían llegado para quedarse los supernanoinos: gracias por hacer del grupo una pequeña familia con su punto de locura y alegría sin fin. En especial quiero dar las gracias a mi despacho 2.18: siempre ruidoso, pero también rebosante de compañerismo y ánimos a los que estábamos en la recta final. Gracias especiales también a Judit, Ramón, Guillem, Carles y David. Gracias Solène por contarme que para escribir la tesis solo tenía que superar la energía de activación, ¡tenías razón! Gracias también a Nathaly y Natascia por sus consejos, su ejemplo y por cuidarme tanto. Muchas gracias a mis primeras amigas en Barcelona, Dayana, Estela, Lourdes y después también Manel. Hicisteis que empezar de cero en una nueva ciudad fuera una aventura alucinante.

En mi vida tiene mucha importancia la divulgación científica, y durante este viaje de tesis me ha mantenido a flote muchas veces (en todos los sentidos). Por eso, quiero dar las gracias a todos mis compañeros de NAUKAS: vuestras palabras de cariño, de comprensión y de ánimo cada vez que las necesitaba me han empujado a seguir en la brecha. Quiero agradecer especialmente a los jefes de NAUKAS el haber confiado en que yo era capaz de subirme a un escenario. Gracias a todos los socios de Hablando de Ciencia por mis añitos de presidencia que me han hecho aprender mucho.

Desgranando Ciencia fue mi primer evento de divulgación científica: gracias por hacer sentirse valorada y querida a mi alter ego Ununcuadio. Gracias a Ignite con Julia a la cabeza por permitirme y empujarme a dar la charla más personal y de la que más orgullosa estoy. Gracias al equipo organizador de BCNspiracy por proponerme tantos retos, por el apoyo incondicional y por tantas alegrías y amistades.

Muchas gracias a mi familia catalana de Carlos y Maricarmen Arregui por acogerme desde el principio, aunque nos hayamos visto poco, pero la orientación profesional que Carlos siempre me ha dado la agradezco de todo corazón.

Muchas gracias a mi psiquiatra, el Dr. Adrián Cano, y a mi psicóloga Susanna García por estar disponibles siempre, y no permitir que perdiera el rumbo. Muchas gracias a Mn Bruno por aguantarme durante tantas horas y a todos los de la Delejovebcn por el worship, la amistad y tantas risas, sobre todo de mis queridos Calçotets (ahora Calçotiets). Gracias también a todos los amigos del Monjibus y a mi sisterhood de Marta, Isabel y Marta. Gracias a Ian y a todos mis grandes referentes del Reading Club: I want to be like you when I'll grow wiser! Gracias a Araceli: tenías razón, después de tantos "nunca acabaré la tesis", finalmente aquí está. Thank you Postcrossing and especially my postcrosser friends (Uly, Charlene, Kapila, Mawanda Robert, Irina). Gracias a todos los que de una manera u otra me habéis acompañado y animado durante todo este tiempo (ahora mismo se me vienen a la cabeza Rosafu, Dario y Víctor, pero han sido muchos y muchos más).

No me gustaría acabar sin dar las gracias a mi familia por estar siempre al pie del cañón conmigo: gracias Jose, Oqueber, Miguel, Euge, Cris y Carmen. Y aquí llega el punto más difícil de todos: ¿cómo te doy las gracias, mamá? Esta tesis nunca hubiera sido posible sin tu trabajo, la formación que me has transmitido, tus ánimos, tu confianza ciega en mí, tu amor incondicional, tu... todo. Tú me has enseñado lo más importante de mi vida, cómo quién se rompe no es por ser débil sino por amar mucho, y que uno siempre saca fuerzas para levantarse de nuevo, aunque sea a rastras y apoyado en ti. ¡Gracias madre por acompañarme hasta el final de este viaje!

Y por último, aunque ocupa el lugar más importante de esta aventura: muchas gracias Jefe, menuda vuelta al mundo que nos hemos marcado juntos. Per moltes més!

Preamble

Great part of this PhD Thesis has been performed under the frame of collaborative projects. This is why besides the results obtained by the author, it has been decided to include some experiments performed by other scientists, which complete and reinforce the work presented in this manuscript.

Content

| | |
|---|----|
| 1. Introduction and Objectives..... | 21 |
| 1.1. Introduction..... | 21 |
| 1.1.1. Vesicles as self-assembled structures | 23 |
| 1.1.1.1. Preparation of vesicles | 25 |
| 1.1.1.1.1. Conventional methods..... | 25 |
| 1.1.1.1.2. Compressed fluids (CFs)-based technologies | 26 |
| 1.1.1.1.2.1. DELOS-SUSP | 27 |
| 1.2. Objectives | 30 |
| 2. Nanovesicle-GLA conjugates as nanomedicine candidates for the treatment of the Fabry disease | 31 |
| 2.1. Introduction..... | 31 |
| 2.2. Impact of the GLA liposomes-RGD_ether composition and supramolecular organization on its biological activity | 36 |
| 2.2.1. Impact of GLA supramolecular organization on its in vitro efficacy | 36 |
| 2.2.2. Impact of RGD peptide on the internalization of GLA nanoliposomes | 48 |
| 2.2.3. Stability in different media | 53 |
| 2.3. Substitution of His-GLA for commercial Replagal® | 55 |
| 2.4. Increase of nanoformulation enzyme concentration to perform in vivo testing | 57 |
| 2.5. Changing the dispersant medium to isotonic one, and changing the counterion of cholesterol_PEG200_RGDether..... | 65 |
| 2.6. Testing different enzymes in order to increase the enzymatic activity | 68 |
| 2.7. In vivo testing: pharmacokinetics, toxicity and efficacy..... | 73 |
| 2.8. Encapsulation of chelators to perform biodistribution by radiolabelling | 77 |

| | | |
|------------|---|-----|
| 2.9. | Conjugation with new peptides for crossing the blood brain barrier | 81 |
| 2.10. | Summary and conclusions..... | 84 |
| 3. | Development of an HPLC methodology for the quantification of the components of the liposome-RGD_ether membrane..... | 85 |
| 3.1. | Introduction..... | 85 |
| 3.2. | Development of the HPLC methodology..... | 88 |
| 3.2.1. | Preliminary studies | 88 |
| 3.2.2. | HPLC-ELSD methodologies | 93 |
| 3.2.2.1. | Method parameters | 95 |
| 3.2.2.2. | Standard solutions preparation | 96 |
| 3.2.2.3. | Sample preparation..... | 96 |
| 3.2.2.4. | Method validation results | 97 |
| 3.2.2.4.1. | Linearity and goodness of fit..... | 97 |
| 3.2.2.4.2. | Limit of detection (LOD) and limit of quantification (LOQ) | 99 |
| 3.2.2.4.3. | Test of dilution of a standard stock solution | 101 |
| 3.2.2.4.4. | Sample dilution test | 103 |
| 3.2.2.4.5. | Accuracy | 105 |
| 3.2.2.4.6. | Precision | 108 |
| 3.2.2.4.7. | Quality criteria | 109 |
| 3.2.2.5. | Sample analysis: quantification of lipids in liposomal formulations | 110 |
| 3.3. | Summary and conclusions..... | 111 |
| 4. | Optimization of the preparation method of liposomes-RGD and their chemical composition..... | 112 |
| 4.1. | Introduction..... | 112 |
| 4.2. | Solvents for dissolving cholesterol_PEG200_RGDether | 113 |
| 4.3. | pH monitoring | 115 |

| | | |
|----------|--|-----|
| 4.4. | Summary and conclusions..... | 124 |
| 5. | Impact of RGD peptide functionalization mode of nanoliposomes on their cellular internalization..... | 125 |
| 5.1. | Introduction..... | 125 |
| 5.2. | Preparation of liposomes by DELOS-SUSP | 129 |
| 5.3. | Physicochemical characterization | 132 |
| 5.3.1. | Determination of size, polydispersity index and Z potential | 132 |
| 5.3.2. | Sample analysis: quantification of lipids in liposomal formulations..... | 134 |
| 5.3.3. | Morphological analysis | 135 |
| 5.3.4. | Lamellarity determination | 136 |
| 5.3.5. | Quantification of DiD in the liposomal formulations | 137 |
| 5.4. | Biological Characterization of liposomes | 138 |
| 5.4.1. | Flow cytometry..... | 138 |
| 5.4.2. | Laser confocal scanning microscopy | 139 |
| 5.5. | Summary and conclusions..... | 140 |
| 6. | Conclusions..... | 141 |
| 7. | Experimental Section | 143 |
| 7.1. | Materials..... | 143 |
| 7.2. | Preparation of nanovesicle-bioactive conjugates. Equipments and procedures. | 144 |
| 7.2.1. | Preparation of nanovesicle-bioactive conjugation by DELOS-SUSP..... | 144 |
| 7.2.1.1. | Equipment..... | 144 |
| 7.2.1.2. | Procedure | 145 |
| 7.2.1.3. | Types of liposomes prepared | 146 |
| 7.2.2. | Preparation of liposomes functionalized with gold nanoparticles by thin film hydration (TFH) | 153 |
| 7.2.2.1. | Procedure | 153 |

| | | |
|----------|--|-----|
| 7.2.2.2. | Types of liposomes prepared | 154 |
| 7.3. | Physicochemical characterization of the nanovesicle-bioactive conjugates. Instruments, techniques and procedures | 155 |
| 7.3.1. | Determination of size, polydispersity index and Z potential | 155 |
| 7.3.2. | Determination of pH..... | 155 |
| 7.3.3. | Quantification of membrane components (cholesterol, DPPC and cholesterol_PEG200_RGD)..... | 155 |
| 7.3.3.1. | Preliminary studies..... | 155 |
| 7.3.3.2. | Optimization and validation of HPLC-ELSD methodology..... | 156 |
| 7.3.4. | Morphological analysis | 159 |
| 7.3.5. | Lamellarity determination | 160 |
| 7.4. | Determination of the degree of loading/functionalization of vesicles | 161 |
| 7.4.1. | Separation and concentration using a diafiltration equipment..... | 161 |
| 7.4.2. | Quantification of GLA in liposomes | 162 |
| 7.5. | Synthesis and characterization of bioactive compounds..... | 163 |
| 7.5.1. | Production of GLA-HIS enzyme | 163 |
| 7.5.2. | Dialysis of Replagal | 163 |
| 7.6. | Labelling of nanovesicles with DiD dye | 163 |
| 7.7. | Cellular uptake assays..... | 164 |
| 7.7.1. | Protocol under clean conditions for the preparation of liposomal samples tested in cell and in vivo assays. | 164 |
| 7.7.2. | Cell culture experiments..... | 165 |
| 7.7.2.1. | Cellular uptake of liposomes assessed by laser scanning confocal microscopy..... | 165 |
| 7.7.2.2. | Flow cytometry experiment..... | 165 |
| 7.8. | Biological activity of GLA | 166 |
| 7.8.1. | Specific enzymatic activity..... | 166 |

| | |
|---|-----|
| 7.8.2. In vitro enzymatic efficacy | 166 |
| 7.9. In vivo experiments | 167 |
| 7.9.1. Pharmacokinetics | 167 |
| 7.9.2. Toxicity..... | 167 |
| 7.9.3. Efficacy..... | 167 |
| Annex: Functionalization of liposomes with different gold nanoparticles | 169 |
| A.1. Introduction..... | 169 |
| A.2. Preparation of Au-nanoliposomes | 171 |
| A.3. Summary and conclusions | 177 |
| Bibliography..... | 178 |

1. Introduction and Objectives

1.1. Introduction

Nanotechnology can be defined as the science, engineering and technology developed in the nanoscale¹. The physicist and Nobel Prize winner, Richard Feynman in 1959, predicted the possibilities of nanoscience in *There is Plenty of Room at the Bottom. An invitation to enter a new field of physics*^{2,3}.

According to the European Commission, nanomaterials refer to the material (natural, incidental or manufactured) that comprises particles in an unbound state or as an aggregate wherein one or more external dimensions is in the size range of 1-100 nm for at least 50% of the particles, conforming to the number size distribution. Size distribution is important since the nanomaterial is usually composed of particles of different sizes. It is worth noting that the upper limit in size (100 nm) is arbitrary because the physicochemical and biological characteristics of the nanomaterials do not change abruptly at this size⁴.

Regarding Feynman comments, he spoke about the now called top-down approach, which means the reduction in size of already existing bulk materials into a smaller one or smaller pieces. In contrast, bottom-up strategy is based in the construction of nanostructures atom by atom using self-assembly procedures^{3,4}. Self-assembly means the spontaneous and reversible association of molecular species to form larger and more complex supramolecular entities according to the intrinsic information contained in the components (chemical building blocks⁵). Bottom-up processes allow the design and control of particle size, morphology and internal structure.

One of the sub-disciplines of nanotechnology is nanomedicine, which is the application of innovative nanotechnologies, aiming to offer solutions to the current limitations in diagnosis, treatment and management of human diseases^{1,6}. As well as Feynman's conference dictated the beginnings of nanotechnology, the concept of "magic bullet" of Paul Ehrlich inspired the field of nanomedicine: the aim was developing targeted carriers, or "magic bullets", loaded with drug compounds in order to target diseases with a single treatment^{3,7}. However, nowadays nanomedicine involves research in at least four different areas: development of biosensors for diagnosis, controlled drug delivery for therapeutic action, regenerative medicine like tissue engineering, and theranostics that focus in the combination of the diagnosis and therapeutic functions in one material^{4,8}.

Drug delivery refers to the systems used as transports for therapeutics in the body^{9,10}. Drug delivery systems (DDS) have enhanced the effectiveness and delivery of the drugs because these nanocarriers can protect sensitive biomolecules from degradation and the in vivo attack of the immune system^{11,12,13}. Nanoparticulate carriers can be composed of organic and inorganic materials. Probably the most widely used for drug delivery purposes are vesicle and polymer based nanocarriers^{14,15,16}. Indeed, vesicles have served as convenient delivery vehicles for biologically active compounds since they are non-toxic, biodegradable and non immunogenic^{17,18}. In vesicle-based DDS, the pharmacological properties strongly depend on the structural characteristics of the conjugates^{19,20}. As a consequence, a high degree of structural homogeneity regarding size, morphology and composition is crucial for their optimum performance²¹.

1.1.1. Vesicles as self-assembled structures

Vesicles are spherical objects composed of amphiphilic molecules that enclose a liquid compartment. The amphiphilic molecules generally have a hydrophobic tail and a hydrophilic or polar head. In contact with water this type of molecules are oriented protecting the hydrophobic tails from the water and exposing its polar head towards it, forming closed bilayers. According to their size and number of bilayers (lamellarity), vesicles can be broadly classified in small unilamellar vesicles (SUVs, size < 200 nm and single bilayer), large unilamellar vesicles (LUVs, size ranging from 200-1000 nm and single bilayer), giant unilamellar vesicles (GUVs, size > 1000 nm and single bilayer), multilamellar vesicles (MLVs, consisting of several concentric bilayers) and multivesicular vesicles (MVs, composed by several small vesicles entrapped into larger ones)²².

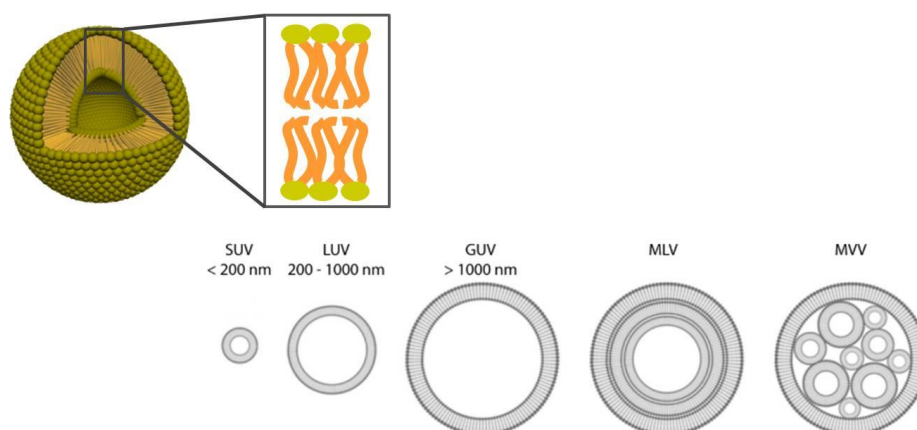


Figure 1.1: Schematic representation of a vesicle composed of amphiphilic molecules. Classification of vesicles regarding size and lamellarity

Vesicles are one of the most studied self-assembled structures due to their diverse and important applications as cell membrane models²³, reaction vessels²⁴ and DDS^{25,26,27}, among others. They are one of the most promising supramolecular assemblies to be used as carriers for drug delivery, due to their great versatility with respect to size, composition, surface characteristics, and capacity for integrating active molecules. The vesicles' unique structure enables them to encapsulate both hydrophobic compounds (within the lipid bilayers) and hydrophilic compounds (within their internal cavity).

Dr. Alec Bangham et al. first described liposomes, vesicles constituted mainly by phospholipids, during their search for a model of cell membranes. When phospholipids were put in contact with water, they spontaneously arranged in vesicles with a bilayered membrane structure²⁸. Although their purpose was to mimic the cellular membrane, soon they were successfully tested as drug delivery systems^{29,30}.

Liposomes present several advantages like biocompatibility, improved solubility of the encapsulated drugs, protection against chemical and/or biological degradation, reduction of the nonspecific side-effects and toxicity of encapsulated drug, among others³¹.

However, the so called “first generation” of liposomes or classic liposomes is rapidly cleared by the mononuclear phagocytic system³². To avoid this effect, “second generation” of liposomes was developed where lipid composition, size and charge are modulated. For instance, cholesterol is added to the formulation in order to increase the stability of the formulation and to reduce the permeability of the system membrane. Also cholesterol can be used as an anchor for the inclusion of hydrophilic carbohydrates or polymers that enhance the half-life of the liposomes in the blood³³. The increased blood circulation time is the main characteristic of this second generation of “stealth” liposomes and is usually accomplished by the addition of polyethylene glycol (PEG) on the surface. PEG chains decrease hydrophobicity and immunogenicity whereas they increase the steric hindrance and stability, protecting against clearance. PEG can be modified attaching specific ligands, entering then in the “third generation” where the liposomes combine various functions like drug delivery, cellular or subcellular targeting, penetration and accumulation, stimuli-sensitive function and imaging/diagnostic. In the case of the stimuli-sensitive liposomes, also called ‘smart’, the systems undergo structural changes in response to certain stimuli like pH, temperature, redox potential changes or magnetic field³².

The great potential and properties of liposomes has led to the first marketed products for the treatment of some major health threats. In fact, Doxil® was the first nanomedicine approved for clinical use in 1995. It consists in a PEGylated liposome formulation encapsulating doxorubicin for the treatment of ovarian cancer. There are also other approved systems, gathered in the literature^{34,35} for diverse applications.

1.1.1.1. Preparation of vesicles

As has been remarked, the optimal performance of the supramolecular formulations is completely related to the structural characteristics. Thus, a tight control over these physicochemical properties is of outstanding importance. In this regard, not only environmental conditions like temperature, pH, ionic strength, composition and concentration of the components are crucial but also the path followed by the self-assembly of the monomer. Therefore, the method of preparation of the systems must be considered. In addition, the manufacturing process should be easily compliant with the regulations of the Food and Drug Administration (FDA) in the United States and the European Medicines Agency (EMA) in Europe. These regulations involve the development and implementation of good manufacturing practices (GMPs), which ensure the quality, safety and traceability of the obtained product³⁶. Also the majority of vesicle preparation methods employ organic solvents that, depending on the final application of the systems, must be reduced below the allowed limits³⁷.

1.1.1.1.1. Conventional methods

The drawback of conventional methodologies to produce vesicles lies in the little control of the self-assembling of the molecules constituting the system, resulting in a high vesicle to vesicle structural heterogeneity^{31,32,33}. That is the case of the thin-film hydration methodology (TFH), also called the Bangham method, which is the most widely used preparation method. In it, lipid components are dissolved in an organic solvent. After the evaporation of this solvent, the thin film formed is rehydrated in an aqueous solvent. Additional operations are needed to correct the heterogeneity of the sample.

Other preparation methods include reverse-phase evaporation, freeze-drying and ethanol injection. However, following these methodologies is necessary to employ additional techniques such as membrane extrusion, sonication, homogenization and/or freeze-thawing, in order to precisely control the size and size distribution³⁵.

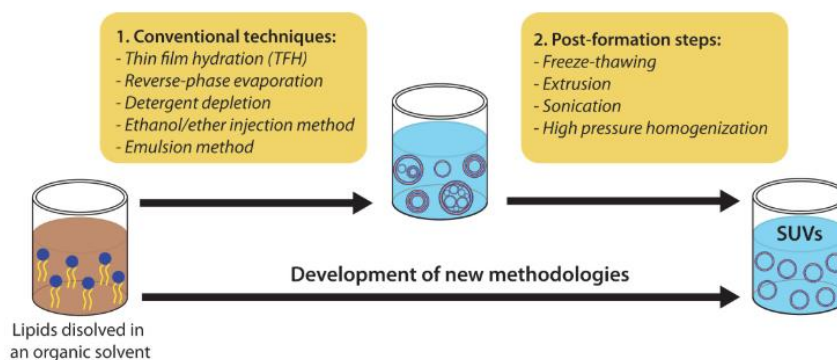


Figure 1.2: Conventional methodologies for the preparation of vesicles and the most common post-formation steps for their homogenization.

Consequently, it is of extreme interest the development of new, efficient and environmentally respectful methodologies that allow the manufacturing of these materials in only one-step but achieving also controlled properties.

1.1.1.1.2. Compressed fluids (CFs)-based technologies

The use of compressed fluid (CFs)-based methodologies, also named as dense gas technologies have emerged as promising alternatives to conventional methodologies for the preparation of nanostructured materials^{38,39,40}, including vesicles. CFs are substances that at normal conditions of pressure (P) and temperature (T) exist as gases but when we increase these factors can be converted into liquids or supercritical fluids. Supercritical region is one of the states of matter that is obtained when the substance is submitted to conditions above its critical pressure (P_c) and temperature (T_c). The most important feature of this supercritical region is the absence of phase boundary between the gas and liquid phases. Therefore, supercritical fluids present properties “hybrids” of the ones associated with liquids and gases, which moreover can be adjustable with small pressure and temperature variations (**Figure 1.3**). Thus, the viscosities and diffusivities are similar to those of the gas phase while the density and solvation power is closer to the liquid phase. Exists the possibility of obtaining this special behavior at conditions below or near the critical point (subcritical region), which means milder conditions of T and P, reducing the cost related to the use of elevated pressures and the risk of damaging the structure and properties of the molecules processed.

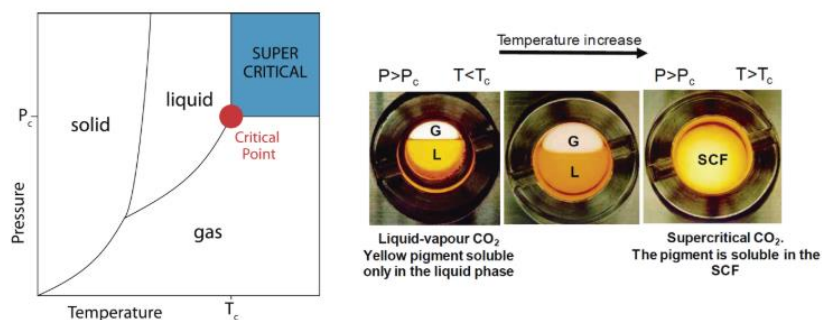


Figure 1.3: Phase diagram of a compressed fluid (left) and images illustrating the different solvating power of CO_2 as a function of its state (right).

The solvent power of a CF, either in the liquid or supercritical state, depends proportionally on its density, which also responds to changes in temperature and pressure around the critical point. Therefore, the solvation power of CFs can be tuned by pressure changes, which propagates much more quickly than the temperature and composition solvent changes. This can offer a better control over the morphology of the materials on the microscopic scale than most of conventional processing techniques. The most widely used dense gas is carbon dioxide (CO_2) since it is non-flammable, non-toxic, noncorrosive, inexpensive, non-polluting and has easily accessible critical parameters of $31.1\text{ }^\circ\text{C}$ and 73.8 bar ⁴¹. Due to these interesting properties, CO_2 has become a “green substitute” to organic solvents in the preparation of lipid-based nanocarriers such as liposomes. Several methodologies that employ CO_2 aim to reduce the amount of organic solvent required in conventional methodologies and at the same time improve the final vesicle structural characteristics^{31,42}. Other advantages of the processing with CO_2 are the sterile operating conditions along with the potential for one-step production processes. However, there are still some drawbacks such as the elevated pressures and temperatures required during the process.

1.1.1.1.2.1. DELOS-SUSP

In the year 2000, the *Nanomol* group of ICMA-B-CSIC where this thesis has been done, developed and patented a new procedure based on the use of compressed CO_2 called *Depressurization of an Expanded Organic Solution (DELOS)* for the production of micron and submicron-sized crystalline particles with high polymorphic purity^{43,44}. In

this process, CO₂ is a co-solvent completely miscible at a given pressure and temperature with an organic solution that contains the solute to be crystallized^{45,46}. DELOS requires milder conditions of pressure (<10 MPa) and temperature (<308 K) than other CFs-based methodologies³¹, allowing the processing of heat labile compounds while reducing the cost of a high pressure plant for the scale-up. Later on, a new and improved procedure based on DELOS process was developed for the preparation of colloidal suspensions: the *Depressurization of an Expanded Organic Solution-Suspension (DELOS-SUSP)* process enables the one-step preparation of cholesterol-rich nanovesicles⁴⁷.

Briefly, the DELOS-SUSP method (**Figure 1.4**) consists in the loading of the membrane lipid components solution and the desired hydrophobic bioactives in an organic solvent (like ethanol) into a high-pressure autoclave previously driven to the working temperature (**Figure 1.4a**). In the second stage, the reactor is pressurized using compressed CO₂ until the working pressure is achieved (10 MPa) (**Figure 1.4b**). Finally, the vesicular conjugates are formed by the depressurization of the CO₂-expanded solution over an aqueous phase containing surfactants and hydrophilic bioactives (**Figure 1.4c**). In this final step, a flow of N₂ at the working pressure is used as a plunger of the CO₂-expanded solution. The expanded organic solution experiences then, a large, abrupt and extremely homogenous temperature decrease produced by the CO₂ evaporation from the expanded solution. This might explain the resulting homogenous vesicles in terms of size, lamellarity and morphology.

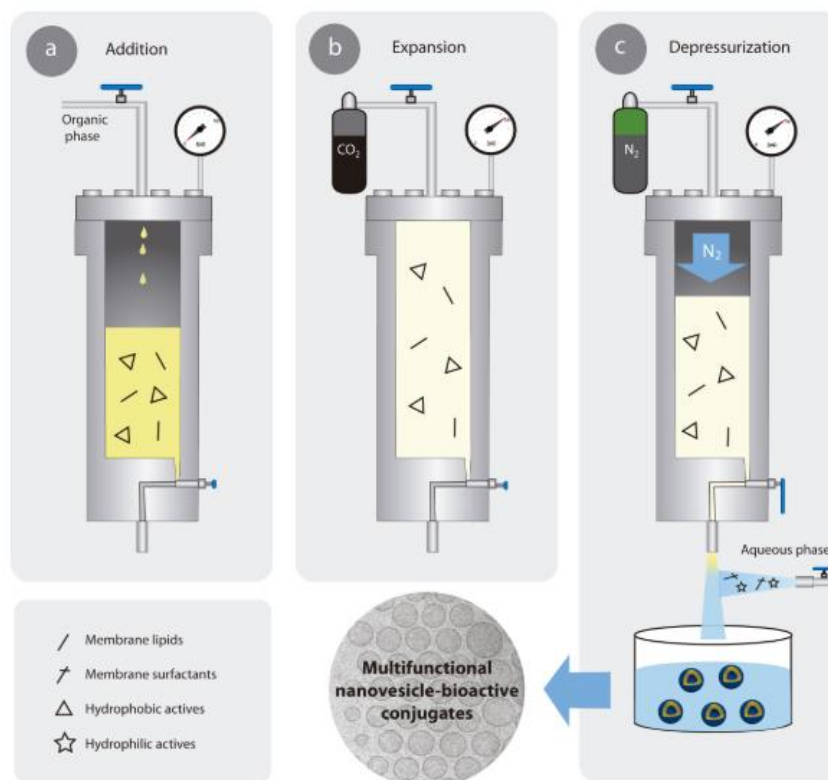


Figure 1.4: Schematic representation of the DELOS-SUSP method for the efficient preparation of multifunctional nanovesicle-bioactive hybrids. The whole procedure includes the loading (a) of an organic solution of the lipidic membrane components and the desired hydrophobic active compounds/molecules into an autoclave at a working temperature (T_w) and atmospheric pressure; the addition of CO₂ (b) to produce a CO₂-expanded solution, at a given X_{CO_2} , working pressure (P_w), and T_w , where the hydrophobic active and membrane components remain dissolved; and finally, the depressurization (c) of the expanded solution over an aqueous solution, which might contain membrane surfactants and hydrophilic biomolecules, to produce an aqueous dispersion of the nanovesicle-bioactive(s) hybrids with vesicle-to-vesicle homogeneity regarding size and morphology.

DELOS-SUSP is thus a simple, robust, scalable and one-step process to prepare a variety of SUVs with different functionalities and high structural homogeneity. Interestingly, this technique allows a high incorporation of cholesterol since there is not a free-solvent state⁴⁸ like in the case of conventional methodologies, i.e. TFH.

DELOS-SUSP has demonstrated its potential to prepare a variety of SUV-biomolecule conjugates with high structural homogeneity and of interest for the development of new nanomedicine candidates⁴⁹.

1.2. Objectives

Following this research line, this thesis is devoted to the study of liposomal systems functionalized with the RGD peptide, in order to correlate their physicochemical properties with their behavior in vitro and, if applicable, in vivo. The RGD peptide was incorporated using a cholesterol molecule covalently bound to a PEG linker that is also attached to the cyclic RGD.

The following main objectives have been addressed:

- Objective 1: To generate a solid experimental proof of concept that opens the door to the pharmaceutical development of nanoliposomes, functionalized with RGD peptide and loaded with α -galactosidase A protein, as a new nanomedicine candidate for the treatment of Fabry disease.
- Objective 2: To study the impact of RGD attachment bond between the cholesterol and the PEG linker in the physicochemical properties of RGD functionalized liposomes and in their cellular internalization.

2. Nanovesicle-GLA conjugates as nanomedicine candidates for the treatment of the Fabry disease

2.1. Introduction

Lysosomal storage disorders (LSDs) include around 70 metabolic genetic diseases characterized by a single mutation that leads to the deficiency of a specific lysosomal enzyme activity and the subsequent accumulation of macromolecular substrates in affected cells^{50,51}. The majority of these disorders are derived from the deficiency of lysosomal hydrolases⁵², although some of them are related to non-enzymatic lysosomal proteins such as lysosomal membrane proteins⁵³. The combined prevalence of LSDs is 1:5000 live births, considering that this may be underestimated because of the difficulties in the diagnosis. However, when considered individually, they are cataloged as rare diseases due to its low incidence.

Lysosomes are cellular organelles with functions that range from protein degradation of macromolecules to fusion with the plasma membrane during cell injury. In some cell types they also have secretory functions⁵⁴. Lysosomes contain digestive enzymes, most of them hydrolases, which are active at the acidic pH of these organelles. In theory, every single mutation in the genes that encode any of these proteins could cause an LSD⁵⁵. Hydrolases are produced in the rough endoplasmic reticulum^{50,56} and

transported to the trans-Golgi network where are tagged with mannose-6-phosphate and secreted to the extracellular milieu⁵⁷. Since endosomes have the mannose-6-phosphate receptors, the enzymes are internalized and delivered to the lysosomes via endocytic pathway⁵⁴.

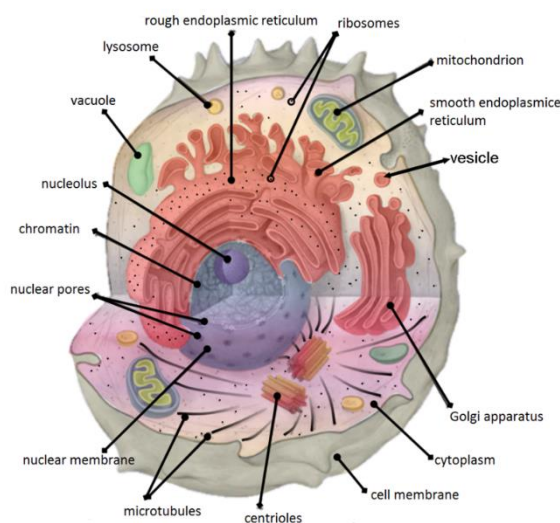


Figure 2.1. Schematic representation of eukaryotic cell organelles (animal). By Koswac [CC BY-SA 4.0 (<https://creativecommons.org/licenses/by-sa/4.0>)]

LSDs can be generally classified based on the macromolecule deposited inside the cells and tissues: sphingolipidoses, mucopolysaccharidoses, mucopolipidoses, oligosaccharidoses, lipidoses and the glycogen storage diseases⁵¹.

Most of the LSDs lack an effective and curative treatment. Some of these disorders benefit from enzyme replacement therapy (ERT) which consists in the intravenous administration of the deficient enzyme. This enzyme is usually obtained by recombinant biotechnology and enriched in mannose 6-phosphate in order to ensure the proper delivery to the lysosome. ERT generally produce significant clinical benefits improving life quality of the patients. However the success is limited due to substantial drawbacks, such as the variability in the efficacy, the clearance from the blood stream, the degradation by proteases⁵⁸, the low effectiveness when the organs are already damaged, immunological reactions and development of resistance to the exogenous enzyme^{50,59,60,61}, high cost of the therapy and inability to cross the blood brain barrier (BBB) to treat neurological impairments^{62,63}. Treatment with ERT usually requires

combination with supportive care consisting in palliative measures in order to treat the multisystemic symptoms^{50,64}. Given all those difficulties, there is a continuous effort towards developing new alternative therapeutic approaches that improve the limitations of the ERT. For instance, some treatment alternatives include gene therapy, substrate reduction, and chaperones. Gene therapy is especially interesting since the lysosomal storage disorders are generated by a single gene mutation⁶⁵, hence is a research area of great interest^{66,67}.

The objective of substrate reduction therapy is to diminish the production of the accumulated material by inhibiting its biosynthesis. Compared with ERT, it is administered orally, does not trigger immune reactions and can potentially cross the blood brain barrier⁶⁵. However, their main limitation is the lack of specificity that may interfere with other anabolic routes⁵⁰.

Chaperones are molecules responsible for the correct folding of proteins. Administering them can result in the recovery of the activity of the affected protein^{50,65}. On the other hand, the effectiveness of this treatment is limited to the cases in which the lack of enzyme activity is due to its misfolding.

In recent years, nanotechnology has emerged as a powerful tool to develop enzyme-loaded nanosystems in order to ameliorate ERT efficacy and minimize its side effects. The objective of these nanomaterials is to increase the bioavailability of the enzyme, avoid its degradation, control the circulation time and release rate. Nanocarriers can be functionalized with targeting units (antibodies, peptides, sugars, aptamers) that provide recognition of markers expressed by sick cells⁶³, thus assuring the correct distribution of the enzyme. In the case of LSDs, the delivery of the enzyme requires targeted delivery into lysosomes^{52,68}.

Fabry disease is a sphingolipidosis⁶⁹, and is one of the most prevalent among LSDs even though its incidence is very low (1:117000⁷⁰). This disease is caused by a gene mutation on the X-chromosome, which encodes α -galactosidase A (GLA) enzyme, a homodimeric glycoprotein. The GLA hydrolyzes terminal α -D-galactosyl residuals from neutral glycosphingolipids⁷¹. Thus, the lack of this enzyme causes the accumulation of these molecules, mainly globotriaosylceramide (Gb3), at the lysosomes of some cells⁷².

The tissue damage caused by the Gb3 deposits is responsible for Fabry disease manifestations. The first symptoms include chronic neuropathic pain, skin abnormalities, gastrointestinal disturbances and corneal opacity. Organ complications typically emerge in young adult patients: renal failure, left ventricular hypertrophy, strokes, among others⁶⁴.

Currently, more than 15 years of clinical experience endorse the ERT for Fabry disease. ERT is presently available in the forms of agalsidase alfa (Replagal[®], from Shire Human Genetic Therapies, Dublin, Ireland) and agalsidase beta (Fabrazyme[®], from Genzyme Corporation, Cambridge, MA). The amino-acid sequences of both enzymes is similar with comparable specific activities per milligram, but differing in the glycosilation patterns⁶⁴. At present, a new recombinant α -galactosidase is in clinical trials: PRX-102 is derived from tobacco-cells and is modified with polyethylene-glycol chains. It shows enhanced half-life, less immunogenicity and similar activity as Replagal[®] and Fabrazyme^{®50}.

Limitations emerge when studying orphan diseases such as Fabry, since there are a small number of patients available for trials. Anyway, the literature shows, for adult male patients, that ERT significantly reduces the deposits of Gb3, improves some cardiac outcomes and stabilizes renal function. Also, it can potentially ameliorate quality of life with a direct impact in the chronic pain⁷³.

Apart from available ERT, chaperone migalastat (Galafold[®], from Amicus Therapeutics, Cranbury, NJ, USA) has been approved for Fabry patients with amenable mutations^{64,70,74}. Currently, 268 mutations are classified as amenable to treatment⁷⁵. Another alternative in clinical trials is Lucerastat, an iminosugar for substrate reduction therapy, applicable for all patients independently of their genotype⁷⁵.

As it was previously exposed, drug delivery systems can be a promising strategy to improve ERT efficacy in LSDs. For instance, targeted polymer nanocarriers coated with intercellular adhesion molecule (ICAM-1) and loaded with α -galactosidase have shown an improved enzymatic release in vascular endothelial cells achieving Gb3 degradation^{50,71}. Another example is the ionically cross-linked polyelectrolyte complex

composed of trimethyl chitosan and GLA which improve GLA activity when compared with the free enzyme⁵⁷.

In the doctoral thesis of Dr. Ingrid Cabrera, it was determined that liposomes functionalized with cyclic RGD are excellent candidates for the specific delivery of active ingredients to endothelial cells⁴⁹. RGD-peptide is a cell targeting peptide, very well known to increase cellular penetration via RGD/integrin recognition, more specifically $\alpha\beta3$ integrins. Integrins are transmembrane heterodimeric glycoprotein cell surface receptors present in vascular endothelial cells normally overexpressed in cancer⁷⁶.

For the integration of RGD-targeting peptide in the liposomes, the cholesterol is covalently bound to RGD peptides through a PEG linker. Among the different types of RGD peptides available, the cRGDfK has been chosen to functionalize the nanoliposomes due to several advantages related to its cyclic structure which include more stability against degradation and improved binding properties⁷⁷. The cholesterol_PEG200_RGD molecule was designed and produced by the group of Dr. Miriam Royo (Institut de Química Avançada de Catalunya, IQAC-CSIC), and more details about this molecule are given in Experimental Section 7.1. Importantly, the cholesterol is bound to the PEG linker through an ether bond, while the bond between the PEG200 and the cRGDfK is carbamate. Therefore, we called this molecule cholesterol_PEG200_RGDether and the liposomes functionalized with this molecule, liposomes-RGD_ether.

Targeting endothelial cells is an interesting challenge for Fabry disease since alterations in the vasculature are typical in the pathophysiology⁷⁸. Actually, $\alpha\beta3$ integrin expression and urinary excretion are related to the progression of the renal injury in this disease⁷⁹. Dr. Ingrid Cabrera also observed that the enzymatic activity of GLA enzyme with a 6_histidine tag was enhanced when this enzyme was integrated in nanoliposomes functionalized with RGD peptide⁸⁰. This promising result opens the doors to the pre-clinical non-regulatory testing.

During *NanoFabry*⁸¹ project (2009-2014), funded by “Fundació La Marató TV3”, functionalized GLA loaded nanoliposomes were prepared with improved capability for

the specific delivery of the GLA enzyme to endothelial cells. As a continuation of *NanoFabry*, the *Lipocell*⁸² project (2014-2015) was granted, financed by Centro de Investigación Biomédica en Red-Bioingeniería, Biomateriales y Nanomedicina (CIBER-BBN) and the pharmaceutical company BIOPRAXIS, focused in Fabry disease, as well as the *Terarmet*⁸³ project (2014-2017), financed by Spanish ministry MINECO, centered not only in Fabry disease but also in mucopolysaccharidosis type III or Sanfilippo syndrome. The promising in vitro efficacy results observed in *Lipocell* and *Terarmet* projects, and the possibility to easily scale up the methodology used for the fabrication of this new nanomedicine candidate, also proved in these projects, open the doors to the pre-clinical in vivo testing currently explored under *Smart-4-Fabry*⁸⁴ EU project.

In the frame of the present thesis, a detailed physicochemical characterizations and in vitro/in vivo studies of these new GLA-nanoliposomes were performed in order to generate a solid experimental proof of concept of a potential nanomedicine candidate to treat Fabry disease, achieving the required quality attributes for the intended indication and administration route.

2.2. Impact of the GLA liposomes-RGD_ether composition and supramolecular organization on its biological activity

To become a potential drug product for the treatment of Fabry disease, the precise understanding of the nanomedicine candidate is necessary and the presence of all the nanoliposomes' components must be justified. For instance, the RGD moiety must demonstrate its role for the proper cellular internalization and biological activity of the nanoconjugate. In order to address these issues, different liposomes were prepared and tested regarding both the internalization and the in vitro efficacy.

2.2.1. Impact of GLA supramolecular organization on its in vitro efficacy

Liposomes were prepared by DELOS-SUSP (Experimental Section 7.2.1) with a membrane composition of cholesterol, phospholipid dipalmitoylphosphatidylcholine (DPPC) and cholesterol_PEG200_RGDether molecule in a theoretical molar ratio 6:10:1 (see **Figure 2.2**).

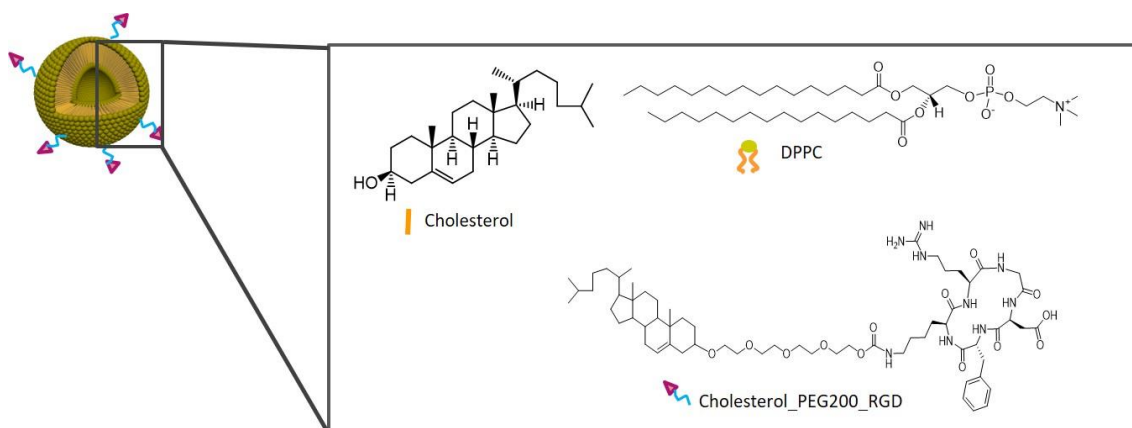


Figure 2.2: Schematic composition of liposomes-RGD_ether composed of cholesterol, DPPC and cholesterol_PEG200_RGDether.

For the DELOS-SUSP procedure, an ethanolic suspension of the three membrane components was added to a reactor of 7.5 mL and pressurized with compressed CO₂. The nanoconjugates were formed with the depressurization of this CO₂-expanded solution of lipids over an aqueous solution of GLA enzyme in water.

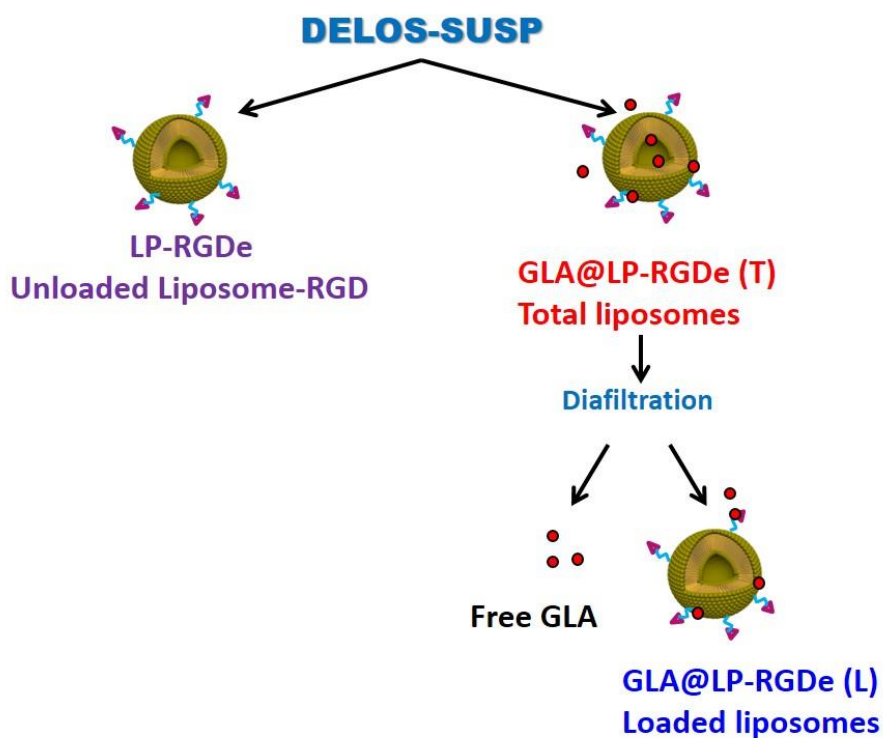


Figure 2.3: Schematic representation of the different GLA nanoliposomes prepared for the physicochemical characterization.

The sample collected from the reactor is named **total liposomes** (GLA@LP-RGDe (T)). Three different theoretical enzyme concentrations, 8.5, 20.0 and 42.5 $\mu\text{g mL}^{-1}$ were tested in the production of liposomes.

In these total liposomal formulations, part of the present GLA is adsorbed in the surface of the liposomes both in the inner and outer faces of the membrane. There is also nonconjugated GLA free in the dispersant medium, i.e. water, of the nanoformulation. In order to eliminate the free GLA, samples were diafiltrated following the procedure described in Experimental Section 7.4.1., to produce nanoliposomal formulations without free GLA, which were called **loaded liposomes** (GLA@LP-RGDe (L)).

Unloaded liposomes-RGD_ether (LP-RGDe) were also prepared by DELOS-SUSP for comparison purposes.

Total, loaded and unloaded liposomes are represented in **Figure 2.3**. The composition of ethanolic and aqueous phases to produce these liposomal formulations of GLA is gathered in **Table 2.1**.

Table 2.1: Compositions and ratios used for the preparation of GLA loaded liposome-RGD conjugates by DELOS-SUSP using CO₂-expanded ethanolic suspensions at 10MPa, 308K and X_{CO2} = 0.85.

| Liposomal systems (GLA concentration) [number of batches] | Organic phase | Aqueous phase | Total lipidic concentration ^a (µg mL ⁻¹) |
|---|--|------------------------|---|
| LP-RGDe [6] | Cholesterol (17 mM) + DPPC (27 mM) + Chol-PEG ₂₀₀ -RGD (2.8 mM) | Water | 1.4 |
| GLA@LP-RGDe (8.5 µg mL ⁻¹) [2] | Cholesterol (17 mM) + DPPC (27 mM) + Chol-PEG ₂₀₀ -RGD (2.8 mM) | GLA in water (89.2 nM) | 1.4 |
| GLA@LP-RGDe (20.0 µg mL ⁻¹) [11] | Cholesterol (17 mM) + DPPC (27 mM) + Chol-PEG ₂₀₀ -RGD (2.8 mM) | GLA in water (200 nM) | 1.4 |
| GLA@LP-RGDe (42.5 µg mL ⁻¹) [2] | Cholesterol (17 mM) + DPPC (27 mM) + Chol-PEG ₂₀₀ -RGD (2.8 mM) | GLA in water (425 nM) | 1.4 |

^aRatio between the total mass of molecules forming the membrane of the liposomes and the volume of the final vesicular suspension. All the systems were prepared following the methodology explained in Experimental Section 7.2.1.

The particle size, polydispersity index (Pdl), and Z potential of the nanoconjugates were measured using a dynamic light scattering (DLS) equipment and are collected in **Table 2.2**. All the systems were in the nanoscale range, but their average sizes and polydispersity are strongly influenced by the GLA concentration in the liposomal system, being higher when the enzyme cargo was increased. For the **total liposomes**, the Z potential was also dependent on the GLA quantity. The Z potential is an indicator of the colloidal stability: in principle high values, either positive or negative, correspond to more stable systems since similar charges are repelled preventing thus the particles aggregation. Correspondingly, the more stable liposomes were the ones with lower GLA concentration, although when the systems were diafiltrated (**loaded liposomes**) the Z potential values turned out to be similar and higher than the total samples, indicating more stability.

Table 2.2: Physicochemical characteristics, entrapment efficiencies (EE), and enzyme loading of nanoliposome conjugates. The physicochemical characteristics of the conjugates after the separation of the nonloaded enzyme are given between brackets.

| Liposomal systems (Initial GLA concentration) | Size | | Z potential (mV) | EE (%) | GLA loading ^c ($\mu\text{g mg}^{-1}$) | GLA conc. ^d ($\mu\text{g mL}^{-1}$) |
|--|-------------------------------|--------------------------------------|--------------------------------|-------------|---|---|
| | Mean ^a (nm) | PdI ^b | | | | |
| LP-RGDe | 160 \pm 1 | 0.38 \pm 0.02 | 30 \pm 2 | - | - | - |
| GLA@LP-RGDe (8.5 $\mu\text{g mL}^{-1}$) | 168 \pm 1 (146 \pm 1) | 0.33 \pm 0.01 (0.29 \pm 0.03) | 18 \pm 1 (-33 \pm 1) | 39 \pm 10 | (2.3 \pm 0.6) | 8 \pm 1 (3 \pm 1) |
| GLA@LP-RGDe (20.0 $\mu\text{g mL}^{-1}$) | 216 \pm 8 (195 \pm 1) | 0.40 \pm 0.01 (0.40 \pm 0.01) | 14 \pm 1 (-24 \pm 2) | 37 \pm 9 | (6 \pm 1) | 20 \pm 2 (7 \pm 2) |
| GLA@LP-RGDe (42.5 $\mu\text{g mL}^{-1}$) | 226 \pm 3 (215 \pm 56) | 0.45 \pm 0.04 (0.33 \pm 0.02) | 9.8 \pm 0.4 (-32 \pm 1) | 38 \pm 8 | (11 \pm 2) | 40 \pm 2 (16 \pm 3) |

^aIntensity weighted mean hydrodynamic size (diameter) measured by dynamic light scattering.

^bPolydispersity index showing the width of the particle size distribution. ^cMass of the integrated enzyme (determined by Western blot), divided by the total mass of the membrane components forming the vesicles. ^dMass of enzyme present divided by the volume of the vesicular suspension. Error margins are SD.

This tendency towards less stable systems when increasing the GLA concentration in the nanoformulation was corroborated by cryo-TEM (**Figure 2.4**), which provides a direct inspection of the sample. Images show that when there is no protein loaded, the vesicles are spherical and unilamellar. The formulations become more polydisperse and oligolamellar with increasing GLA loading.

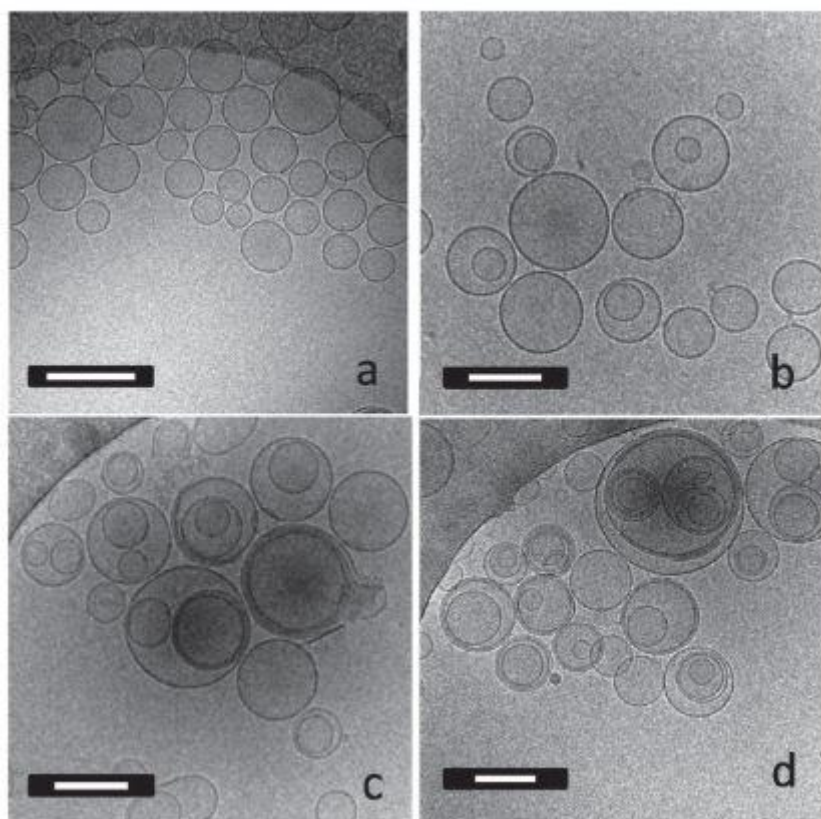


Figure 2.4: Cryo-TEM pictures showing the morphology of the nanoconjugates with different GLA concentrations: a) LP-RGDe, b) GLA@LP-RGDe (L) $8.5 \mu\text{g mL}^{-1}$, c) GLA@LP-RGDe (L) $20.0 \mu\text{g mL}^{-1}$, d) GLA@LP-RGDe (L) $42.5 \mu\text{g mL}^{-1}$. Figure extracted from *Adv. Healthcare Mat.*, 2016⁸⁵.

In comparison with cryo-TEM, SAXS gives a more averaged structural characterization. SAXS measurements corroborated the observations performed by cryo-TEM. As instance, when the GLA concentration is $42.5 \mu\text{g mL}^{-1}$, the broadness increment of the SAXS curve indicates a higher polydispersion in the interbilayer distance compared with the rest of the systems (**Figure 2.5**).

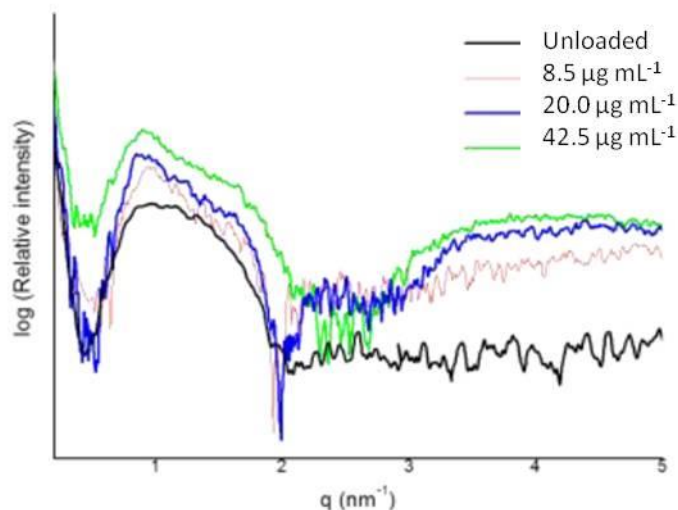


Figure 2.5: SAXS intensity profile versus the scattering vector modulus (q) recorded from unloaded liposomes-RGD_ether (black) and GLA loaded liposomes (at different enzyme concentrations) at 298K. Figure extracted from *Adv. Healthcare Mat.*, 2016⁸⁵, Supporting information.

The amount of incorporated enzyme in the samples was measured using SDS-PAGE and Western blot as explained in Experimental Section 7.4.2. The entrapment efficiency (EE) (**Table 2.2**) was calculated dividing the mass of integrated enzyme by the total initial mass used in the experiment. Despite GLA loading of nanoconjugates enhanced with the increase of GLA concentration of the liposomal system, the EE values were very similar to $\approx 40\%$ in all cases, indicating that the integrated enzyme vs free enzyme ratio was kept constant.

After the physicochemical characterization, the specific enzymatic activity of GLA was assessed using the fluorescent methodology explained in Experimental Section 7.8.1. Briefly, the samples were incubated with a nonfluorescent substrate (4-methylumbelliferyl-d-galactoside, 4-MUG) that renders a fluorescent product (4-methylumbelliferone, 4-MU) when the GLA split it. Measuring the increase of the fluorescent signal, the specific activity of GLA was established.

Specific activity was compared among total and loaded liposomes, and with free GLA solubilized in water (withdrawn from the aqueous phase used in experiments). Remarkably, the specific activity of the GLA always increases when it is conjugated to the liposomes. In the loaded systems with 8.5 and 20.0 $\mu\text{g mL}^{-1}$ the specific activity

increased 3-fold but was only 1.3-fold for the loaded with $42.5 \mu\text{g mL}^{-1}$. As a control we used unloaded liposomes-RGD_ether and GLA in solution. GLA in solution was prepared depressurizing a CO_2 -expanded ethanol solution over water with GLA. The unloaded system presented no fluorescence, indicating that the carrier does not affect the enzymatic assay. The GLA in solution result matched the one of free GLA in water, implying that there is no influence of the CO_2 and ethanol in the determination of the specific activity. It can be concluded that the activity enhancement is related to the enzyme-liposome association.

Table 2.3: Specific enzymatic activities ($\mu\text{mol 4-MU mg}^{-1} \text{GLA h}^{-1}$) of GLA liposomal systems.

| Liposomal systems (Initial GLA concentration) | Total liposomes ^a | Loaded liposomes ^b | Free GLA in water ^c |
|---|------------------------------|-------------------------------|--------------------------------|
| LP-RGDe | 0 | 0 | 0 |
| GLA ($20.0 \mu\text{g mL}^{-1}$) in solution ^d | 364 ± 18 | - | 385 ± 9 |
| GLA@LP-RGDe ($8.5 \mu\text{g mL}^{-1}$) | 913 ± 27 | 924 ± 89 | 304 ± 14 |
| GLA@LP-RGDe ($20.0 \mu\text{g mL}^{-1}$) | 846 ± 270 | 1253 ± 65 | 400 ± 49 |
| GLA@LP-RGDe ($42.5 \mu\text{g mL}^{-1}$) | 879 ± 140 | 705 ± 88 | 548 ± 200 |

^aTotal liposomes, corresponding to the fraction prior diafiltration in which the non-loaded and the loaded GLA coexist together. ^bLoaded liposomes, corresponding to the fraction obtained after the diafiltration process, ^cfree GLA, corresponding to the initial GLA aqueous solution before its conjugation, ^dInfluence of DELOS-SUSP process in the enzymatic activity of GLA. Error margins are SEM.

The theoretical analysis of the interaction of the GLA protein with the bilayer performed using a thermodynamic model showed that the GLA dimer is incorporated as a peripheral protein. Indeed, only eight residues of a single GLA monomer are embedded in the lipid bilayer. In order to better understand the results, a large-scale molecular dynamic simulation was performed. In this case, only one GLA monomer

was considered since only one monomer of the dimer interacts with the membrane, according to the previous thermodynamic calculations. The results confirmed that only the eight residues are responsible of the interaction with the liposome membrane, whereas the active center is located far from the bilayer. This suggests that the enzyme is adsorbed onto the nanocarriers' surface by its second domain (see **Figure 2.6**). Thereby, the GLA without any modification in its structure, has its first domain oriented exposing the active site towards the aqueous phase, which can explain the increased enzymatic activity observed experimentally⁸⁵. Since increasing the GLA loading liposomes become more polydisperse and oligolamellar, the access of the enzyme is less available to the substrate which could explain the smaller specific activity increase observed for the conjugates with the highest GLA loading (1.3-fold instead of 3-fold increment).

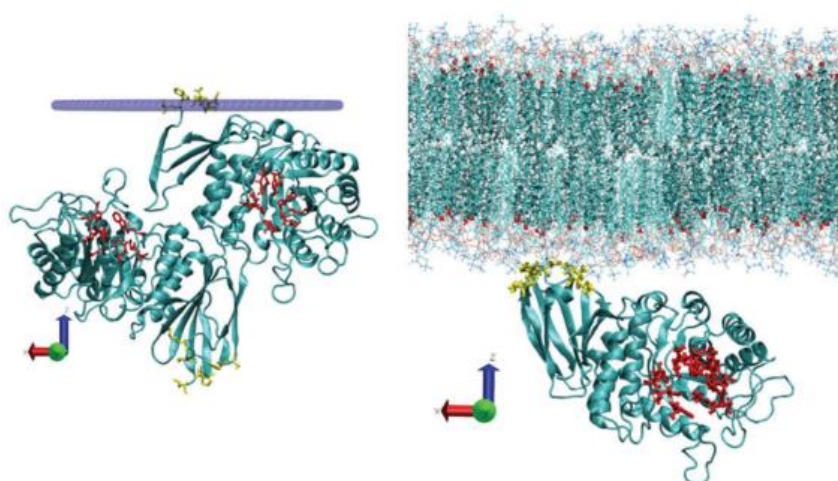


Figure 2.6: In the left is the simulation of the GLA dimer obtained using thermodynamic calculation. In the right is the simulation of a GLA monomer obtained with molecular dynamics. In both cases, the protein residues involved in the interaction with the liposomal membrane are shown as yellow bonds and the residues involved in the active enzymatic region are shown as red bonds. Figure extracted from *Adv. Healthcare Mat.*, 2016⁸⁵.

We can distinguish, then, two phenomena related with the increased activity of the loaded systems: the immobilization of the enzyme in the bilayer and the accessibility of the enzyme if the system is homogenous and unilamellar. The formulation with 20.0 $\mu\text{g mL}^{-1}$ GLA content was then selected for the next experiments, because of the good physicochemical properties and enhanced enzymatic activity.

The following step was to test the ability of the GLA@LP-RGDe to degrade the Gb3 deposited inside the lysosomes. For this purpose, it was used a cellular model of Fabry disease consisting in mouse aortic endothelial cells (MAEC) from GLA knock out (KO) mice. These cells have also been described to overexpress $\alpha\beta3$ integrins⁷⁶, justifying the importance of using RGD moiety. The procedure is described in Experimental Section 7.8.2. The samples were co-incubated with NBD-Gb3 in the MAEC cells. The NBD dye covalently attached to the Gb3 molecules exhibits higher fluorescence than when is free in solution. The lower fluorescence values measured by fluorescence flow cytometry indicates that the conjugates are actively degrading the Gb3.

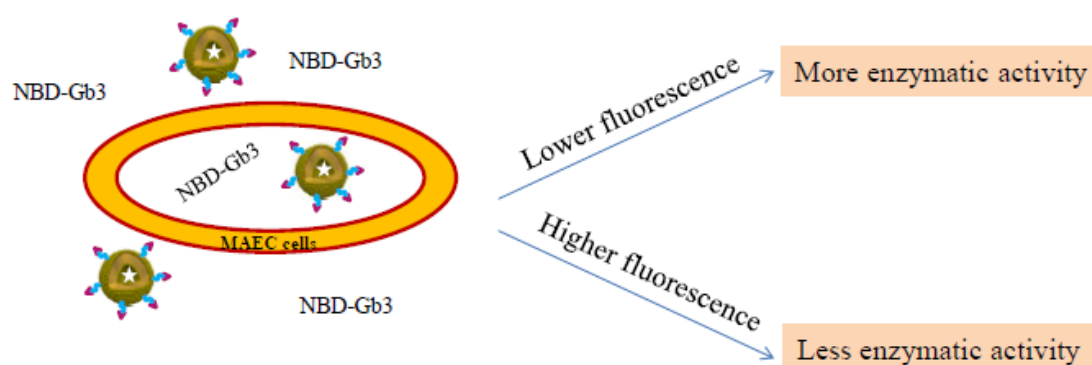


Figure 2.7: Schematic representation of the efficacy test performed with MAEC cells. Extracted from Cabrera, 2013⁸⁰.

From previous studies by immunomicroscopy^{80,85}, GLA seemed anchored in the membrane, as was also assessed in the theoretical simulations. However, in order to study the impact of the GLA localization in the liposomes on the degradation of Gb3, other prototypes represented in **Figure 2.8** were prepared. Apart from the **total** and **loaded liposomes**, **adsorbed** and **artificial total liposomes** were also prepared and tested.

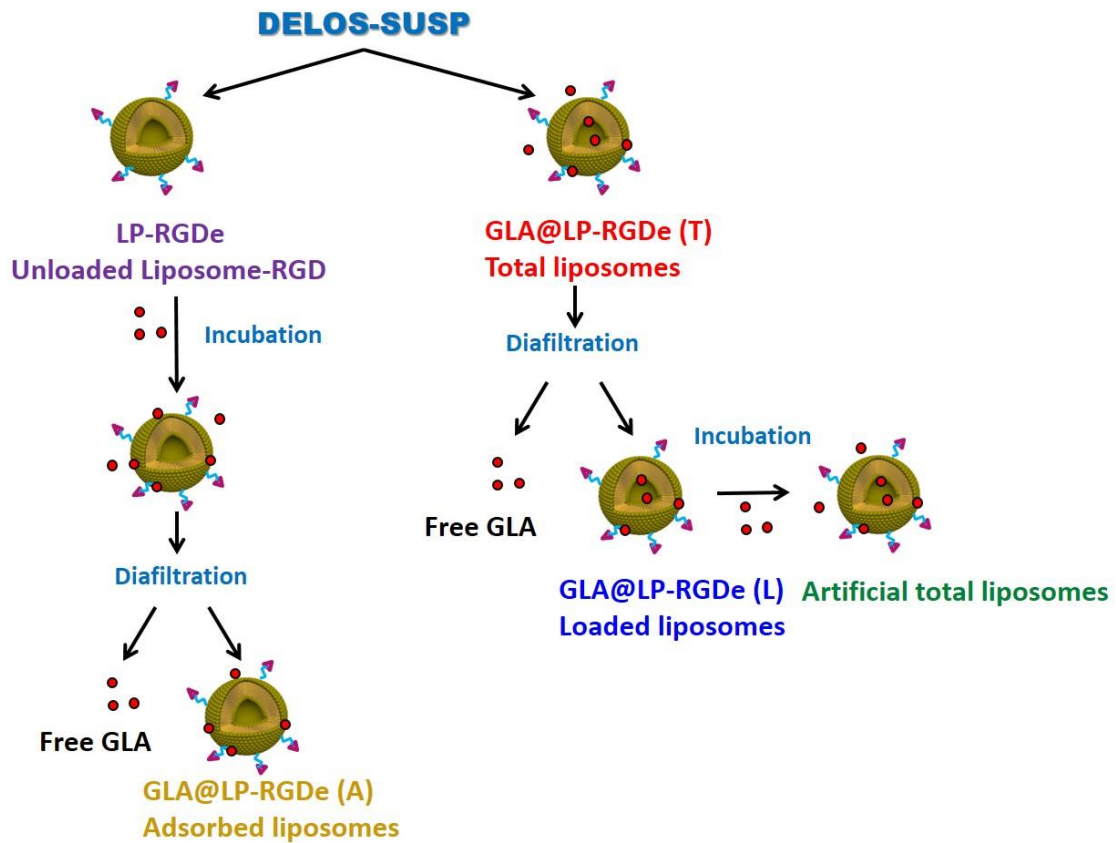


Figure 2.8: Schematic representation of the different GLA nanoliposomes prepared for the *in vitro* efficacy testing.

Unloaded liposomes-RGD_ether were prepared by DELOS-SUSP and then incubated during 24 hours with free GLA at room temperature. Afterwards, they were diafiltrated to eliminate the non-attached GLA to obtain the **adsorbed liposomes** (GLA@LP-RGDe (A)), where all the GLA supposedly is adsorbed in the outer membrane, since the protein is hydrophilic and cannot cross the lipophilic bilayer of the liposomes. GLA loading is less in consequence. In addition, the enzymatic activity did not show the increment observed in the GLA of the total and loaded liposomes.

Artificial total liposomes were formed adding GLA over the loaded liposomes to simulate what happens with the total liposomes obtained directly from DELOS-SUSP. Theoretically, this should behavior in the same way than the total prototype. Indeed, this sample showed a similar content of GLA and similar specific activity of the protein to the usual **total liposomes** obtained from the reactor. The artificial total liposomes were not characterized in terms of size and Z-potential.

Table 2.4: Physicochemical characteristics, entrapment efficiencies (EE), loading of conjugates and specific enzymatic activities of nanoliposomes prototypes (adsorbed and artificial total)

| Liposomal systems (Initial GLA concentration) | Size | | Z potential (mV) | EE (%) | GLA loading ^c (μg mg ⁻¹) | GLA conc. ^d (μg mL ⁻¹) | Specific activity (μmol mg ⁻¹ h ⁻¹) |
|--|------------------------|------------------|------------------|--------|---|---|--|
| | Mean ^a (nm) | Pdl ^b | | | | | |
| Adsorbed liposomes (GLA@LP-RGDe (A)) | 141±2 | 0.38±0.02 | -18.9±0.4 | 8±2 | 2.5±0.5 | 3.5±0.7 | 498±5 |
| Artificial total liposomes | - | - | - | - | - | 17±1 | 1089±54 |

^aIntensity weighted mean hydrodynamic size (diameter) measured by dynamic light scattering.

^bPolydispersity index showing the width of the particle size distribution. ^cMass of the integrated enzyme (determined by Western-blot), divided by the total mass of the membrane components forming the vesicles. ^dMass of enzyme present divided by the volume of the vesicular suspension. Error margins are SD.

As it can be observed in **Figure 2.9**, when the protein is conjugated to the liposomes-RGD_ether (either total, loaded or adsorbed systems) there is a better performance reducing the lysosomal Gb3 deposits. To explain the differences among the formulations we can distinguish three types of GLA based on its location: GLA in water, GLA immobilized on the outside surface of the liposome bilayer and GLA encapsulated inside the liposome and thus, less accessible. The adsorbed system reduced more the Gb3 deposits since it is completely formed by the most active GLA according to the theoretical studies, which is the GLA immobilized with the active site exposed to the aqueous phase. However, as it has been commented before in **Table 2.4**, the specific enzymatic activity was lower in this sample in comparison with the loaded liposomes. At the moment, we cannot explain this discrepancy. Total systems (the one obtained from the reactor and the artificial one prepared to mimic it) presented the three types of GLA (free, immobilized and encapsulated) which explains the curves, slightly lower

in comparison with the adsorbed formulation. The loaded liposomes contain two types of GLA, immobilized and encapsulated, which illustrate why they are superior to the free GLA in water, but inferior to the adsorbed and total systems.

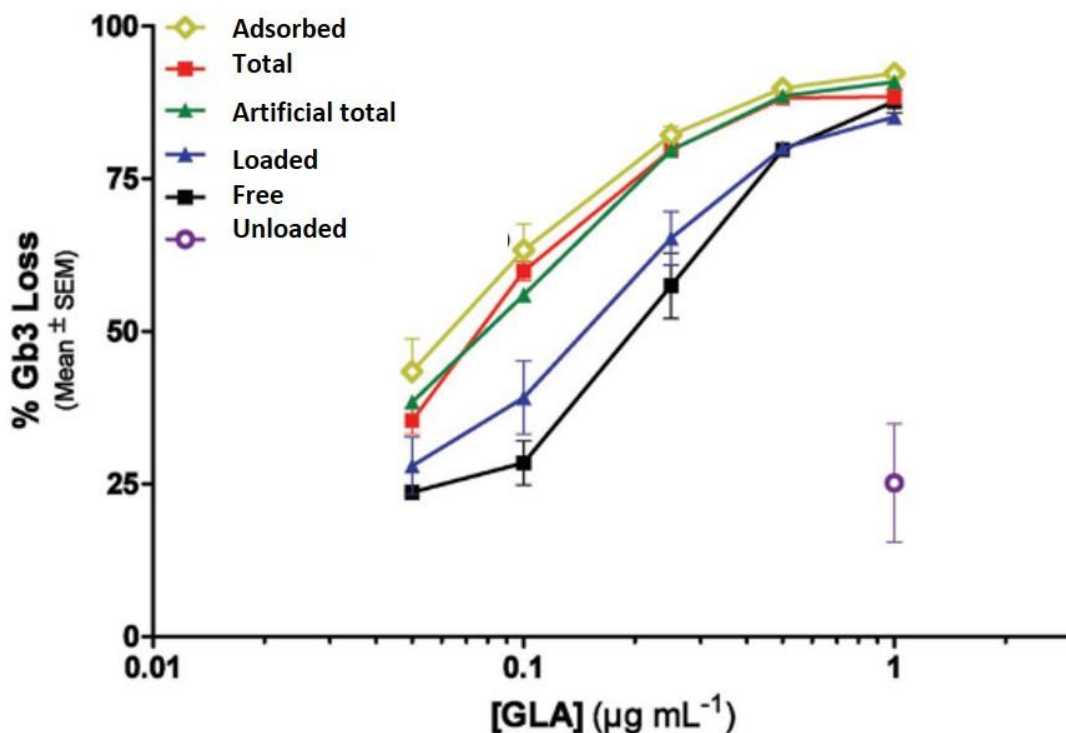


Figure 2.9: Effect of different formulations of GLA in the reduction of Gb3 deposits in aortic endothelial cells of Fabry KO mice. For all the formulations it has been used the same GLA batch with an enzymatic activity of $519 \mu\text{mol h}^{-1} \text{mg}^{-1}$. Represented values correspond to mean \pm SEM value. Figure adapted from *Adv. Healthcare Mat.*, 2016⁸⁵.

2.2.2. Impact of RGD peptide on the internalization of GLA nanoliposomes

Although in a previous work the enhanced cellular internalization of liposomes-RGD_ether was demonstrated⁴⁹, in order to distinguish the effect of GLA from the RGD impact in cellular internalization, different systems were prepared: loaded liposomes-RGD_ether at two different concentrations (8.5 and 20.0 $\mu\text{g mL}^{-1}$), unloaded liposomes-RGD_ether, GLA loaded plain liposomes (without RGD) and unloaded plain liposomes.

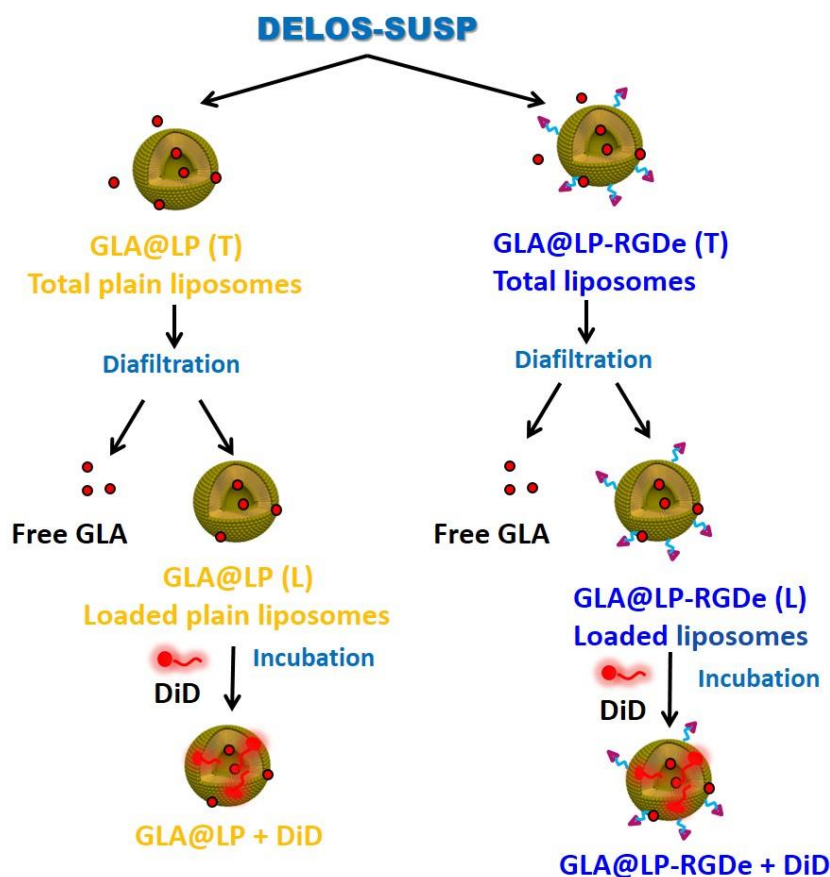


Figure 2.10: Schematic representation of the different GLA nanoliposomes prepared for the *in vitro* internalization studies.

All the systems were prepared by DELOS-SUSP and after the production were incubated with 50 nM of the carbocyanine dye 1,1'-dioctadecyl-3,3,3',3'-tetramethylindodicarbocyanine perchlorate (DiD) following the procedure described in detail in Experimental Section 7.6. DiD is a hydrophobic dye from the family of carbocyanines, widely used for cell membrane and lipids labeling. It interacts with the lipidic membranes through hydrophobic interactions enabling the detection by flow cytometry and laser scanning confocal microscopy (LSCM). The theoretical characteristics of the systems are collected in **Table 2.5**.

Table 2.5: Compositions and ratios used for the preparation of GLA loaded liposome conjugates by DELOS-SUSP using CO₂-expanded ethanolic solutions at 10MPa, 308K and X_{CO2} = 0.85. After production, the systems were incubated with DiD dye.

| Liposomal systems (GLA concentration) [number of batches] | Organic phase | Aqueous phase | Lipidic concentration ^a (µg mL ⁻¹) | Incubation with DiD (nM) |
|---|---|---------------------------|--|-----------------------------|
| GLA@LP-RGDe + DiD (8.5 µg mL ⁻¹) [1] | Cholesterol (17 mM) + DPPC (27 mM) + Chol-PEG ₂₀₀ -RGD (2.8 mM) | GLA in water (89.2 nM) | 1.4 | 50 |
| GLA@LP-RGDe + DiD (20.0 µg mL ⁻¹) [1] | Cholesterol (17 mM) + DPPC (27 mM) + Chol-PEG ₂₀₀ -RGD (2.8 mM) | GLA in water (200 nM) | 1.4 | 50 |
| LP-RGDe + DiD [2] | Cholesterol (17 mM) + DPPC (27 mM) + Chol-PEG ₂₀₀ -RGD (2.8 mM) | Water | 1.4 | 50 |
| LP + DiD [2] | Cholesterol (19 mM) + DPPC (27 mM) | Water | 1.3 | 50 |
| GLA@LP + DiD (20.0 µg mL ⁻¹) [2] | Cholesterol (19 mM) + DPPC (27 mM) | GLA in water (200 nM) | 1.3 | 50 |

Before performing the internalization studies, all the samples of **Table 2.5** were characterized in terms of size, polydispersity index, Z potential and GLA concentration. All the physicochemical characteristics are collected in **Table 2.6**.

Table 2.6: Physicochemical characteristics, entrapment efficiencies (EE), and loading of nanoliposome conjugates. The physicochemical characteristics of the conjugates after the separation of the nonloaded enzyme are given between brackets. The GLA concentration of the total samples was not tested since it is not relevant for the purpose of the study

| Liposomal systems (Initial GLA concentration) | Size | | Z potential (mV) | EE (%) | GLA loading ^c (µg mg ⁻¹) | GLA conc. ^d (µg mL ⁻¹) |
|--|--------------------------|----------------------------|-------------------------|--------|---|---|
| | Mean ^a (nm) | Pdl ^b | | | | |
| GLA@LP-RGDe (8.5 µg mL ⁻¹) | 148.8±0.8 (163.5±0.8) | 0.26±0.01 (0.25±0.02) | 3.2±0.2 (-10.9±0.8) | 53±1 | (3.2±0.2) | (4.5±0.1) |
| GLA@LP-RGDe (20.0 µg mL ⁻¹) | 129±2 (146±3) | 0.33±0.01 (0.44±0.01) | 26.0±0.4 (-1.7±0.2) | 45±10 | (6±1) | (9±2) |
| LP-RGDe | 125±3 | 0.226±0.003 | 13.9±0.6 | - | - | - |
| LP | 126±2 | 0.203±0.008 | 4.1±0.2 | - | - | - |
| GLA@LP (20.0 µg mL ⁻¹) | 133±1 (182±4) | 0.185±0.007 (0.40±0.01) | 7.0±0.1 (-12.7±0.03) | 44±9 | (3.8±0.8) | (5±1) |

^aIntensity weighted mean hydrodynamic size (diameter) measured by dynamic light scattering.

^bPolydispersity index showing the width of the particle size distribution. ^cMass of the integrated enzyme (determined by Western blot), divided by the total mass of the membrane components forming the vesicles. ^dMass of enzyme present divided by the volume of the vesicular suspension. Error margins are SD.

HMEC-1 cells were used for flow cytometry and laser scanning confocal microscopy, since they are endothelial cells known to overexpress $\alpha v \beta 3$ integrins necessary for RGD targeting⁷⁶. For the flow cytometry assays, the cells were incubated during 30 and 180 min at 16 °C and 37 °C with 0.3 mg mL⁻¹ of DiD-labeled liposomes (Experimental Section 7.7.2.2.). In **Figure 2.11**, blue and green bars refer to cells incubated at 16 °C where the liposomes are attached to the cellular membrane but not internalized, since internalization is inhibited at this temperature. Yellow and red bars correspond to cells incubated at 37 °C.

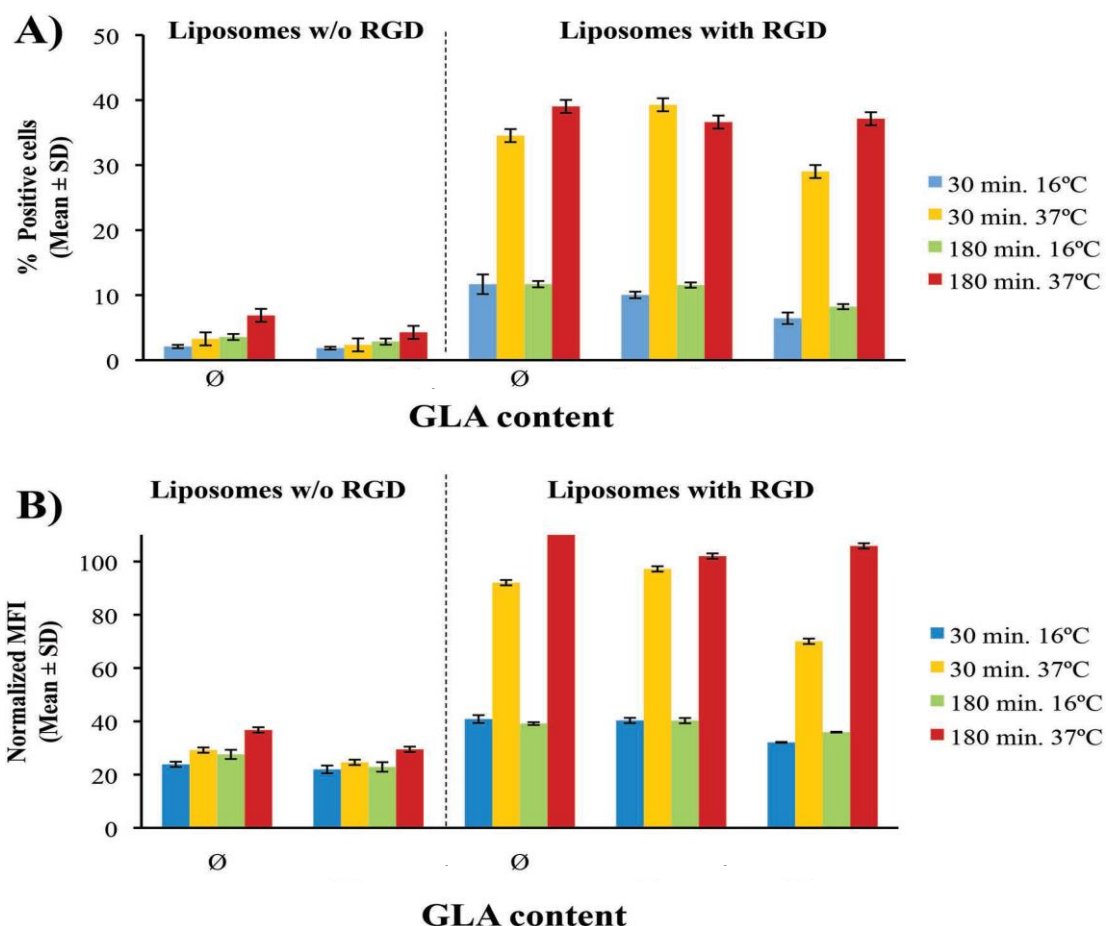


Figure 2.11: Internalization of nanovesicles on endothelial cells assessed by flow cytometry after 30 and 180 min of incubation at 16 °C and 37 °C: A) Flow cytometry quantification of the fraction of cells that internalized plain liposomes and liposome-RGD_ether conjugates as the percentage (%) of DiD-positive cells among the total number of cells. B) Mean fluorescence intensity (MFI) of DiD in the cells normalized to the maximum fluorescence intensity. Figure extracted from *Adv. Healthcare Mat.*, 2016⁸⁵.

After 180 min of incubation, 38±1% of the cells showed internalization of the DiD labeled liposomes-RGD_ether systems, whereas this percentage was 6±2% for cells incubated with DiD labeled plain liposomes (**Figure 2.11A**). Quantifying the mean fluorescence intensity associated to the cells that have internalized the DiD labeled liposomes, gave significantly higher MFI values to the liposomes-RGD_ether (**Figure 2.11B**). This was expected since our group reported previously that liposomes-RGD_ether internalized 30-fold more than plain liposomes⁴⁹.

Regarding the GLA loaded liposomes-RGD_ether, the internalization kinetics was faster for the conjugates less loaded (8.5 μg mL⁻¹). However, at 180 min the uptake of both systems was very similar.

For the laser scanning confocal microscopy, HMEC-1 cells were incubated for 180 min with DiD labeled liposomes at 37 °C, to promote internalization (Experimental Section 7.7.2.1.). Cells were also stained with LysoTracker green. The results were comparable to the ones by flow cytometry: the complete internalization was observed for liposomes-RGD_ether loaded and unloaded, after 180 min of incubation. Moreover, the liposomes were localized within the lysosomes, which is crucial for the adequate release of GLA cargo at the target organelle (**Figure 2.12**).

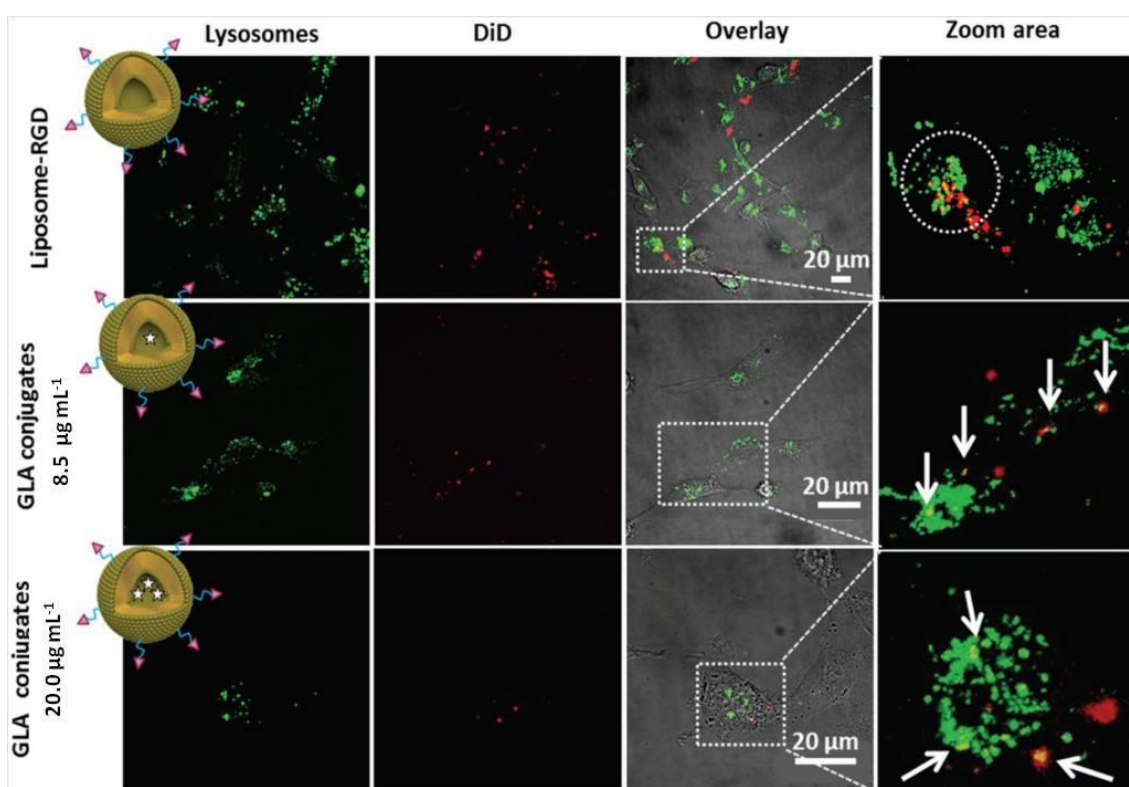


Figure 2.12: Confocal images of the cellular uptake of GLA loaded liposome-RGD_ether conjugates and unloaded liposome-RGD_ether after 3 h incubation at 37 °C. The arrows denote the sites of colocalization between the labeled conjugates and the lysosomes. Figure extracted from *Adv. Healthcare Mat.*, 2016⁸⁵

With the results from flow cytometry and confocal, it can be concluded then that the RGD moiety is essential for a fast and specific internalization, and that the GLA does not alter the RGD function.

2.2.3. Stability in different media

Since the physicochemical parameters change in contact with complex systems like the physiological media or the intracellular environment, the stability of the loaded systems

was also tested in different dispersant media by measuring the change in the mean particle size (diameter) with time. The media selected for this purpose were the buffer PBS and cellular growth medium. Cellular growth medium is water-based and is composed of basal medium, which contains essential amino acids and salts, and 10% of fetal bovine serum. The growth medium selected for this purpose was DMEM (Dulbecco's Modified Eagle Medium).

A small volume of liposomes (400 μL) was diluted with 1600 μL of water, PBS or cellular growth medium. The samples were incubated mimicking the conditions of the cells cultured for the internalization studies: 310 K in a humidified atmosphere with 5% CO_2 for 48 hours. The particle size was measured at different incubation times (0, 4, 19 and 40 h) using the dynamic light scattering equipment.

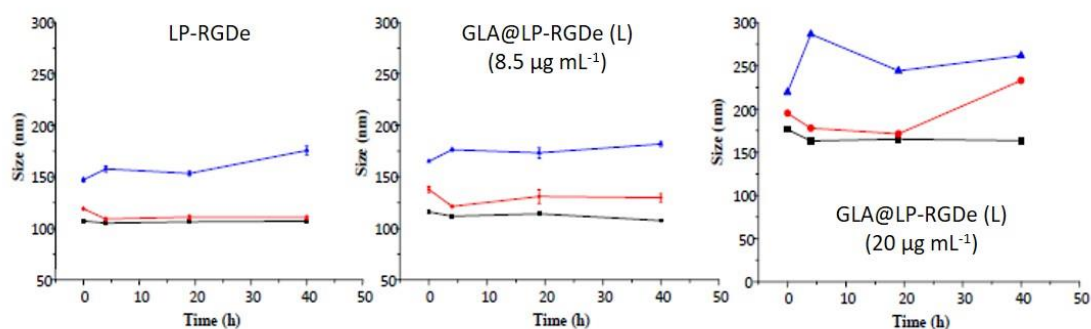


Figure 2.13: Stability of GLA liposome-RGD_ether conjugates with different loading in water (black), PBS (red) and cellular growth medium (blue).

All the systems studied (LP-RGDe, GLA@LP-RGDe (L) at 8.5 and 20.0 $\mu\text{g mL}^{-1}$) were stable in both media (**Figure 2.13**). The GLA conjugates in PBS increased around 15 nm compared with the samples incubated in water and remained stable for 40 hours without signs of vesicle aggregation. However, this increase was larger (70 nm) in the case of GLA conjugates containing 20.0 $\mu\text{g mL}^{-1}$ after 40 hours. This may be due to some degree of instability in PBS related to the ionic strength. Furthermore, in cellular growth medium there was an increment of size that remains quite constant during the time of incubation. This increment is consistent with the protein corona effect: when a nanoparticle is in contact with a biological medium it becomes covered with proteins⁸⁶.

2.3. Substitution of His-GLA for commercial Replagal®

Until this moment, the GLA employed was a His-tagged human α -Galactosidase A produced by Dr. José Luis Corchero from the Instituto de Biotecnología y Biomedicina (IBB-UAB). This GLA enzyme has a 6₆-histidine tag in its structure (100 kDa) that allows the enzyme purification in a single step. The production procedure is described in Experimental Section 7.4. However, the enzymatic activity of this His-GLA was not enough for the translation to in vivo studies. Furthermore, the histidine tag of the His-GLA could be immunogenic and therefore is preferable to avoid its use in clinical applications. We decided, then, to change the enzyme His-GLA incorporated in our liposomes up to now by commercially available Replagal®. There are differences between the His-GLA previously employed and the Replagal®. For instance, the histidine tail, absent in Replagal®, and the dissolution media of each enzyme. While His-GLA is in acetic buffer, Replagal® is in a mixture of sodium phosphate monobasic, monohydrate, polysorbate 20, sodium chloride, sodium hydroxide and water.

Systems were prepared like GLA@LP-RGDe, maintaining the same proportion between lipids and the enzyme. Instead of using GLA in water, the CO₂ ethanolic lipid solution is depressurized over Replagal in water at a concentration of 20.0 $\mu\text{g mL}^{-1}$. The non-incorporated Replagal was separated using diafiltration process.

Table 2.7: Physicochemical characteristics, entrapment efficiencies (EE), loading of nanoliposome conjugates and enzymatic activities. The physicochemical characteristics of the conjugates after the separation of the nonloaded enzyme are given between brackets.

| Liposomal systems (Initial GLA concentration) | Size | | Z potential (mV) | EE (%) | GLA loading ^c (µg mg ⁻¹) | GLA conc. ^d (µg mL ⁻¹) | Enzymatic activity (µmol mg ⁻¹ h ⁻¹) |
|--|------------------------|----------------------------|------------------|--------|---|---|---|
| | Mean ^a (nm) | Pdl ^b | | | | | |
| GLA@LP-RGDe (20.0 µg mL ⁻¹) | 216±8 (195±1) | 0.40±0.01 (0.40±0.01) | 14±1 (-24±2) | 37±9 | (6±1) | 20±2 (7±2) | 846±270 (1253±65) |
| Replagal@LP-RGDe (20.0 µg mL ⁻¹) | 185±3 (164±1) | 0.22±0.01 (0.191±0.005) | -14±1 (-37±1) | 40±9 | (5.7±0.7) | 20±4 (8±1) | 510±54 (362±42) |

^aIntensity weighted mean hydrodynamic size (diameter) measured by dynamic light scattering.

^bPolydispersity index showing the width of the particle size distribution. ^cMass of the integrated enzyme (determined by Western-blot), divided by the total mass of the membrane components forming the vesicles. ^dMass of enzyme present divided by the volume of the vesicular suspension. Error margins are SD.

The physicochemical properties of the Replagal® nanoconjugates are smaller and have lower polydispersity indexes. Interestingly, the Z-potential of Replagal loaded liposomes is higher than the GLA loaded systems, maybe pointing to a more stable formulation. The incorporation of GLA tested by Western blot is very similar in both systems. Although the enzymatic activity is lower in the case of Replagal, in vitro efficacy is similar in both Replagal and GLA loaded liposomes-RGD_ether conjugates as is shown in **Figure 2.15**. We concluded, that the enzyme seems to interact in a similar way with the membrane components⁸⁰. These results opened the door for the ongoing in vivo experiments.

2.4. Increase of nanoformulation enzyme concentration to perform in vivo testing

The enzyme concentration of the formulation developed up to now was very low compared to the one used in current Fabry patients' treatment, resulting in an insufficient drug concentration to observe in vivo a minimal therapeutic effect, i.e. reduction of Gb3 deposits, at the maximum feasible administration dose. Therefore, in order to reach the GLA concentration ($\geq 200 \mu\text{g mL}^{-1}$) required to achieve in vivo therapeutic doses, and taking into account the limited GLA loading capacity of the liposomes as explained in section 2.2.1 (**Table 2.2**) in the framework of this thesis we made great efforts to develop a methodology to concentrate the nanovesicles in order to increase the Replagal concentration in the liposomes-RGD_ether formulation. For this purpose, we used the samples obtained from DELOS-SUSP process with an enzyme concentration of around $20 \mu\text{g mL}^{-1}$, and proceeded to diafiltrated and concentrate them using the protocol described in Experimental Section 7.4.1. Basically, dispersant medium was extracted through the diafiltration column while the liposomes remained in the circuit. One batch of 24 mL was enough to concentrate x2 and x3. The systems maintained the physicochemical features and the enzymatic activity, as is shown in **Table 2.8**.

Table 2.8: Physicochemical characteristics, entrapment efficiencies (EE), loading, and specific enzymatic activity of nanoliposome conjugates prepared for their concentration x2 and x3.

| Liposomal systems | Size | | Z potential (mV) | EE (%) | GLA loading ^c ($\mu\text{g mg}^{-1}$) | GLA conc. ^d ($\mu\text{g mL}^{-1}$) | Enzymatic activity ($\mu\text{mol mg}^{-1} \text{h}^{-1}$) |
|-----------------------|------------------------|------------------|------------------|--------|--|--|--|
| | Mean ^a (nm) | Pdl ^b | | | | | |
| Replagal (commercial) | - | - | - | - | - | - | 1087±71 |
| Replagal in water | - | - | - | - | - | 12±1 | 506±52 |
| Replagal@LP-RGDe (T) | 185±3 | 0.22±0.01 | -14±1 | - | - | 20±4 | 510±54 |
| Replagal@LP-RGDe (L) | 164±1 | 0.191±0.005 | -37±1 | 40±9 | 5.7±0.7 | 8±1 | 362±42 |
| Replagal@LP-RGDe (x2) | 164±2 | 0.21±0.01 | -35±1 | - | 12±1 | 17±2 | 448±57 |
| Replagal@LP-RGDe (x3) | 160±1 | 0.33±0.01 | -32±1 | - | 18±2 | 26±3 | 578±26 |

^aIntensity weighted mean hydrodynamic size (diameter) measured by dynamic light scattering.

^bPolidispersity index showing the width of the particle size distribution. ^cMass of the integrated enzyme (determined by Western-blot), divided by the total mass of the membrane components forming the vesicles. ^dMass of enzyme present divided by the volume of the vesicular suspension. Error margins are SD, except for enzymatic activity that are SEM.

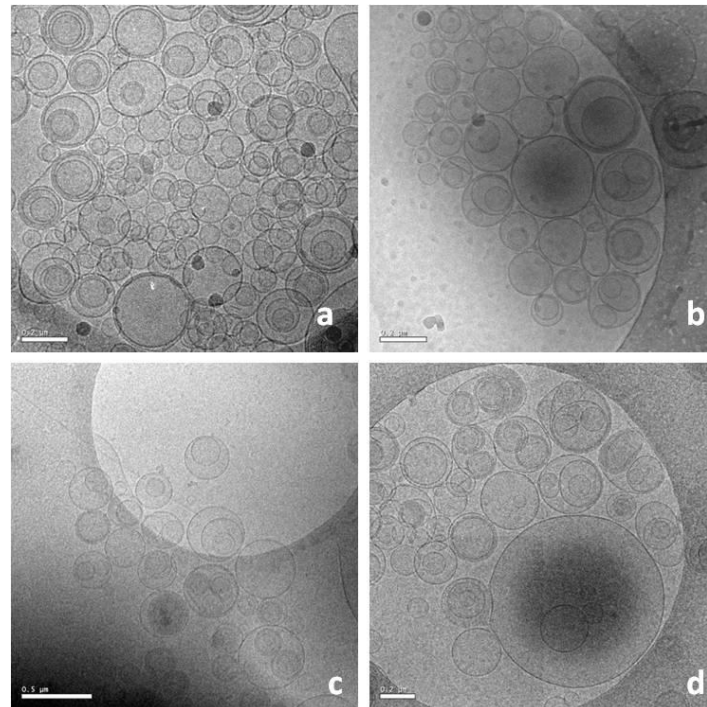


Figure 2.14: Cryo-TEM pictures showing the morphology of the nanoconjugates with Replagal: a) Replagal@LP-RGDe (T), b) Replagal@LP-RGDe (L), c) Replagal@LP-RGDe (x2), d) Replagal@LP-RGDe (x3). Scale bars are 500 nm.

Before the in-vivo study, the systems were also tested in vitro using MAEC cells to assess the capability of reducing the Gb3 (**Figure 2.15**).

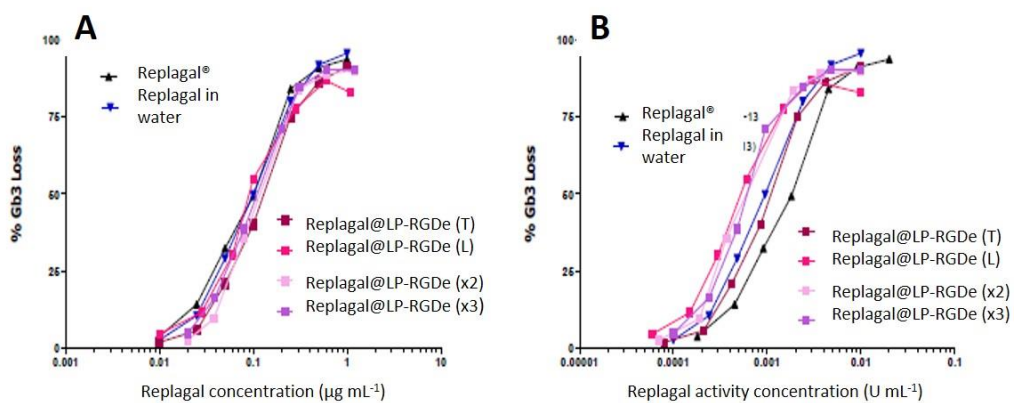


Figure 2.15: Efficacy of different formulations of Replagal in the reduction of Gb3 deposits in aortic endothelial cells (MAEC) of Fabry KO mice. In A, data is represented in protein concentration ($\mu\text{g mL}^{-1}$) and in B the data is represented in activity concentration (U mL^{-1}). U ($\mu\text{mol min}^{-1}$) refers to the amount of Replagal that catalyzes one micromole of Gb3 per minute under the conditions of the assay method (see Experimental Section 7.8.1).

When the data is represented based on protein concentration (**Figure 2.15A**), the nanoconjugates present similar efficacy in cell culture, and there is no difference between free Replagal® and the liposome conjugates. However, when represented based on enzymatic activity concentration (**Figure 2.15B**), the liposomes have an increased efficacy compared with free Replagal®. Another remark is that the concentrated systems x2 and x3 do not present differences in efficacy, thus enabling us to increase the concentration up to x15.

To prepare a sample concentrated x15 it was necessary to use at least three batches of 24 mL of liposomal formulation prepared by DELOS-SUSP. According to the cryoTEM (**Figure 2.17**) and DLS results (**Table 2.9**), concentrating the sample x15 in water was possible without jeopardizing the physicochemical features.

Table 2.9: Physicochemical characteristics, entrapment efficiencies (EE), loading, and specific enzymatic activity of nanoliposome conjugates prepared for their concentration x3 and x15.

| Liposomal systems | Size | | Z potential (mV) | EE (%) | GLA loading ^c (µg mg ⁻¹) | GLA conc. ^d (µg mL ⁻¹) | Enzymatic activity (µmol mg ⁻¹ h ⁻¹) |
|---|------------------------|------------------|------------------|--------|---|---|---|
| | Mean ^a (nm) | Pdl ^b | | | | | |
| Replagal in water | - | - | - | - | - | 17.1±0.1 | 1366±4 |
| Replagal@LP-RGDe (T): pool of 3 batches | 172.2±0.3 | 0.313±0.008 | 7.59±0.07 | - | - | 16.0±0.4 | 1742±40 |
| Replagal@LP-RGDe (L) | 176±2 | 0.38±0.01 | -5.8±0.1 | 41±3 | 4.6±0.3 | 6.5±0.4 | 1514±73 |
| Replagal@LP-RGDe (x3) | 166±1 | 0.28±0.01 | -25.5±0.6 | - | 5.66±0.07 | 23.8±0.3 | 1473±17 |
| Replagal@LP-RGDe (x15) | 174±3 | 0.29±0.02 | -27.1±0.4 | - | 4.6±0.7 | 96±14 | 1461±110 |

^aIntensity weighted mean hydrodynamic size (diameter) measured by dynamic light scattering.

^bPolydispersity index showing the width of the particle size distribution. ^cMass of the integrated enzyme (determined by Western blot), divided by the total mass of the membrane components forming the vesicles. ^dMass of enzyme present divided by the volume of the vesicular suspension. Error margins are SD, except for enzymatic activity that are SEM.

Given that the concentration x15 was possible, another experiment was designed in order to explore if increasing the concentration x20 and x30 was also feasible. For this experiment, several batches of Replagal® loaded liposomes-RGD_ether were prepared in order to obtain x3, x15, x20 and x30 systems. The systems are schematized in **Figure 2.16**.

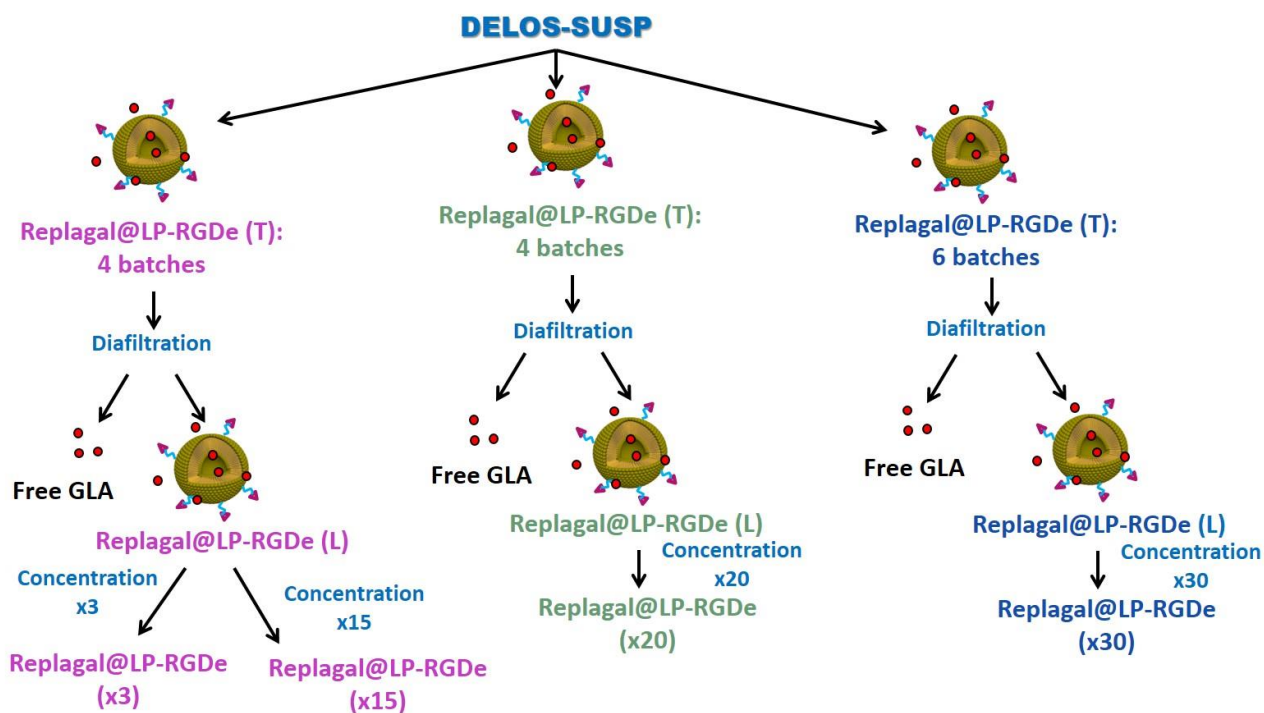


Figure 2.16: Schematic representation of the different GLA nanoliposomes prepared concentrating the samples by the diafiltration equipment.

As it is shown in **Table 2.10** and **Figure 2.17**, the concentration x20 and x30 using diafiltration was possible. The final physicochemical features depend more on the initial properties than on the procedure of concentration itself. Results displayed that the concentration of Replagal augmented following the process, while specific enzymatic activity was affected upon concentration. However, when the systems were tested in MAEC cells for the Gb3 reduction test, this enzymatic activity difference did not affect the outcome of the experiment and all the different samples presented a similar efficacy to commercial Replagal in terms of Gb3 reduction (**Figure 2.18**).

Table 2.10: Physicochemical characteristics, entrapment efficiencies (EE), loading, and specific enzymatic activity of nanoliposome conjugates.

| Liposomal systems | Size | | Z potential (mV) | EE (%) | GLA loading ^c ($\mu\text{g mg}^{-1}$) | GLA conc. ^d ($\mu\text{g mL}^{-1}$) | Enzymatic activity ($\mu\text{mol mg}^{-1} \text{h}^{-1}$) |
|---|------------------------|------------------|------------------|-----------|--|--|--|
| | Mean ^a (nm) | Pdl ^b | | | | | |
| Replagal in water | - | - | - | - | - | 23±3 | 1235±88 |
| Replagal@LP-RGDe (T): pool of 4 batches | 172±8 | 0.58±0.04 | -7.8±0.1 | - | 11.6±0.6 | 16.2±0.8 | 1498±134 |
| Replagal@LP-RGDe (L) | 209±16 | 0.49±0.06 | -10.2±0.3 | 30±2 | 3.4±0.2 | 4.8±0.3 | 1366±145 |
| Replagal@LP-RGDe (x3) | 171±4 | 0.49±0.01 | -23.8±0.3 | - | 4.3±0.2 | 18±1 | 909±70 |
| Replagal@LP-RGDe (x15) | 191±8 | 0.53±0.04 | -27.1±0.4 | - | 3.8±0.3 | 79±6 | 921±61 |
| Replagal@LP-RGDe (T): pool of 4 batches | 184±4 | 0.50±0.07 | -9.3±0.2 | - | 16±3 | 22±4 | 947±19 |
| Replagal@LP-RGDe (L) | 174±2 | 0.445±0.006 | -10.7±0.6 | 21±4 | 3.4±0.1 | 4.7±0.2 | 1460±56 |
| Replagal@LP-RGDe (x20) | 197±9 | 0.55±0.05 | -18.1±0.1 | - | 3.9±0.3 | 108±9 | 715±83 |
| Replagal@LP-RGDe (T): pool of 6 batches | 160±6 | 0.45±0.05 | -7.3±0.7 | - | 8±2 | 11±3 | 1843±86 |
| Replagal@LP-RGDe (L) | 157±4 | 0.30±0.06 | -12±1 | 53±1 5 | 4.1±0.4 | 5.8±0.6 | 1182±77 |
| Replagal@LP-RGDe (x30) | 164±3 | 0.32±0.01 | -17±1 | - | 3.9±0.8 | 163±37 | 1058±48 |

^aIntensity weighted mean hydrodynamic size (diameter) measured by dynamic light scattering.
^bPolydispersity index showing the width of the particle size distribution. ^cMass of the integrated enzyme
(determined by Western blot), divided by the total mass of the membrane components forming the
vesicles. ^dMass of enzyme present divided by the volume of the vesicular suspension. Error margins are SD,
except for enzymatic activity that are SEM.

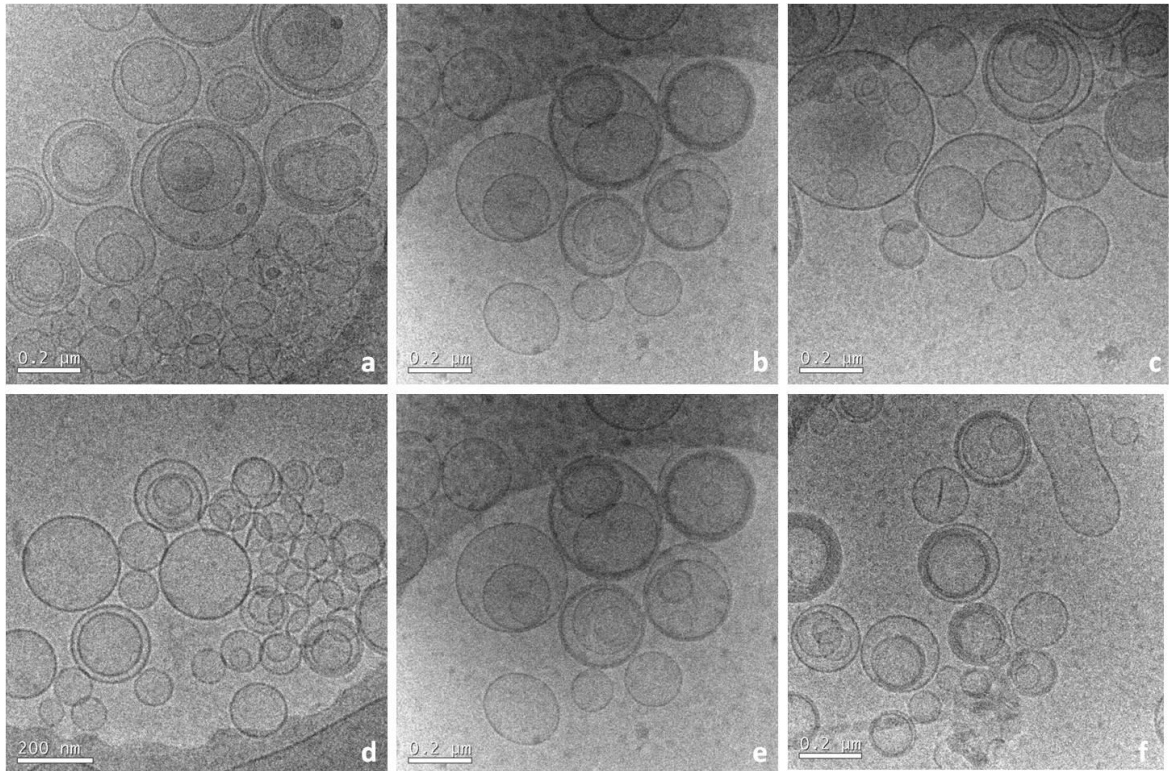


Figure 2.17: Cryo-TEM pictures showing the morphology of the nanoconjugates with Replagal: a) Replagal@LP-RGDe (T), b) Replagal@LP-RGDe (L), c) Replagal@LP-RGDe (x3), d) Replagal@LP-RGDe (x15), e) Replagal@LP-RGDe (x20), f) Replagal@LP-RGDe (x30). Scale bars are 200 nm.

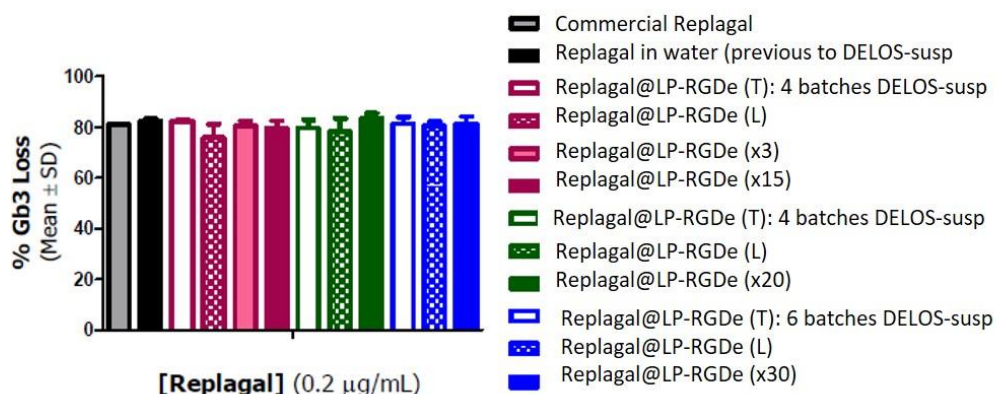


Figure 2.18: In vitro efficacy assays of different Replagal loaded liposomal formulations

2.5. Changing the dispersant medium to isotonic one, and changing the counterion of cholesterol_PEG200_RGDether

In the cholesterol_PEG200_RGD molecular unit, the arginine has trifluoroacetic acid (TFA) as counterion. Considering that this TFA can interfere with the in vivo studies enhancing cellular growth⁸⁷ or even inhibiting cellular proliferation⁸⁸ in certain cellular types, the interchange with chloride counterion was assayed. However, when liposomes were prepared with the new cholesterol_PEG200_RGD, they sedimented. Therefore, the use of chloride was discarded. In addition, we have found that the TFA is approved by the Food and Drug Administration (FDA) as an inactive ingredient in drug products for intravenous administration without toxicity issues.

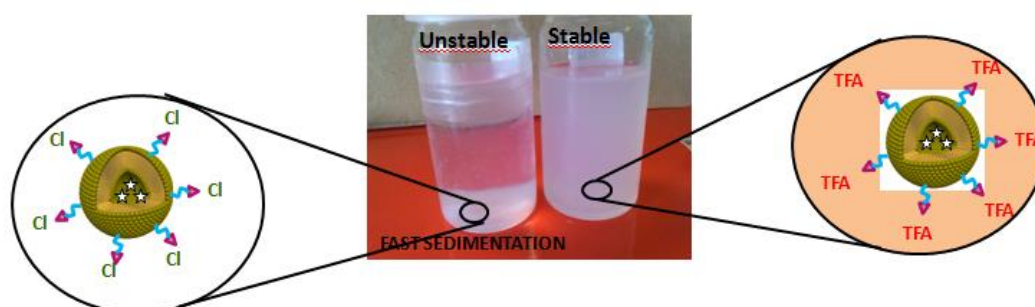


Figure 2.19: The new liposomal formulations with chloride as counterion sedimented while the usual ones with TFA remained stable.

Other challenge was to modify the dispersant medium of the liposome nanoconjugates to an isotonic one. In the present thesis, we have tested the substitution of water by PBS and NaCl 0.9%, more appropriate for intravenous administration. First, we tried to prepare the systems directly in commercial PBS instead of depressurizing over water. Since the resultant liposomes sedimented within hours, we changed the protocol: the systems were produced by DELOS-SUSP as usually and, when diafiltrated, the medium was changed from water with 5% ethanol to PBS, and then concentrated three fold (x3). Liposomes were also prepared directly in NaCl 0.9% by DELOS-SUSP. The physicochemical properties of the different nanoliposomal systems in PBS and NaCl 0.9% are collected in **Table 2.11**.

After changing the medium to PBS, the nanoconjugates became bigger and with higher polydispersity index, but more importantly, during diafiltration the GLA loading is lost. We had to reject PBS as an alternative dispersant medium for our systems.

In the case of systems prepared in NaCl 0.9%, not only the samples were polydisperse but also the protein loading and enzymatic activity were substantially reduced. Hence, NaCl 0.9% was discarded as an alternative isotonic medium for our samples.

Table 2.11: Physicochemical characteristics, entrapment efficiencies (EE), loading, and specific enzymatic activity of Replagal nanoliposome conjugates in PBS and NaCl 0.9%.

| Liposomal systems | Size | | Z potential (mV) | EE (%) | GLA loading ^c ($\mu\text{g mg}^{-1}$) | GLA conc. ^d ($\mu\text{g mL}^{-1}$) | Enzymatic activity ($\mu\text{mol mg}^{-1} \text{h}^{-1}$) |
|--|------------------------|------------------|------------------|------------|--|--|--|
| | Mean ^a (nm) | PdI ^b | | | | | |
| Replagal in water | - | - | - | - | - | 17.5 \pm 0.2 | 406 \pm 25 |
| Replagal@LP -RGDe (T) | 248 \pm 11 | 0.48 \pm 0.08 | 6.09 \pm 0.05 | - | - | 17 \pm 1 | 451 \pm 57 |
| Replagal@LP -RGDe (L) in PBS | 214 \pm 5 | 0.45 \pm 0.05 | -6.1 \pm 0.5 | 0 | 0 | 0 | 32 \pm 1 |
| Replagal@LP -RGDe (L) in water (control) | 205 \pm 5 | 0.38 \pm 0.02 | -27.0 \pm 0.5 | 40 \pm 9 | 1.50 \pm 0.01 | 2.10 \pm 0.01 | - |
| Replagal@LP -RGDe (x3) in PBS | 215 \pm 4 | 0.50 \pm 0.02 | -4.7 \pm 0.8 | 0 | 0 | 0 | 21 \pm 0.7 |
| Replagal in water | - | - | - | - | - | 16.2 \pm 0.7 | 338 \pm 42 |
| Replagal@LP -RGDe (T): pool of 3 batches | 207 \pm 2 | 0.41 \pm 0.04 | - | - | - | 14.9 \pm 0.5 | 467 \pm 20 |
| Replagal@LP -RGDe (x15) in PBS | 199 \pm 2 | 0.42 \pm 0.05 | -5 \pm 1 | 0 | 0 | 0 | 49 \pm 2 |
| Replagal in NaCl 0.9% | - | - | - | - | - | 17.85 \pm 0.06 | 795 \pm 51 |
| Replagal@LP -RGDe (T) in | 277 \pm 6 | 0.64 \pm 0.02 | -2.2 \pm 0.1 | - | - | 15.7 \pm 0.2 | 1535 \pm 54 |

| | | | | | | | |
|-------------------------|--------|-----------|----|----------|-----------|-----------|-------|
| NaCl 0.9% | | | | | | | |
| Replagal@LP | | | | | | | |
| -RGDe (L) in NaCl 0.9% | 276±18 | 0.69±0.1 | QR | 11.1±0.3 | 1.25±0.03 | 1.75±0.04 | 111±7 |
| Replagal@LP | | | | | | | |
| -RGDe (x3) in NaCl 0.9% | 231±18 | 0.53±0.06 | QR | 32.5±0.6 | 1.22±0.01 | 5.11±0.06 | 144±5 |

^aIntensity weighted mean hydrodynamic size (diameter) measured by dynamic light scattering.

^bPolydispersity index showing the width of the particle size distribution. ^cMass of the integrated enzyme (determined by Western blot), divided by the total mass of the membrane components forming the vesicles. ^dMass of enzyme present divided by the volume of the vesicular suspension. QR: not meeting quality requirements of the DLS equipment. Error margins are SD, except for enzymatic activity that are SEM.

We decided to continue using water as dispersant medium since the benefits of using an isotonic nanoformulation in front of the risks associated with the impairment of the physicochemical properties due to the presence of salts did not compensate. Besides, for the in vivo studies, the injection volume of the nanoformulation is too small (generally between 100-200 µL, depending on the weight of the mice) to expect any reaction due to the not adjusted tonicity. Therefore, next experiments were performed with water.

2.6. Testing different enzymes in order to increase the enzymatic activity

Although the systems with Replagal are very similar to those produced with the His-tagged GLA as was previously shown in this Chapter (Section 2.3), we observed that the increase in specific enzymatic activity is more pronounced in the His-GLA (i.e. **Table 2.7**). We attributed this difference to the excipients present in commercial Replagal® formulation, the sodium phosphate monobasic, monohydrate, polysorbate 20, sodium chloride, sodium hydroxide and water. In order to test this hypothesis, we decided to dialyze the Replagal in presence of acetic buffer (Experimental Section 7.6.) and to

perform the enzymatic activity. As it is shown in **Table 2.12**, the enzymatic activity experiments a significant increment when the Replagal is dialyzed.

Table 2.12: Enzymatic activity of dialyzed Replagal in comparison with commercial Replagal

| Type of Replagal | GLA conc. ($\mu\text{g mL}^{-1}$) | Enzymatic activity ($\mu\text{mol h}^{-1}\text{mg}^{-1}$) |
|----------------------|-------------------------------------|---|
| Commercial Replagal® | 1023±13 | 1309±121 |
| Dialyzed Replagal | 904±13 | 2494±117 |

We decided then to prepare the loaded liposomes-RGD_ether with dialyzed Replagal (dReplagal) and compared them with commercial Replagal and His-GLA loaded systems. For this, systems were prepared maintaining the same proportion between lipids, the same total concentration of lipids and the same ratio lipid-enzyme. The CO₂ ethanolic lipid solution is depressurized over either His-GLA, Replagal or dialyzed Replagal in water at a concentration of 20.0 $\mu\text{g mL}^{-1}$. The non-incorporated Replagal was separated using diafiltration process.

Physicochemical features of the systems are displayed in **Table 2.13** and **Figure 2.20**. The size and Z-potential of the dialyzed Replagal loaded liposomes-RGD_ether is very similar to the commercial loaded ones, with an improved polydispersity index. In this case, the His-GLA loaded system did not present as good properties as in other experiments. The cryo-TEM images (**Figure 2.19**) showed very similar morphologies for the three systems.

Table 2.13: Physicochemical characteristics of nanoliposome conjugates with the three different enzymes: His-GLA, commercial Replagal and dialyzed Replagal.

| Liposomal systems | Size | | Z potential (mV) |
|-----------------------|------------------------|------------------|------------------|
| | Mean ^a (nm) | Pdl ^b | |
| Replagal@LP-RGDe (L) | 136±1 | 0.32±0.01 | -18.3±0.1 |
| dReplagal@LP-RGDe (L) | 137±2 | 0.24±0.1 | -17.40±0.05 |
| GLA@LP-RGDe (L) | 173±6 | 0.58±0.02 | -5.8±0.2 |

^aIntensity weighted mean hydrodynamic size (diameter) measured by dynamic light scattering.

^bPolydispersity index showing the width of the particle size distribution. Error margins are SD.

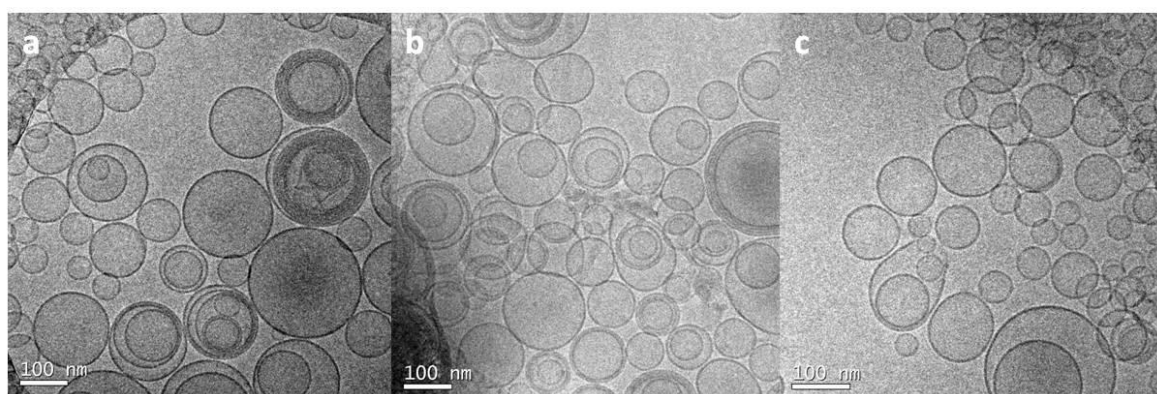


Figure 2.20: Cryo-TEM pictures showing the morphology of the nanoconjugates with the three types of protein: a) Replagal@LP-RGDe (L), b) dReplagal@LP-RGDe, c) GLA@LP-RGDe. Scale bars are 100 nm.

We did a comparative analysis of all the total and loaded batches produced at the moment with the three different enzymes, in order to select which type of enzyme is more convenient for the next experiments. Each total and loaded batch was compared with the free enzyme. As it can be seen in **Table 2.14**, the enzymatic activity of GLA@LP-RGDe was measured in eight total and nine loaded batches. Seven of eight total batches showed a mean increment of enzymatic activity, whereas the other did not increase with respect to free His-GLA. For Replagal@LP-RGDe were tested seven total and six loaded batches. Half the total batches experienced a little increase in the enzymatic activity compared with free commercial Replagal. In the case of dReplagal@LP-RGDe, only three total and three loaded batches were tested. Remarkably, the three total showed an important increment in the enzymatic activity. For the loaded only one batch

experienced an increment, compared with free dialyzed Replagal. Although there are few experiments with dialyzed Replagal, it seems to provide an improvement in the enzymatic activity when it is used. Given all the data, we decided to continue the experiments with dReplagal@LP-RGDe.

Table 2.14: Comparison of enzymatic activity (EA) increase in loaded liposomes-RGD_ether with respect to the free enzyme. As explained before the only difference between the three systems is the protein (His-GLA, Replagal or dialyzed Replagal). In general, all experiments performed rendered systems with mean size less than 200 nm and polydispersity indexes lower than 0.3 (see **Table 2.2** for His-GLA, **Tables 2.8, 2.9** and **2.10** for Replagal, and **Table 2.13** for dialyzed Replagal).

| Type of GLA | Type of liposome system | INCREASE | | DO NOT INCREASE | | | TOTAL |
|--------------------------|-------------------------|-------------------|-------------------|---------------------------|-------------------|---------------------------|---------|
| | | Number of Batches | Number of batches | Relative mean EA increase | Number of batches | Relative mean EA increase | |
| His-GLA | Total | 8 | 7/8 | 2.6 | 1/8 | 1.0 | 2.4±0.5 |
| | Loaded | 9 | 5/9 | 3.29 | 4/9 | 0.81 | 2±1 |
| Replagal | Total | 7 | 4/7 | 1.24 | 3/7 | 0.82 | 1.1±0.2 |
| | Loaded | 6 | 1/6 | 1.56 | 5/6 | 0.81 | 0.8±0.3 |
| Dialyzed Replagal | Total | 3 | 3/3 | 3.47 | | | 3.5 |
| | Loaded | 3 | 1/3 | 1.78 | 2/3 | 0.83 | 1.1±0.5 |

With these promising results, we performed the production of a dReplagal@LP-RGDe (x35), in order to have the appropriate enzyme concentration for in vivo experiments. DLS measurements and Cryo-TEM images, depicted in **Figure 2.21**, indicate that this liposomal formulation has a large heterogeneity and do not meet quality criteria.

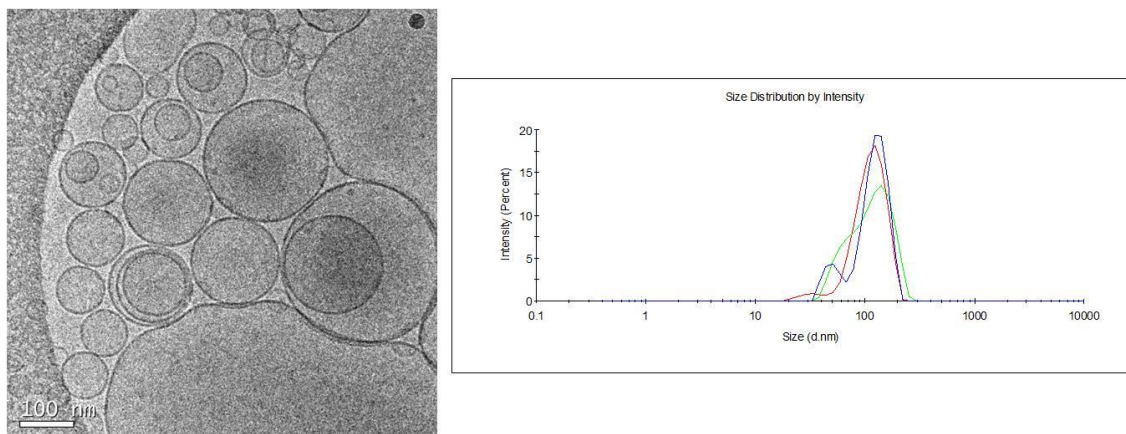


Figure 2.21: Cryo-TEM picture showing the morphology of the nanoconjugate concentrated x35, and the size distribution of this sample measured by DLS

The protein concentration and specific enzymatic activities are shown in **Table 2.15**. As it can be seen, the great activity of the dialyzed Replagal (see **Table 2.12**) is lost when the dialyzed enzyme is conjugated with liposomes-RGD_ether to reach a system with an enzyme concentration around $300 \mu\text{g mL}^{-1}$, which also has a theoretical concentration of liposome membrane components of 50 mg mL^{-1} . Since this loss of enzymatic activity was not observed with commercial Replagal, when it is conjugated to the same type of liposomes, using the same enzyme concentration and the same molar ratios “enzyme/liposome membrane components”, we decided to move back to the production of nanoliposomes with Replagal not dialyzed for upcoming experiments.

Table 2.15: Protein concentration and specific enzymatic activity of the dReplagal@LP-RGDe with an EE around 40%

| Liposomal systems | GLA conc. ^a ($\mu\text{g mL}^{-1}$) | Enzymatic activity ($\mu\text{mol mg}^{-1} \text{ h}^{-1}$) |
|---|---|--|
| dReplagal in water | 22±3 | 685±38 |
| dReplagal@LP-RGDe (T): mix of 10 batches | 25±5 | 881±42 |
| dReplagal@LP-RGDe (x35) | 349±62 | 689±35 |

^aMass of present enzyme divided by the volume of the vesicular suspension. Error margins are SD in the case of Replagal concentration and SEM for the enzymatic activity.

2.7. In vivo testing: pharmacokinetics, toxicity and efficacy

In vivo experiments were performed by Dr. Ibane Abasolo team with Natalia García at CIBBIM (Hospital Universitari Vall d'Hebron) and are included in this thesis because of the relevance of the obtained results.

Pharmacokinetics (PK) is the study of the time course of absorption, metabolism, and excretion of a drug compound administered to the body⁸⁹, in terms of the relationship between a dose and the plasma concentration over time. Instead, pharmacodynamics refers to the body's biological response to drugs and provides an idea of the efficacy.

A preliminary pharmacokinetic study was carried out measuring the GLA activity in plasma at three time points: 1, 5 and 60 min (**Figure 2.22**). For this, a mouse model of Fabry disease, specifically the GLA KO mice (GlatmKul), was employed, using three animals per time point. The free Replagal and the Replagal@LP-RGD (x3) (physicochemical details presented in **Table 2.8** and **Figure 2.14**) were administered as a single dose intravenously (Experimental Section 7.9.1.). Free Replagal experienced a higher clearance rate than the encapsulated in the functionalized nanoliposomes. Accordingly, the plasma half-life of the nanoconjugates suffered an important increase, almost 4 times higher: 14.7 min for the Replagal loaded systems while 4.7 min was determined for free Replagal. This is a promising result achieved on the non-regulatory pre-clinical phase, since nanoliposomes seems to prolong the enzyme circulation time in the blood, which could be translated in a higher enzyme biodistribution allowing an increase in the efficacy.

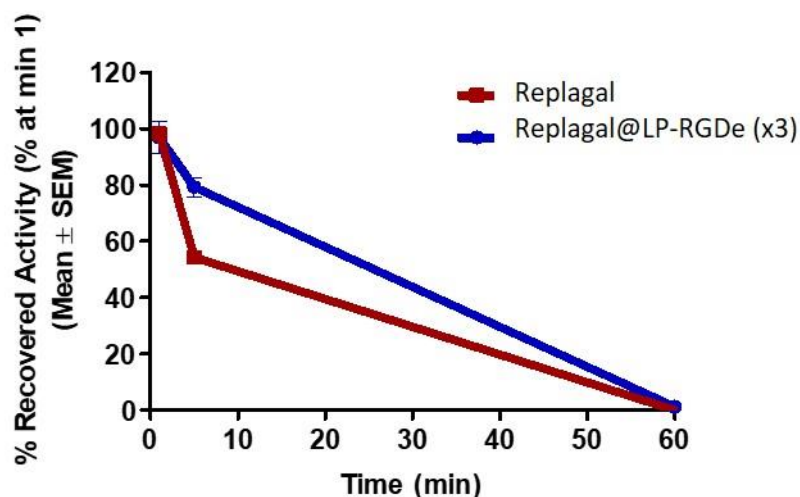


Figure 2.22: Pharmacokinetics analysis of Replagal@LP-RGDe (x3) with a Replagal concentration of $26 \pm 3 \mu\text{g mL}^{-1}$, measuring the enzymatic activity.

Furthermore, the **Figure 2.23** shows a very preliminary study of tissue biodistribution in which the percentage of enzymatic activity of Replagal loaded nanoliposomes was compared to free Replagal 30 minutes after injection. These preliminary results evidence that Replagal bioavailability is improved when delivered in liposomes-RGD_ether since its activity is higher in plasma when it is nanoformulated (in accordance with the pharmacokinetics of **Figure 2.22**), and its uptake by the liver, which is not a target organ in Fabry disease, is lower. Therefore, higher levels of circulating enzyme will be available to the target organs, when Replagal is conjugated to the nanoliposomes. Nevertheless, although it has been observed that the accumulation in kidney (a target organ) is similar for free Replagal and Replagal@LP-RGDe, other organs must be tested such as spleen, lung, etc. to extract conclusions.

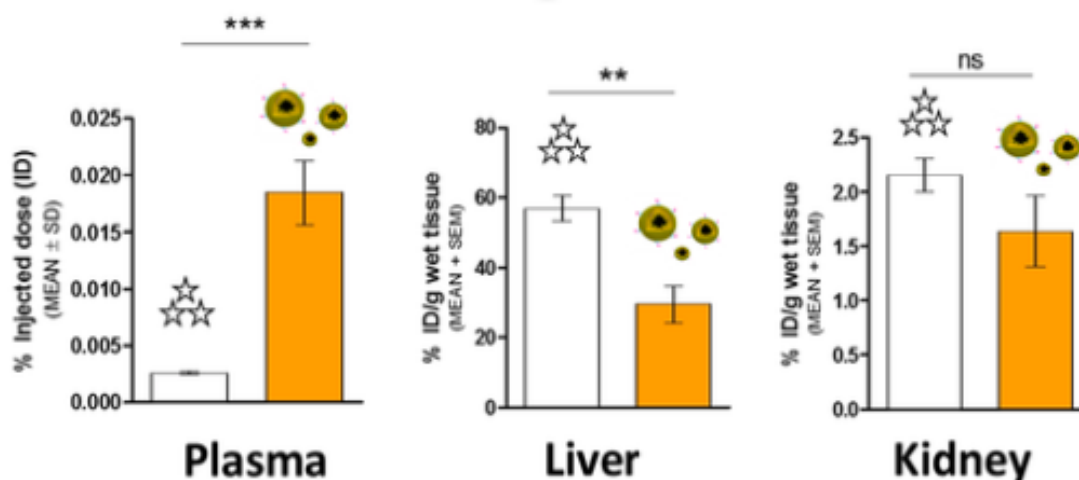


Figure 2.23: Preliminary study of tissue biodistribution in which Replagal nanoformulation was compared to free Replagal after a single administration. In white is represented the free Replagal, and in orange the Replagal@LP-RGDe.

Preliminary toxicity assays were performed with the administration of the maximum feasible dose (MFD) which in this case was of 300 mg kg⁻¹ in lipid content, equivalent to 1.5 mg kg⁻¹ of Replagal. This MFD was Replagal@LP-RGDe (x30) in Milli-Q water. Fabry mice were monitored for 21 days post-administration and then euthanized in order to do gross necropsy (Experimental Section 7.9.2.). No signs of toxicity were observed based on physical examinations (body weight and food consumption). The necropsy showed no gross anatomical alterations.

The Replagal@LP-RGDe (x30) formulation (physicochemical characteristics in **Table 2.10** and **Figure 2.17**) was also used to perform a preliminary efficacy assay. The efficacy in pharmacology is the therapeutic response or effect that a given drug produces. The cardiac remodeling genes involved in Fabry disease were used for evaluating the efficacy in this preliminary assay.

A real-time polymerase chain reaction (RT-PCR) is a laboratory technique of molecular biology based on the polymerase chain reaction (PCR). It monitors the amplification of a targeted DNA molecule during the PCR. In our case, it was used to determine the mRNA levels of cardiac remodeling genes as indicators of cardiac alterations in Fabry mice.

The cardiac remodeling is a progressive response of the heart to acute and chronic injuries (damage) regardless its etiology. Cardiac remodeling involves molecular, cellular, and interstitial changes that manifest clinically as changes in size, shape, and function of the heart after injury or stress stimulation. The results of efficacy are the read-out of the changes in the mRNA expression of cardiac remodeling genes (by RT-PCR).

Six cardiac remodeling genes were studied after administration of Replagal to Fabry mice (Experimental Section 7.9.3.). After three weeks, it was performed a RT-PCR analysis of the heart and it was determined in two independent assays that the genes that better responded to the treatment were *Serpine1* and *TBSH2*. The efficacy of the Replagal@LP-RGDe (x30) administered at 1.5 mg kg^{-1} was compared in a preliminary study to the free Replagal. Results (see **Figure 2.24**) showed that Replagal@LP-RGDe (x30) had the same efficacy than free Replagal when administered at 1.5 mg kg^{-1} of Replagal, reaching the wild type levels (healthy mice). Nevertheless, further assays must be performed at lower doses, in order to see if the Replagal loaded liposomes-RGD_ether increases its efficacy *in vivo*.

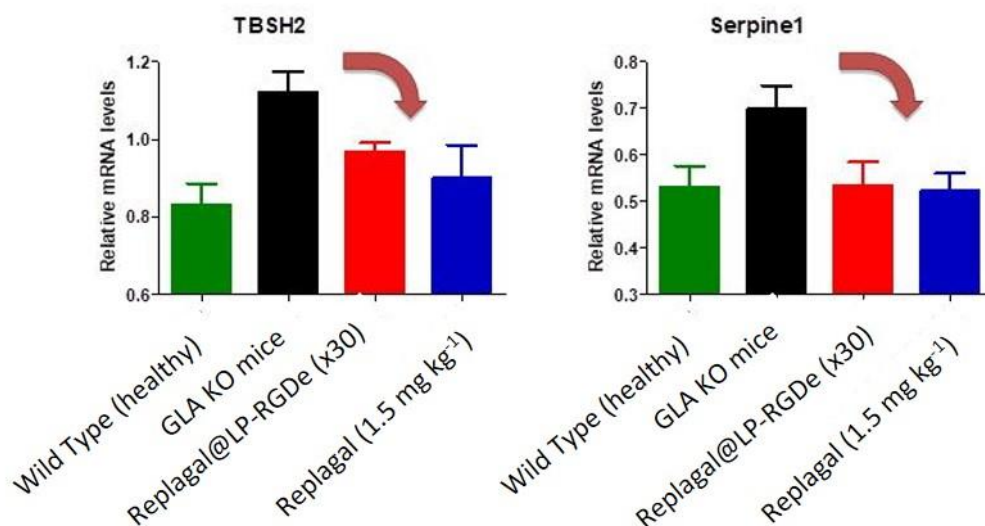


Figure 2.24: Preliminary efficacy assays where after the administration of 1.5 mg kg^{-1} of Replagal, the animals were euthanized three weeks later. Two cardiac remodeling genes were analyzed by RT-PCR. Results showed that Replagal@LP-RGDe (x30) had the same efficacy than free Replagal when administered at 1.5 mg kg^{-1} of Replagal.

2.8. Encapsulation of chelators to perform biodistribution by radiolabelling

The objective of biodistribution studies is the tracking of a given compound inside animal or human subjects, determining the travel and retention in organs of patients. In vivo biodistribution can be accomplished with nuclear medicine imaging using radiolabelling, optical imaging using fluorophores, magnetic resonance imaging (MRI) using contrast agents, among others⁹⁰. Isotopic (radio)labelling is one of the most powerful methods for nanoparticle tracking in experimental studies. This in vivo imaging using radiopharmaceuticals is very important for drug development. The imaging techniques that employ radionuclides (gamma and positron emitters) are single photon emission computed tomography (SPECT) and positron emission tomography (PET). There are several methods for the incorporation of a radionuclide in liposomes, mainly passive encapsulation, membrane labelling, surface chelation and remote loading⁹¹. Due to the characteristics of our facilities that do not allow the use of radionuclides, our possibilities to label the liposomes were the remote loading of a hydrophilic agent, or using bifunctional chelators (BFCs).

As represented in **Figure 2.25**, we started with the first approach, trying to encapsulate diethylenetriaminepentaacetic acid (DTPA) in the inner cavity of our liposomes-RGD_ether. This hydrophilic chelator will entrap the ⁶⁷Ga radionuclide once it is transported across the lipid bilayer by means of a lipophilic chelator.

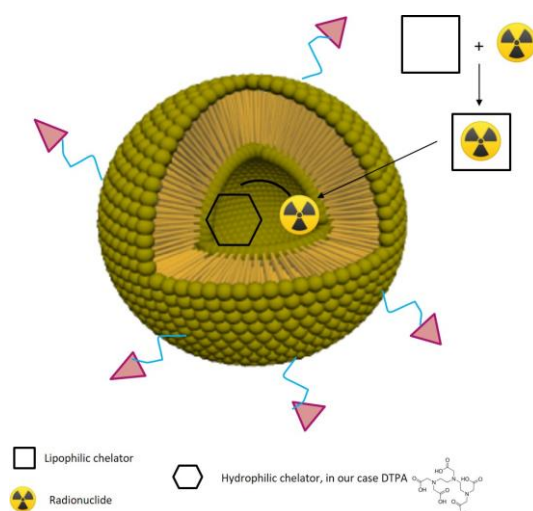


Figure 2.25: Schematic representation of the strategy of remote loading of DTPA loaded liposomes-RGD_ether (DTPA@LP-RGDe): a lipophilic chelators transport the radionuclide through the lipid bilayer. The radionuclide is trapped forming a complex with a second hydrophilic chelator previously entrapped in the inner cavity of the liposome. In our case, this entrapped hydrophilic chelator is DTPA.

DTPA@LP-RGDe were prepared following the DELOS-SUSP procedure described in Experimental Section 7.2.1.2. As always, a mixture of the membrane components (cholesterol, DPPC and cholesterol_PEG200_RGDether at a molar ratio 6:10:1) was suspended in ethanol, added to the reactor and then expanded with CO₂. The CO₂ expanded solution was then depressurized over DTPA dissolved in the depressurization water in order to achieve its encapsulation. Given that the final concentration of DTPA necessary for radiolabelling was 6 mM, we put an excess of DTPA calculated assuming a 10% of final entrapment efficiency (after diafiltration and concentration x30). In addition, we tried to quantify the encapsulated DTPA by UV absorbance, destroying the liposomes-RGD_ether with Triton X-100. However, the DTPA did not show any distinct peak and we could not quantified this chelator.

We produced seven batches of DTPA@LP-RGDe by DELOS-SUSP that were diafiltrated to eliminate the DTPA non-encapsulated and concentrated x30. The physicochemical characteristics are gathered in **Table 2.16** and **Figure 2.26**. As it can be observed, all the samples presented high polydispersity indexes, which are in accordance with what is observed in cryo-TEM images: the systems not only have small unilamellar vesicles

but also tubular structures, more abundant in the total samples in comparison with the concentrated x30.

Table 2.16: Physicochemical characteristics of DTPA loaded liposomes-RGD_ether

| Liposomal systems | Size | | Z potential (mV) |
|---------------------------------------|------------------------|------------------|---------------------|
| | Mean ^a (nm) | Pdl ^b | |
| DTPA@LP-RGDe (T): mix of 7 batches | QR | QR | +29±1 |
| DTPA@LP-RGDe (L) | 138±1 | 0.39±0.04 | +8.8±0.2 |
| DTPA@LP-RGDe (x30) | 136±1 | 0.43±0.01 | +2.4±0.2 |

^aIntensity weighted mean hydrodynamic size (diameter) measured by dynamic light scattering.

^bPolydispersity index showing the width of the particle size distribution. Error margins are SD. QR: not meeting quality requirements of the DLS equipment.

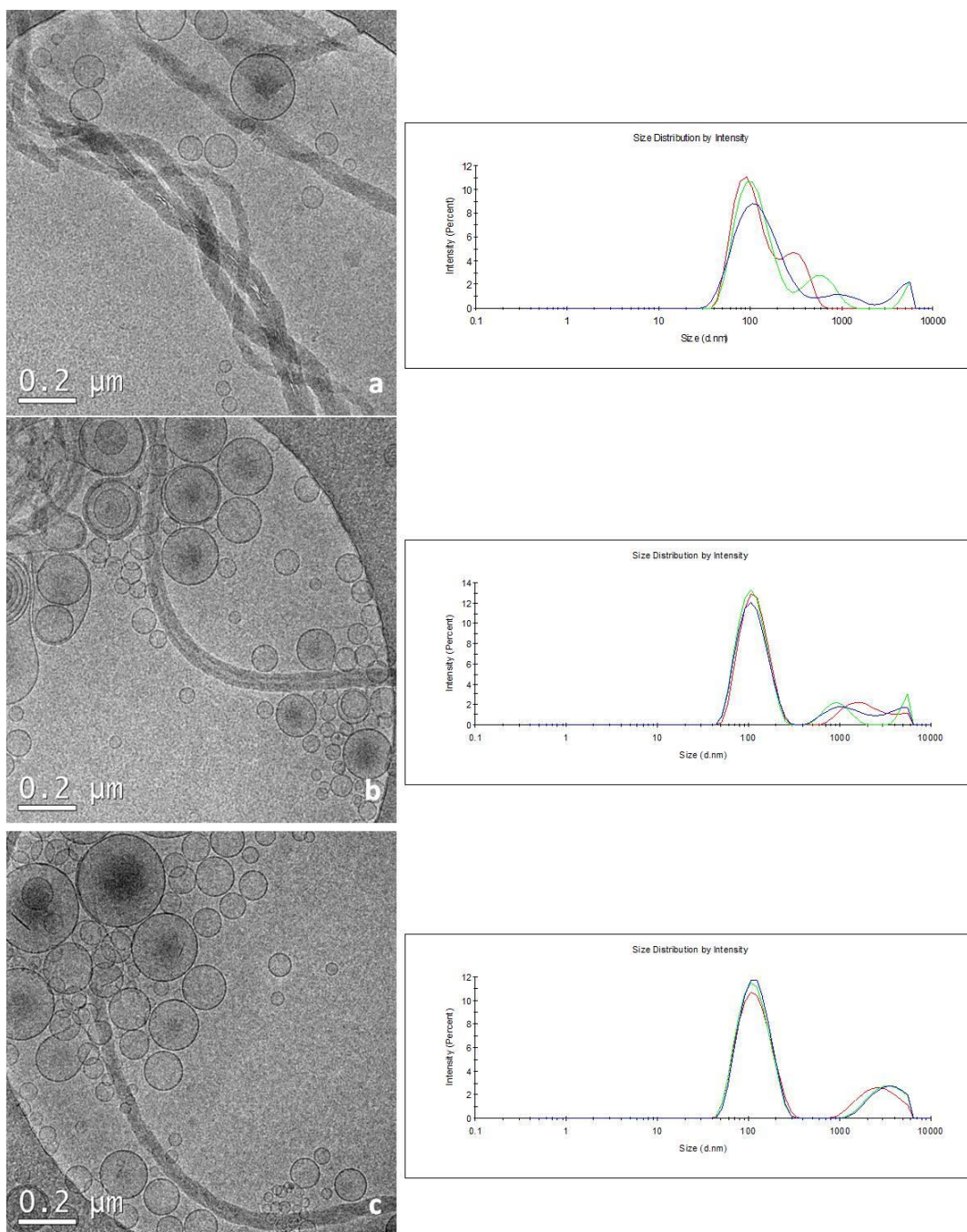


Figure 2.26: Cryo-TEM pictures and DLS measurements showing the morphology and average size of the nanoconjugates with DTPA: a) DTPA@LP-RGDe (T) b) DTPA@LP-RGDe (L), c) DTPA@LP-RGDe (x30). Scale bars are 200 nm.

It is probable that DTPA promotes the formation of tubular structures as it is shown in **Figure 2.26a**. When diafiltrated, and furthermore, when concentrated x30, the DTPA is eliminated from the sample giving more unilamellar liposomes. Given the heterogeneity of the sample and the probable loss of DTPA, we had to discard the encapsulation of DTPA and turned to other techniques, as instance using bifunctional

chelators. This approach needs to be completely developed in upcoming experiments, out of the scope of the present thesis.

2.9. Conjugation with new peptides for crossing the blood brain barrier

Blood brain barrier refers to a barrier of highly specialized endothelial cells attached between them via tight junctions. This barrier covers the entire brain in order to protect it from harmful substances. However, the endothelial cells express in their surfaces several receptors and transporters that allow the entrance of molecules such as nutrients. This way of access can be exploited by nanoparticles decorated with peptides that are recognized by the receptors/transporters⁹².

Although Fabry disease is characterized by the lack of major central nervous system involvement⁵⁰, there are neurological symptoms both in the peripheral and central nervous system mainly related to cerebral vasculopathy with increased risk of cerebrovascular events⁷². Since ERT cannot cross the BBB, it would be of extreme interest to have a nanocarrier able to traverse it using targeting units⁶². As 50% of the LSDs, other than Fabry, presents central nervous system disorders⁶³, it is very interesting to have an appropriate nanocarrier which can cross the BBB.

It is still unknown, since biodistribution has not been performed yet, if our liposomal formulation (tagged with the RGD peptide) will be able to cross the BBB, although there is favorable input from literature⁹³. Meanwhile, the design and development of a new platform of cholesterol_PEG200_peptide conjugation with high potential for BBB crossing was contemplated. Two peptides-cholesterol conjugates were selected in order to study the physicochemical features when incorporated in liposomes: transferrin and glutathione.

Transferrin (pTf1) is a protein that is in charge of transporting de iron through the body. Transferrin receptor is highly expressed in the brain in order to supply its iron needs⁹³. Glutathione (GSH) is a tripeptide with functions that range from antioxidant to detoxification. The mechanism of internalization by glutathione transporter remains

unclear. Anyway, since glutathione is an essential molecule is greatly internalized through the BBB⁹².

The current methodology to synthesize cholesterol-(PEG)_n-peptide molecular units consists of a versatile cholesterol-(PEG)_n-maleimide platform designed to incorporate any cysteine-derivative peptide by means of a thioether bond formation. Using the cholesterol-PEG200-RGD synthesis as a reference, the group of Dr. Miriam Royo at the Institut de Química Avançada synthesized cholesterol-PEG200-pTf1 and cholesterol-PEG200-GSH Catalunya (IQAC), more details of the molecules are given in Experimental Section 7.1.

Cholesterol-PEG200-pTf1 resulted soluble in ethanol, whereas cholesterol-PEG200-GSH remained as a suspension very similar to the one of cholesterol-PEG200-RGDether. In either case, the solution/suspension with cholesterol, DPPC and cholesterol-PEG200-peptide was added to the reactor following the same procedure used to prepare liposomes-RGD_ether (see Experimental Section 7.2.1.2). The differences between the obtained systems started with the macroscopic appearance: liposomes-pTf1 looked more translucent than liposomes-GSH (**Figure 2.27**). This matched also the measurement data by DLS (see **Table 2.17**): liposomes-pTf1 are smaller than the liposomes-GSH although both systems present low polydispersity index and high Z-potentials values (positive for liposomes-pTf1 and negative for liposomes-GSH). Cryo-TEM images also revealed important differences between both systems: whereas liposomes-pTf1 are mostly small unilamellar vesicles, liposomes-GSH are more heterogeneous with big and multilamellar vesicles that tend to aggregate. Interestingly, in the liposomes-pTf1 sample small sticks appear (that are indicated with the white arrows in **Figure 2.27**), and which presence we cannot explain yet. From these very preliminary results, we discarded liposomes-GSH for its bad physicochemical properties. Liposomes-pTf1 will be tested in the near future in biodistribution assays when the methodology for performing it is completely developed and tuned.

Table 2.17: Physicochemical properties of liposomes-pTf1 and liposomes-GSH

| Liposomal systems | Batch | Size | | Z potential (mV) |
|-------------------|-------|------------------------|------------------|------------------|
| | | Mean ^a (nm) | PdI ^b | |
| LP-pTf1 | #1 | 113.4±0.4 | 0.215±0.009 | +51±1 |
| | #2 | 123 ±2 | 0.218 ±0.004 | +55±1 |
| LP-GSH | #1 | 173±2 | 0.19±0.03 | -23±1 |
| | #2 | 156.4±0.5 | 0.203±0.009 | -22.4±0.6 |

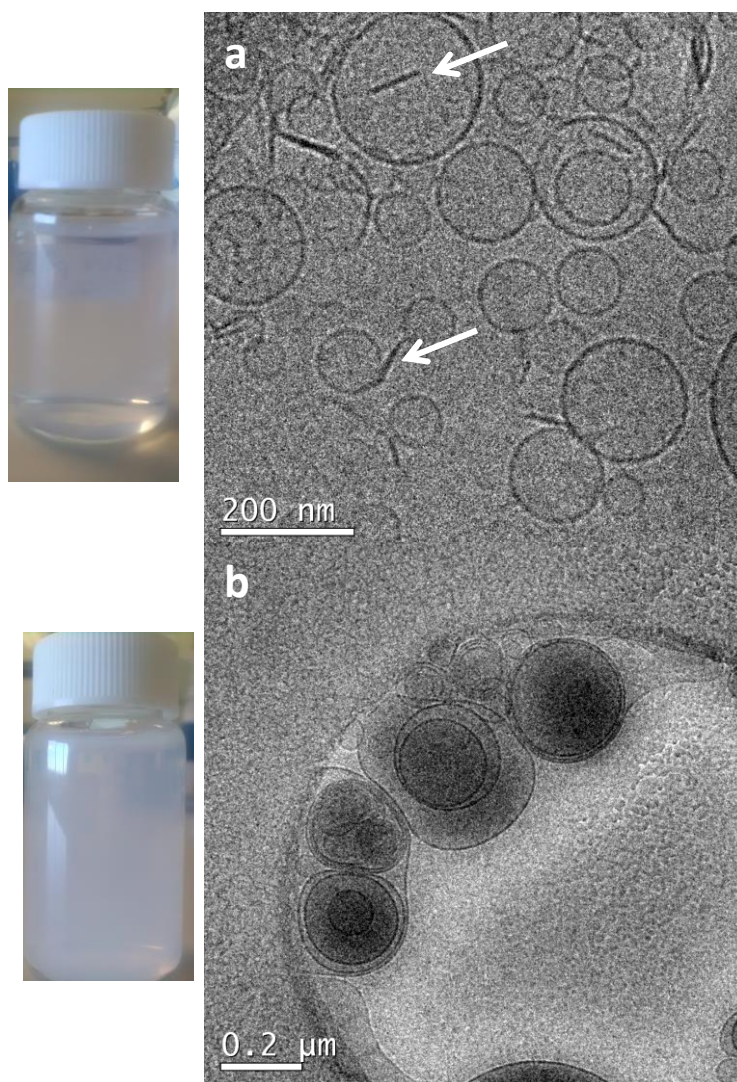


Figure 2.27: Macroscopic appearance and cryoTEM images of: a) liposomes-pTf1, b) liposomes-GSH.

2.10. Summary and conclusions

- DELOS-SUSP renders GLA loaded liposomes-RGD_ether with entrapment efficiencies around 40%. Their physicochemical characteristics strongly influence the biological activity. GLA loaded liposomes-RGD_ether present higher enzymatic activity than free GLA, and the GLA liposomal systems are capable of degrading in vitro the Gb3 cellular deposits.
- The concentration of Replagal loaded liposomes-RGD_ether up to near 300 $\mu\text{g mL}^{-1}$ of enzyme concentration, necessary for the in vivo testing, is possible using a diafiltration methodology. This new GLA liposomal formulations fulfill the quality physicochemical criteria to face in vivo evaluation .
- The change between chloride and trifluoroacetic, more desired from a pharmaceutical point of view, as counterion of the cholesterol_PEG200_RGDether was not possible, since unstable nanoliposomes were obtained.
- The use of PBS and NaCl 0.9% was not possible as dispersant media for the preparation of Replagal loaded liposomes-RGD_ether at the desired enzyme concentration and molar ratios between enzyme and liposome membrane components.
- Although dialyzed Replagal presents higher enzymatic activity than non-treated commercial Replagal, when formulated in the liposomes-RGD_ether, this activity is lost.
- The pharmacokinetics revealed that the blood half-life of Replagal loaded liposomes-RGD is almost 4 times higher than free Replagal.
- Efficacy assays showed the capacity of Replagal loaded liposomes-RGD_ether to revert cardiac remodeling genes to the levels of healthy individuals.
- The preparation of DTPA loaded liposomes-RGD_ether for performing the biodistribution by radiolabelling was not possible, since the physicochemical characteristics do not meet quality criteria.
- Liposomes-pTf1, to be used as nanocarriers for BBB crossing, were successfully prepared by DELOS-SUSP with appropriate physicochemical characteristics.

3. Development of an HPLC methodology for the quantification of the components of the liposome-RGD_ether membrane

3.1. Introduction

Liquid chromatography is one of the most used techniques in pharmaceutical analysis. This separation technique is based on the different distribution of species between two immiscible phases: the mobile and the stationary phases. The mobile phase consists of a liquid that passes through the stationary phase placed in a column⁹⁴. Hence, liquid chromatography depends mainly on mechanisms of adsorption, mass distribution, ion exchange and size exclusion⁹⁵.

The components of high-performance liquid chromatography (HPLC) equipment involve usually a pumping system, an injector, a chromatographic column, a detector and a data acquisition system. The pump uses high pressure to push the mobile phase at a defined flow rate, either at constant (isocratic elution) or varying composition (gradient elution). The injector places a small volume of liquid sample into a tube packed with porous particles (stationary phase). The small particles inside the column cause the high backpressure at normal flow rates. The sample interacts physically or chemically with the column, being partially retained or eluted. The separated

components are collected at the end of the column and identified by an external measurement technique based in a physicochemical property like UV-absorbance, refractive index, etc., depending on the analyte nature. This response is digitally amplified and registered in the data acquisition system as the chromatogram, determining also the time of elution (retention time), sample components (qualitative analysis) and the amount of analyte (quantitative analysis).



Figure 3.1: HPLC components, courtesy of Agilent Technologies, Inc.

Liquid chromatography is classified in normal or reverse phases depending on the polarity of the mobile and stationary phases. Normal phase is the traditional chromatography where the analyte is adsorbed and desorbed onto a polar stationary phase, typically silica or alumina. However, at present, reversed chromatography is more used. As its name indicates, is the opposite of normal chromatography: the stationary phase is a hydrophobic column and the mobile phase is a polar solvent. Using less polar solvents reduces the hydrophobic interaction between the analyte and the column until desorption is accomplished. The reversed phase columns are composed of silica functionalized with hydrocarbons. Changing the alkyl chain influences the retention time, achieving lower retention times when the chain is shorter¹.

The most commonly used detector is the ultraviolet/visible (UV/Vis) where an ultraviolet beam is conducted through a flow cell and a sensor measures the light passing by the cell. The detector converts thus this transmitted light into absorbance values. The absorbance depends on the analyte concentration and is based on Beer's law.

Evaporation light scattering detectors (ELSD) are of extreme utility when the analytes do not possess chromophores detectable by UV/Vis. However, volatile mobile phases are required and also that the analyte is less volatile than these mobile phases⁹⁶.

ELSD were first introduced in the 1980s and nowadays there are commonly employed being classified as a quasi-universal detector (it is not applicable for mobile phases less volatile than the analyte)⁹⁷. That is because in ELSD the target analytes are transformed into a fine spray by a nebulizer and heated until only the mobile phase is evaporated. Light beam is directed at the remaining solute and the scattered light is detected. The involved steps in the detector are the nebulization of the sample, the evaporation of the solvent and finally the light scattering of the particles.

Nebulizers are based in the Venturi effect of a carrier gas (normally, air or nitrogen), that flows coaxially to the mobile phase which comes from the chromatographic column and converts the mobile phase into small droplets. These droplets are transported by the nebulizer gas into a heated drift tube where the solvent is evaporated and transformed in a cloud with non-volatile analyte present in the mobile phase. The analyte particles arrive to the detector cell passing through a light beam where they scattered light by four main processes which are Rayleigh scattering, Mie scattering, reflection and refraction. Thus, the detector response is a result of these four light scattering mechanisms that are regulated by the particle size distribution (radius) compared to the wavelength of the light beam, independently of the nature of the analyte. It should be noted that this response is non-linear.

Quantification of the lipid content in liposomal formulations is relevant because this concentration influences both efficacy and stability⁹⁸. For instance, this quantification is required to guarantee the quality of any liposomal pharmaceutical formulation and for the understanding of their biological behavior, for instance cellular internalization. According to a recent study⁹⁹, the phospholipid content is not always characterized in liposome's literature. However, in other studies phospholipid concentration, composition and hydrolysis, and cholesterol concentration and autooxidation are assessed as usual characterization methods for quality control^{100,101}.

There are several techniques for the quantitative lipid analysis, such as Bartlett , ascorbic acid and other molybdate-containing reagents assays, enzymatic assays and finally chromatographic methodologies¹⁰². In the case of chemical and enzymatic reactions, the total lipid content is analyzed but not the specific composition of individual components. Another limitation of the preceding techniques is the required step of derivatization. Taking all into account, HPLC becomes the best method for the determination of phospholipids and cholesterol in liposomes^{99,101}.

In HPLC methodologies, membrane components of a liposome are separated based on their different chain lengths, head groups, and polarities. Separation is accomplished with a variety of columns, eluent systems (isocratic as well as gradient) and detectors like phosphorus analyzer, UV, radioactive flow, flame ionization, fluorescence, and evaporative light-scattering¹⁰³.

In this thesis, we have developed and validated an HPLC procedure for the precise quantification of the membrane components of liposomes-RGD_ether: cholesterol, the phospholipid dipalmitoylphosphatidylcholine (DPPC) and the cholesterol_PEG200_RGDether. Cholesterol acts as a membrane stabilizing molecule. Cholesterol_PEG200_RGDether has an important role in targeting specific cells and biological pathways, and in the distribution of active molecules in the body. Therefore, it cannot be considered as a simple inactive ingredient and its quantification is very important. As explained in Chapter 2, this cholesterol_PEG200_RGDether is a molecule composed of cholesterol covalently bound to a linker PEG200 through an ether bond. The PEG200 is bound to the cyclic cRGDFK peptide through a carbamate bond. Liposomes-RGD_ether composition is represented in the previous Chapter 2, **Figure 2.2**.

3.2. Development of the HPLC methodology

3.2.1. Preliminary studies

At first the idea was to develop an HPLC-UV methodology to determine the concentrations of cholesterol and cholesterol_PEG200_RGDether, and, if possible, the quantity of DPPC, using an UV-Vis detector. The final goal for these studies was to

provide an analytical methodology to quantify the chemical composition of the liposome membrane components, which could be accepted by regulators and facilitate entrance to clinical phases in the future. For the development of a liposomal product is interesting the use of mass spectrometry (MS) to identify the composition of the formulation and its degradation products. MS is very versatile since other detectors, for example UV, can be connected to it, without the necessity of developing two chromatographic methods¹⁰⁴.

This part of the work was performed in collaboration with Dr. Miriam Royo group at Institut de Química Avançada de Catalunya (IQAC-CSIC), with the valuable support of Dr. Daniel Pulido.

Most of the studies using UV detector for phospholipid separation were old^{105,106,107} as the one reporting a method to detect simultaneously cholesterol and 1,2-dioleoyl-sn-glycero-3-phosphocholine (DOPC)¹⁰⁸. Although there are important structural differences between DOPC, presenting two unsaturated bonds, and DPPC, which is a saturated phospholipid (see **Figure 3.2**), the method reported by Singh et al. (2005) was used as a starting point for the development of the HPLC method to quantify membrane components of liposomes-RGD_ether.

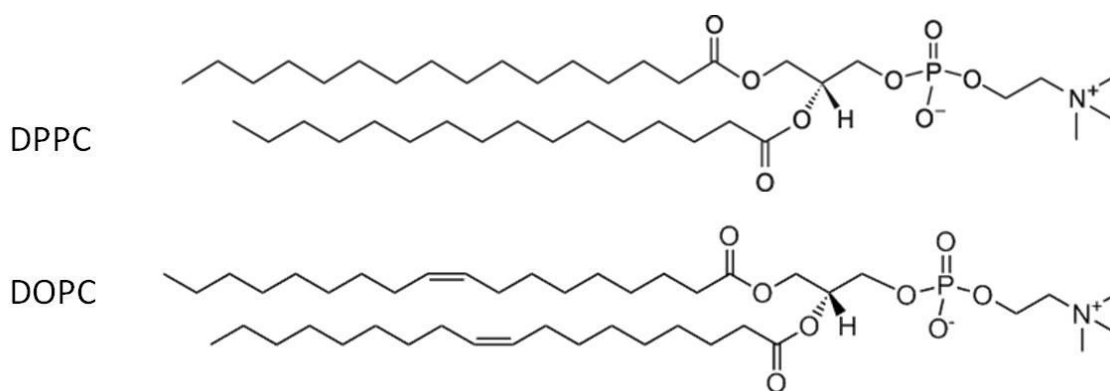


Figure 3.2: DPPC and DOPC chemical structures

The appropriate column choice is critical for success in HPLC. In literature the employed columns for the separation of cholesterol and phospholipids were C₁₈, octadecylsilane¹⁰⁹, and C₈, octylsilane¹⁰⁸. In accordance to these previous HPLC data, we tested two different C₁₈ and two different C₈ columns, plus a C₄ column, butylsilane, for the development of the new HPLC-UV methodology. It is worthy to

mention that the C₄ column is the one used for the determination of the purity of the cholesterol_PEG200_RGDether⁴⁹.

The standards used for the HPLC method feasibility study and development, were solutions of cholesterol, cholesterol_PEG200_RGDether and DPPC in ethanol. The concentrations employed for the preparation of the standards were the theoretical ones weighed to produce liposomes using DELOS-SUSP divided by 10 (95 ppm DPPC, 32 ppm cholesterol and 16 ppm of cholesterol_PEG200_RGDether). Since cholesterol_PEG200_RGDether is barely soluble in ethanol, it is probable we were injecting less quantity of this analyte. Therefore, this working procedure is not appropriate for the quantification of cholesterol_PEG200_RGDether but it suited us for the preliminary detection of this molecule. All the solvents used were HPLC grade quality. In **Table 3.1**, are gathered the majority of the HPLC methodologies tested.

Table 3.1: HPLC-UV methodology conditions tested for the quantification of the membrane components of liposomes-RGD_ether.

| Number | Column | Gradient/ Isocratic | T (°C) | Flow (mL/ min) | Time (min) | Mobile phase A | Mobile phase B |
|--------|----------------------------------|------------------------|---------------|----------------------|------------|-------------------|----------------|
| #1 | C ₁₈ 4.6x150 mm | Isocratic | 40 | 1 | 30 | Acetonitrile | Isopropanol |
| | | | | | | 85 | 15 |
| #2 | C ₄ 4.6x250 mm | Gradient | 40 | 1 | 0 35 | Milli-Q water | Isopropanol |
| | | | | | | 95 | 5 |
| #3 | C ₈ 2.1x50m m | Gradient | 25 | 0.3 | 0 15 | Milli-Q water | Acetonitrile |
| | | | | | | 80 | 20 |
| #4 | C ₈ 2.1x150 mm | Gradient | 25, 40, 60 | 0.3 | 0 20 | Milli-Q water | Acetonitrile |
| | | | | | | 80 | 20 |
| #5 | C ₈ 2.1x150 mm | Gradient | 25 | 0.3 | 5 7 | Methanol+ | Isopropanol |
| | | | | | | 10% PIC* | 0 |
| | | | | | | 100 | 40 |

*1-acid heptanesulfonic.

More experimental details can be found in Experimental Section 7.3.5.1. The injection volume was 20 μ L in all methods.

Using C₁₈ columns, the conditions best suited for cholesterol were not appropriate for cholesterol_PEG200_RGDether and vice versa. Furthermore, both eluted at the same retention time (RT).

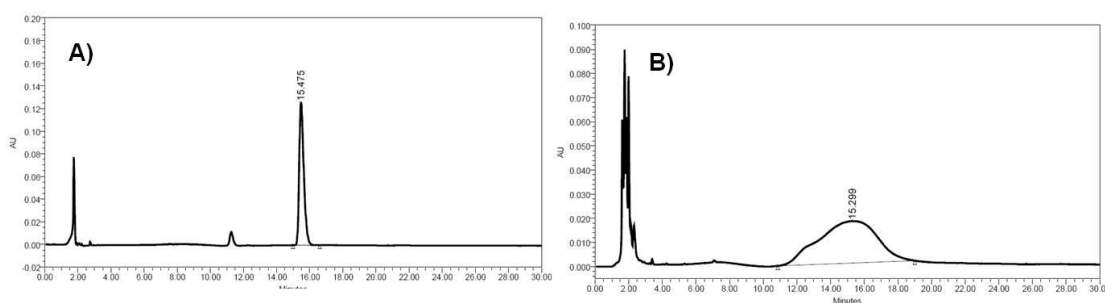


Figure 3.3: Chromatograms corresponding to the analysis of 20 μ L ethanolic solutions of **A)** 32 ppm cholesterol (RT: 15.5 min), and **B)** 16 ppm cholesterol_PEG200_RGDether (RT: 15.2 min), using methodology #1

It was not possible to get appropriate separation of cholesterol and cholesterol_PEG200_RGDether using C₄ column following methodology #2 (see **Figure 3.4**).

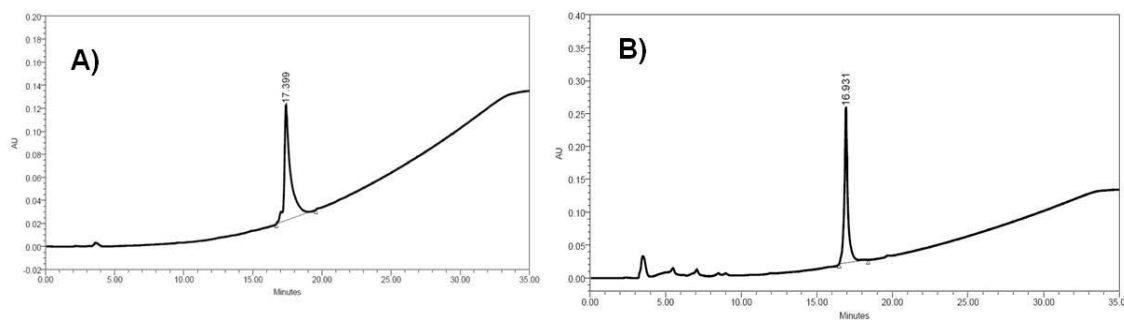


Figure 3.4: Chromatograms corresponding to the analysis of 20 μ L ethanolic solutions of **A)** 32 ppm cholesterol (RT: 17.3 min), and **B)** 16 ppm cholesterol_PEG200_RGDether (RT: 16.9 min), using methodology #2

Instead, with C₈ column in method #3 the peaks were well resolved.

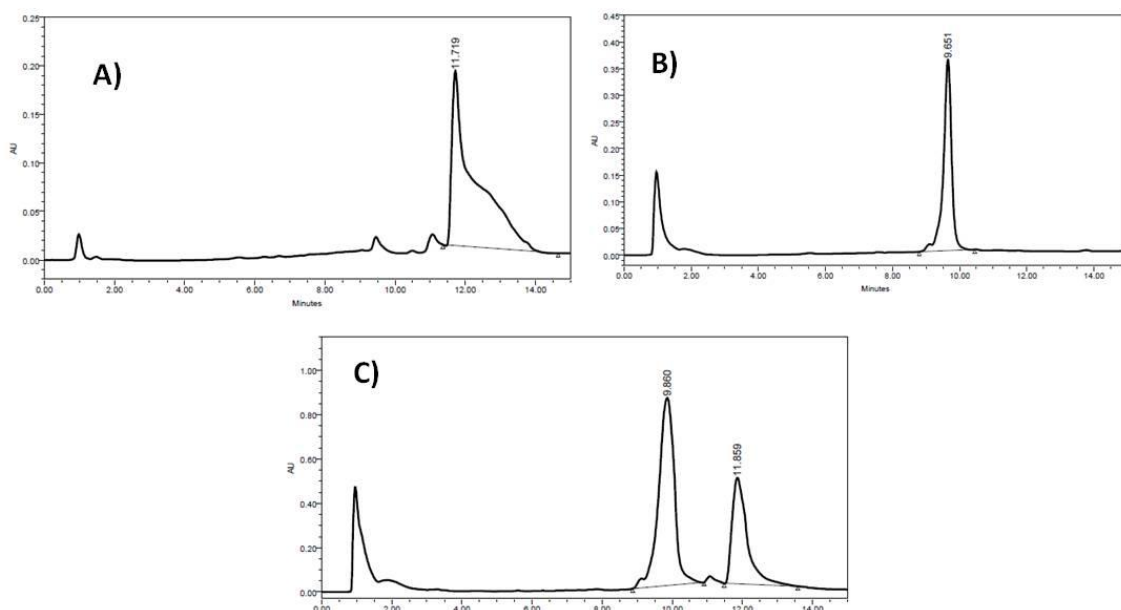


Figure 3.5: Chromatograms corresponding to the analysis of 20 μL ethanolic solutions of **A)** 32 ppm cholesterol (RT: 11.2 min), and **B)** 16 ppm cholesterol_PEG200_RGDether (RT: 12.5 min) and **C)** co-injection of 32 ppm cholesterol (RT: 9.9 min) and 16 ppm cholesterol_PEG200_RGDether (RT: 11.8 min), using methodology #3

Since C_8 2.1x50mm was a very short column, we tried another one (C_8 2.1x150 mm) in order to improve the results. There were detected also impurities in each peak.

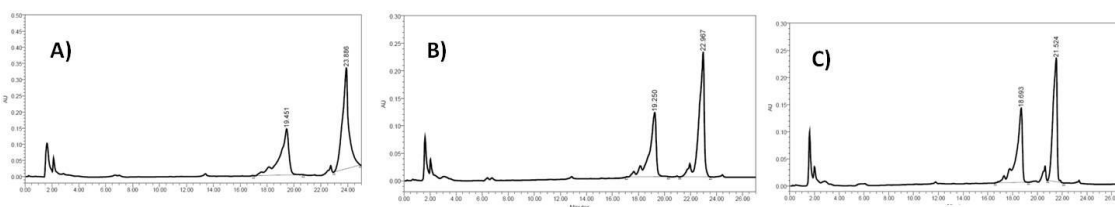


Figure 3.6: Chromatograms corresponding to the analysis of 20 μL of a solution of 32 ppm cholesterol and 16 ppm cholesterol_PEG200_RGDether co-injection, using methodology #4, **A)** 25 °C cholesterol (RT: 19.4 min) and cholesterol_PEG200_RGDether (RT: 23.8 min), **B)** 40 °C cholesterol (RT: 19.2 min) and cholesterol_PEG200_RGDether (RT: 22.9 min), and **C)** 60 °C cholesterol (RT: 18.6 min) and cholesterol_PEG200_RGDether (RT: 21.5 min)

Once detected and separated both cholesterol and cholesterol_PEG200_RGDether, we tried to detect the DPPC. After several trials, we added 1-heptanesulfonic acid (PIC) to the mobile phase following the conditions reported by Morales et al.,2006¹⁰⁹.

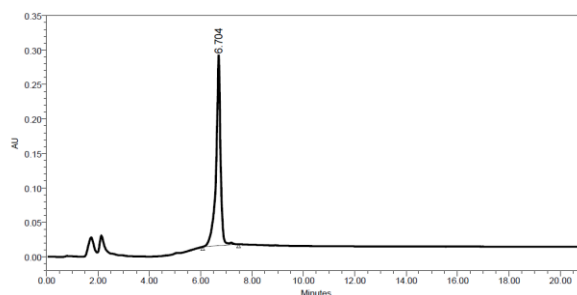


Figure 3.7: Chromatogram of 20 μL of a solution of 95 ppm of DPPC, using methodology #5

As it was previously said, the final goal for these studies is to pass through clinical-grade regulatory conditions, coupling UV to MS, but PIC is incompatible with MS. Trying another column (C_{18} 5 μm 4.6x150 mm) it was possible to resolve the three components and detect them by UV. However, there were some problems related to the low cholesterol_PEG200_RGDether and DPPC sensitivities. After considering all the pros and cons, we decided to change the detection method to ELSD, the commonest for lipids and other molecules without chromophores, although it cannot be coupled to a MS detector, since it involves the destruction of the sample. Therefore, further development of two separate methods will be needed if required.

3.2.2. HPLC-ELSD methodologies

This part of the thesis was performed in collaboration with the Chemistry Analysis Service at Universitat Autònoma de Barcelona (UAB) and with valuable support from Dr. Alba Eustaquio.

Since cholesterol_PEG200_RGDether is barely soluble in ethanol, the first step, before HPLC method development, involved the trial of different solvents like acetone, isopropanol (IPA), 1-butanol, chloroform (CHCl_3), dimethyl sulfoxide (DMSO) and dimethylformamide (DMF) to achieve the complete dissolution of this substance. Mixtures of solvents, for example a mixture of isopropanol, DMF and chloroform, were also tested in order to dissolve simultaneously the three membrane components (cholesterol, cholesterol_PEG200_RGDether, DPPC). At first, chloroform seemed an appropriate solvent for cholesterol_PEG200_RGDether but the recovery achieved of the compound, after HPLC analysis, was not acceptable being very low.

Finally, the disruption of the liposomes and the complete dissolution of the three components was accomplished in two steps: a mixture of CHCl_3 :IPA (1:9 v/v) was used to solubilize the cholesterol and DPPC, while another mixture of DMF:IPA (1:9 v/v) was suitable to solubilize cholesterol_PEG200_RGDether. The challenge was to find a unique solvent for all the components. Another protocol was established employing IPA with formic acid to solubilize cholesterol and DPPC, and methanol/water (95:5 v/v) to solubilize cholesterol_PEG200_RGDether, which reduced the time of analysis from 40 to 20 min. Afterwards, it was found that pure methanol was able to solubilize the three components simultaneously. Therefore, methanol was selected as a good solvent for the preparation of the standards of the membrane components and samples of liposomes-RGD_ether, and as a suitable mobile phase for HPLC-ELSD.

Pre-treatment of liposomes to disrupt the lipid bilayers is frequently needed prior to the injection of the sample, depending on the mobile phase and the lipid solubility¹¹⁰. Although in other works liposomes were straightforward dissolved in short chain alcohols such as methanol or 2-propanol^{99,108,111}, in our case, the components were too diluted to be detectable using this procedure. Thus, it was established a freeze-drying procedure of the samples with the only purpose of eliminating the water, before the dissolution of the liposomes-RGD_ether membrane components with the methanol.

Several mobile phases, column temperatures and flows were tested until the final method was established. Once developed, the method must undergo validation. The objective of validating an analytical procedure is to demonstrate that it is suitable for its intended purpose. In our case, the method was validated by assessing the linearity, the stock dilution test, the samples dilution test, the accuracy test, the precision, the limit of quantification (LOQ) and the limit of detection (LOD). Linearity, LOQ, LOD and the stock dilution test was determined using standards, and the rest of the mentioned parameters were measured with real samples.

These samples were prepared using DELOS-SUSP procedure, as explained in detail in Experimental Section 7.2.1. Briefly, 1.2 mL of an ethanolic suspension of cholesterol_PEG200_RGDether, cholesterol and DPPC is added to the reactor, which is pressurized with compressed CO_2 . Afterwards, the samples are depressurized over 24 mL of Milli-Q water.

3.2.2.1. Method parameters

The HPLC method #6 developed for the separation and quantification of the membrane components of liposome-RGD_ether is based on the use of a C₁₈ column, 5 µm, 4.6x150 mm. A gradient eluent system is used by combining mobile phase A and mobile phase B, following the gradient elution mode described in **Table 3.3**. Mobile phase A consisted in methanol/water (95/5%, v/v) and mobile phase B in 0.1% of formic acid in isopropanol. The injection volume is 20 µL. Column temperature was fixed at 25 °C, while the nebulization temperature is 40 °C and the evaporation temperature 80 °C. Detection was performed with a gain of 2.

Table 3.3: Gradient elution mode for quantitative analysis of cholesterol_PEG200_RGDether, cholesterol and DPPC in liposomes-RGD_ether.

| Time (minutes) | Mobile phase A (%) | Mobile phase B (%) | Flow rate (mL/min.) |
|----------------|--------------------|--------------------|---------------------|
| 0 | 97 | 3 | 1 |
| 3.0 | 97 | 3 | 1 |
| 4.0 | 88 | 12 | 2 |
| 16.0 | 88 | 12 | 2 |
| 16.5 | 95 | 5 | 2 |
| 19.0 | 97 | 3 | 2 |
| 19.5 | 97 | 3 | 1 |

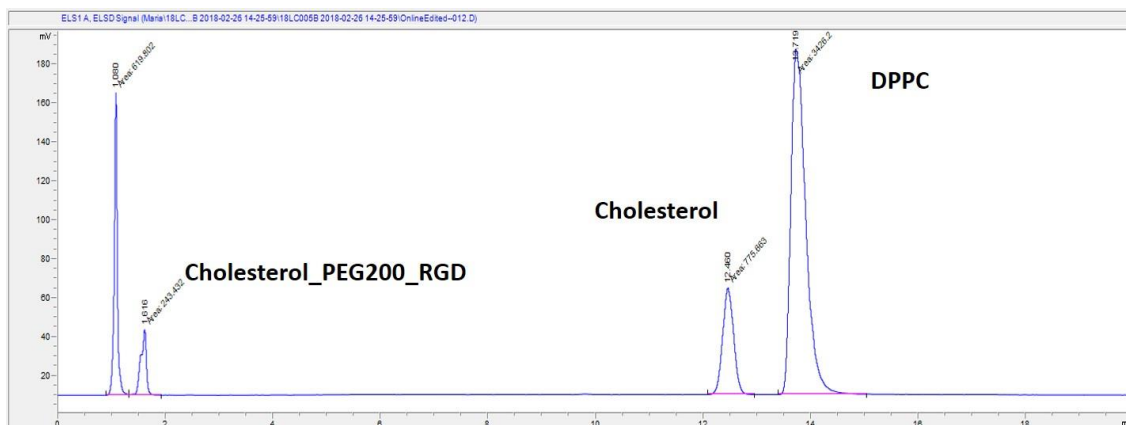


Figure 3.8: Chromatogram of the three components of liposomes-RGD_ether, using standards of 700 ppm DPPC, 250 ppm cholesterol and 100 ppm cholesterol_PEG200_RGDether and following the method #6.

3.2.2.2. Standard solutions preparation

Standard solutions of cholesterol (25 to 250 ppm), DPPC (35 to 700 ppm), and cholesterol_PEG200_RGDether (5 to 100 ppm) were prepared in methanol. Solutions were injected into the HPLC system preceding each measurement with the objective of establishing the calibration curves and as a reference check.

The calibration curve of each compound is performed by plotting the logarithm values of peak area against the logarithm values of analyte concentrations. Correlation (r^2) is determined for all curves by regression analysis.

3.2.2.3. Sample preparation

1 mL of sample is lyophilized in a 4 mL-glass vial. The lyophilization protocol is described in detail in Experimental Section 7.3.5.2. The lyophilization cake of each sample is dissolved in 1 mL of methanol. The sample is filtered and injected the same day of preparation.

3.2.2.4. Method validation results

3.2.2.4.1. Linearity and goodness of fit

Linearity is the relation between the analyte concentration and the response (proportional to the concentration) given by the system when the method is applied.

The use of evaporative light-scattering detectors can result in limited direct linearity, and when larger concentration ranges are required, a standard log–log transformation can be used, with the logarithm of the peak area and the logarithm of the concentration⁹⁸. This limited linearity is solved injecting a calibration curve each time we analyzed samples. Therefore, the results shown here corresponds to one routinely injected calibration curve. The calibration curve is prepared using a solution of the three components as explained in 3.2.2.2.

The points of each calibration curve are gathered in the Experimental Section, **Tables 7.3** for cholesterol_PEG200_RGDether, **7.4** for cholesterol, and **7.5** for DPPC.

The linear correlation between the logarithm of peak's area and the logarithm of cholesterol_PEG200_RGDether concentration is represented in **Figure 3.9**. The linear equation is $y = 1.7578x - 0.5032$ where the y is the logarithm of the peak's area and the x is the logarithm of the cholesterol_PEG200_RGDether divided by 1000 in mg mL^{-1} . The correlation coefficient is 0.9972. This result is suitable for considering it acceptable, since the goodness of fit for this analyte was higher than 0.99, showing good correlation between the peak areas and the concentrations.

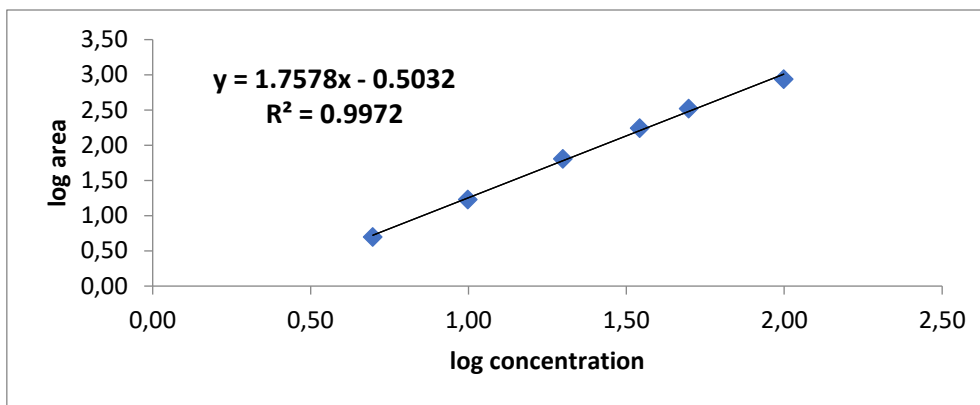


Figure 3.9. Linear equation of the cholesterol_PEG200_RGDether. In the x axis is represented the logarithm of the concentration divided by 1000 in mg mL^{-1} and in the y axis is the logarithm of the peak's area.

The calibration curve of cholesterol is represented in **Figure 3.10**. The linear equation is $y = 1.7779x - 0.7268$ where the y is the logarithm of the peak's area and the x is the logarithm of the cholesterol divided by 1000 in mg mL^{-1} . The correlation coefficient is 0.9993, being suitable for considering it acceptable, since the goodness of fit for this analyte was higher than 0.99, showing good correlation between the peak areas and the concentrations.

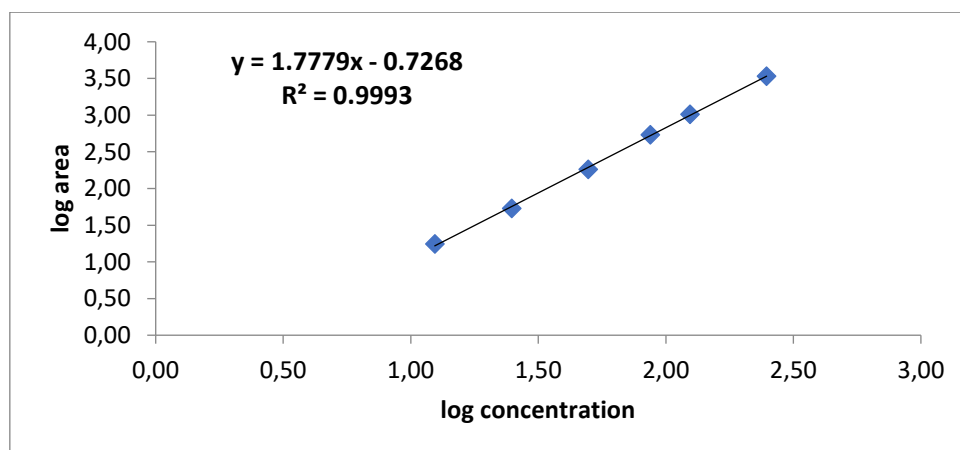


Figure 3.10: Linear equation of the cholesterol. In the x axis is represented the logarithm of the concentration divided by 1000 in mg mL^{-1} and in the y axis is the logarithm of the peak's area.

The calibration curve of DPPC is represented in **Figure 3.11**. The linear equation is $y = 1.7893x - 1.0028$ where the y is the logarithm of the peak's area and the x is the logarithm of the cholesterol divided by 1000 in mg mL^{-1} . The correlation coefficient is

0.9991, being suitable for considering it acceptable, since the goodness of fit for this analyte was higher than 0.99, showing good correlation between the peak areas and the concentrations.

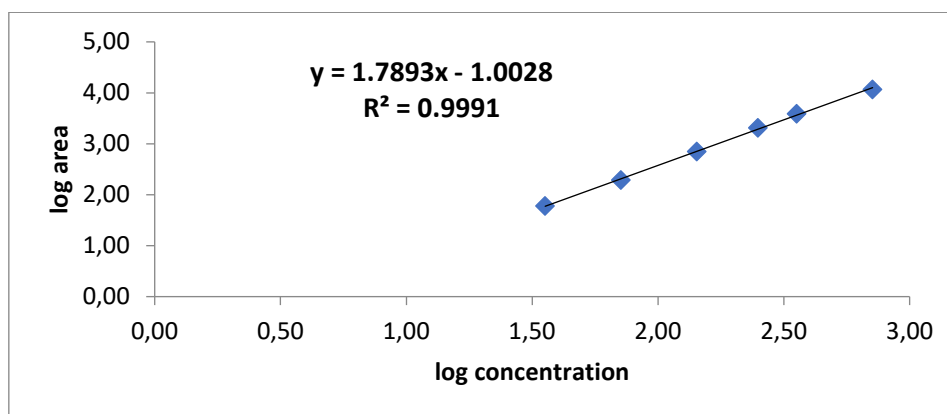


Figure 3.11. Linear equation of the DPPC. In the x axis is represented the logarithm of the concentration divided by 1000 in mg mL^{-1} and in the y axis is the logarithm of the peak's area.

3.2.2.4.2. Limit of detection (LOD) and limit of quantification (LOQ)

The detection limit (LOD) of an analytical procedure is the lowest amount of analyte detected in a sample but not necessarily quantified as an exact value. The quantification limit (LOQ) of an analytical procedure is the lowest amount of analyte in a sample which can be quantitatively determined with precision and accuracy¹¹².

The signal-to-noise is dependent on the response and the slope of the calibration curve. Following ICH guidelines, the LOD is the signal-to-noise of 3, whereas the LOQ is established in 10^{98} .

In **equation 3.1.**, σ is the standard deviation of the response, Y refers to the theoretical concentration, Y_i to the real concentration and n to the points evaluated. Data were obtained from **Tables** in Experimental Section 7.3.5.2: **7.3** (for cholesterol_PEG200_RGDether), **7.4** (for the cholesterol) and **7.5** (for the DPPC). S in **equations 3.2** and **3.3** refers to the slope in the calibration curve (**Figure 3.9** for cholesterol_PEG200_RGDether, **3.10** for cholesterol and **3.11** for DPPC).

$$\sigma = \sqrt{\frac{\sum(Y-Y_i)^2}{n-2}} \text{ (Equation 3.1)}$$

$$LOD = \frac{3\sigma}{S} \text{ (Equation 3.2)}$$

$$LOQ = \frac{10\sigma}{S} \text{ (Equation 3.3)}$$

Table 3.4: Parameters used to calculate the LOD and LOQ of cholesterol_PEG200_RGDether

| Y | Y _i | n | $\sum(Y - Y_i)^2$ | σ | S | LOD | LOQ |
|-------|----------------|---|-------------------|----------|--------|------|------|
| 5.0 | 5.0 | | | | | | |
| 10.0 | 10.0 | | | | | | |
| 20.0 | 19.9 | 6 | 0.22 | 0.23 | 1.7578 | 0.40 | 1.33 |
| 35.0 | 34.9 | | | | | | |
| 40.0 | 39.8 | | | | | | |
| 100.0 | 99.6 | | | | | | |

The LOD and LOQ for cholesterol_PEG200_RGDether is 0.40 and 1.33 ppm.

Table 3.5: Parameters used to calculate the LOD and LOQ of cholesterol

| Y | Y _i | n | $\sum(Y - Y_i)^2$ | σ | S | LOD | LOQ |
|-------|----------------|---|-------------------|----------|--------|------|------|
| 12.5 | 12.4 | | | | | | |
| 25.0 | 24.8 | | | | | | |
| 50.0 | 49.7 | 6 | 3.7 | 0.96 | 1.7779 | 1.62 | 5.41 |
| 87.5 | 86.9 | | | | | | |
| 125.0 | 124.2 | | | | | | |
| 250.0 | 248.4 | | | | | | |

The LOD and LOQ for cholesterol 1.62 and 5.41 ppm.

Table 3.6: Parameters used to calculate the LOD and LOQ of DPPC

| Y | Yi | n | $\sum (Y - Yi)^2$ | σ | S | LOD | LOQ |
|-------|-------|---|-------------------|----------|--------|-------|-------|
| 35.0 | 35.6 | | | | | | |
| 70.0 | 71.6 | | | | | | |
| 140.0 | 142.5 | 6 | 230.64 | 7.59 | 1.7893 | 12.73 | 42.44 |
| 245.0 | 249.4 | | | | | | |
| 350.0 | 356.6 | | | | | | |
| 700.0 | 712.6 | | | | | | |

The LOD and LOQ for DPPC are 12.73 and 42.44 ppm.

3.2.2.4.3. Test of dilution of a standard stock solution

The standard stock dilution test is the verification that the analyte presents no problem of solubility or precipitation in the medium used for the dissolution of the lyophilized samples. The standard stock solution (theoretical concentration) is diluted to half the initial concentration, and the real concentration (experimental concentration) is determined with the calibration curve. These can be accomplished using the diluted stock to prepare three different diluted points. If the theoretical and the experimental concentration are similar, it means there is not precipitation of the sample. The percentage of recovery is calculated using the **Equation 3.4**.

$$\% \text{ Recovery} = \frac{\text{Experimental concentration}}{\text{Theoretical concentration prepared}} \times 100 \quad \text{(Equation 3.4)}$$

A recovery near the 100% (90-110%) indicates that there are no problems with the dissolution of the analyte.

For the stock dilution test of cholesterol_PEG200_RGDether, the stock of 104.0 ppm was diluted to 45.8 ppm, preparing then three points at 9.2, 18.3 and 32.0 ppm. The results are shown in **Table 3.7**.

Table 3.7: Stock dilution test results for cholesterol_PEG200_RGDether.

| Peak area | log area | log concentration | Theoretical Concentration | | %recovery |
|-----------|----------|-------------------|---------------------------|-------|-----------|
| | | | (ppm) | (ppm) | |
| 19.5 | 1.29 | 0.94 | 8.8 | 9.1 | 96 |
| 81.8 | 1.91 | 1.28 | 19.0 | 18.3 | 104 |
| 240.4 | 2.38 | 1.53 | 33.9 | 32.0 | 106 |

Since the recovery is near the 100%, there are no problems of solubility of the stock of cholesterol_PEG200_RGDether.

In the case of cholesterol, the stock of 248.3 ppm was diluted to 125.1 and then three diluted points (25.0, 43.8 and 62.6) were prepared. The results are collected in **Table 3.8**.

Table 3.8: Stock dilution test results for cholesterol.

| Peak area | log area | log concentration | Theoretical Concentration | | %recovery |
|-----------|----------|-------------------|---------------------------|-------|-----------|
| | | | (ppm) | (ppm) | |
| 18.1 | 1.26 | 1.40 | 25.2 | 25.0 | 100.5 |
| 44.6 | 1.65 | 1.61 | 41.2 | 43.8 | 94.0 |
| 83.8 | 1.92 | 1.76 | 58.1 | 62.6 | 92.8 |

The percentage of recovery for the stock dilution test of cholesterol is acceptable for considering the stock dilution test validated.

For the stock dilution test of DPPC, the stock of 699.6 ppm was diluted to 359.5, and then three different diluted points were prepared (179.8, 125.8 and 71.9 ppm). The results are gathered in **Table 3.9**.

Table 3.9: Stock dilution test results for DPPC.

| Peak area | log area | log concentration | Theoretical Concentration concentration | | %recovery |
|--------------|-------------|----------------------|--|-------|-----------|
| | | | (ppm) | (ppm) | |
| 323.6 | 2.51 | 2.26 | 181.3 | 179.8 | 100.9 |
| 153.7 | 2.19 | 2.09 | 124.2 | 125.8 | 98.7 |
| 46.3 | 1.67 | 1.83 | 67.5 | 71.9 | 93.9 |

The percentage of recovery for the stock dilution test of DPPC is acceptable for considering the stock dilution test validated.

3.2.2.4.4. Sample dilution test

Sample dilution test is very similar to the previous test, except that instead of using standards, the solubility of the samples is evaluated. The lyophilized samples are solubilized in different known volumes ($V_1=2$ mL and $V_2=5$ mL). The percentage of recovery is calculated using **Equation 3.5**.

$$\% \text{ Recovery} = \frac{\text{Concentration in } V_1 \times V_1/V_2}{\text{Concentration in } V_2} \times 100 \quad (\text{Equation 3.5})$$

A recovery near the 100% indicates that there are no problems with the solubility of the sample. The acceptance limit is between 90-110% and the relative standard deviation (RSD) must be less than 10%.

Table 3.10: Dilution test results for cholesterol_PEG200_RGDether

| Sample | Volume (mL) | Peak area | RSD % | log area | log concentration | Concentration (ppm) | Average |
|---------------------|-------------|-----------|-------|----------|-------------------|---------------------|---------|
| V ₁ (#1) | | 243.3 | | 2.39 | 1.64 | 44.0 | |
| V ₁ (#2) | 2 | 238.2 | 2.04 | 2.38 | 1.64 | 43.5 | 44.0 |
| V ₁ (#3) | | 248.1 | | 2.39 | 1.65 | 44.5 | |
| V ₂ (#4) | | 54.5 | | 1.74 | 1.27 | 18.8 | |
| V ₂ (#5) | 5 | 56.7 | 2.76 | 1.75 | 1.28 | 19.2 | 19.1 |
| V ₂ (#6) | | 57.5 | | 1.76 | 1.29 | 19.4 | |

The percentage of recovery for the samples dilution test of cholesterol_PEG200_RGDether, according to **Equation 3.5**, using as V₁= 2 mL and V₂= 5 mL is 108%. Thus, the percentage of recovery is validated.

Table 3.11: Dilution test results for cholesterol

| Sample | Volume (mL) | Peak area | RSD % | log area | log concentration | Concentration (ppm) | Average |
|---------------------|-------------|-----------|-------|----------|-------------------|---------------------|---------|
| V ₁ (#1) | | 769.5 | | 2.89 | 2.03 | 107.7 | 108.1 |
| V ₁ (#2) | 2 | 783.3 | 0.92 | 2.89 | 2.04 | 108.8 | |
| V ₁ (#3) | | 773.2 | | 2.89 | 2.03 | 108,0 | |
| V ₂ (#4) | | 143.8 | | 2.16 | 1.62 | 41.9 | 43.0 |
| V ₂ (#5) | 5 | 153.4 | 3.83 | 2.19 | 1.64 | 43.5 | |
| V ₂ (#6) | | 154,,1 | | 2.19 | 1.64 | 43.6 | |

The percentage of recovery for the samples dilution test of cholesterol, according to **Equation 3.5**, is 99%. Thus, the percentage of recovery is validated.

Table 3.12: Dilution test results for DPPC

| Sample | Volume (mL) | Peak area | RSD % | log area | log concentration | Concentration | Average |
|---------------------|-------------|-----------|-------|----------|-------------------|---------------|---------|
| V ₁ (#1) | | 3461 | | 3.54 | 2.54 | 345.5 | |
| V ₁ (#2) | 2 | 3481 | 0.34 | 3.54 | 2.54 | 346.6 | 345.9 |
| V ₁ (#3) | | 3460.3 | | 3.54 | 2.54 | 345.5 | |
| V ₂ (#4) | | 643.3 | | 2.81 | 2.13 | 134.9 | |
| V ₂ (#5) | 5 | 669.5 | 3.93 | 2.83 | 2.14 | 138.0 | 137.9 |
| V ₂ (#6) | | 695.9 | | 2.84 | 2.15 | 141.0 | |

The percentage of recovery for the samples dilution test of DPPC, according to **Equation 3.5**, is 99%. Thus, the percentage of recovery is validated.

3.2.2.4.5. Accuracy

The accuracy of an analytical procedure expresses the closeness of agreement between the real value and the value found¹¹². To assess the accuracy, it was performed the standard addition method.

Matrix refers to the components of the sample that are not the analytes. When the matrix interferes in the measure, it is called matrix effect. To assess this effect, the samples are spiked with standards. For this, three different aliquots are prepared: the standard to test (P) coming from the stock solution containing the three analytes, the sample (S) that contains only the freeze-dried liposomes, and the same sample spiked with standard (S+P). The quantity of P added should be in the range of 50% and 150% of this component in the real sample. The percentage of recovery is calculated using **Equation 3.6**.

$$\% \text{ Recovery} = \frac{[P+S]-[S]}{[P]} \times 100 \quad (\text{Equation 3.6})$$

A recovery near the 100% will indicate the absence of matrix effect and an acceptable accuracy. The acceptance limit is between 90-110% and the RSD must be less than 10%.

Table 3.13: Data results of the accuracy test of cholesterol_PEG200_RGDether

| Sample | Peak area | RSD% | log area | log concentration | Concentration (ppm) | Average |
|-----------------|-----------|------|----------|-------------------|---------------------|---------|
| Sample 1 (S) | 243.3 | | 2.39 | 1.64 | 44.0 | |
| Sample 2 (S) | 238.2 | 2.04 | 2.38 | 1.64 | 43.5 | 44.02 |
| Sample 3 (S) | 248.1 | | 2.39 | 1.65 | 44.5 | |
| Standard (P) | 100.6 | | 2.00 | 1.43 | 26.6 | |
| Standard (P) | 88.5 | 6.50 | 1.95 | 1.39 | 24.8 | 25.83 |
| Standard (P) | 96.9 | | 1.99 | 1.42 | 26.1 | |
| S + P | 484.8 | | 2.69 | 1.81 | 65.2 | |
| S + P | 545.9 | 7.04 | 2.74 | 1.84 | 69.7 | 68.36 |
| S + P | 551.9 | | 2.74 | 1.85 | 70.2 | |

In the accuracy test, the percentage of recovery, following **equation 3.6**, is 94%. Therefore, the method has been demonstrated to be accurate enough for the intended purpose of cholesterol_PEG200_RGDether quantification and adequate for routine analysis.

Table 3.14: Data results of the accuracy test of cholesterol

| Sample | Peak area | RSD % | log area | log concentration | Concentration (ppm) | Average |
|-----------------|-----------|-------|----------|-------------------|---------------------|---------|
| Sample 1 (S) | 769.5 | | 2.89 | 2.03 | 107.7 | |
| Sample 2 (S) | 783.3 | 0.92 | 2.89 | 2.04 | 108.8 | 108.15 |
| Sample 3 (S) | 773.2 | | 2.89 | 2.03 | 108.0 | |
| Standard (P) | 280.9 | | 2.45 | 1.79 | 61.1 | |
| Standard (P) | 262.7 | 3.69 | 2.42 | 1.77 | 58.8 | 59.68 |
| Standard (P) | 264.9 | | 2.42 | 1.77 | 59.1 | |
| S + P | 1670.5 | | 3.22 | 2.22 | 166.5 | |
| S + P | 1667.8 | 1.05 | 3.22 | 2.22 | 166.4 | 167.03 |
| S + P | 1699.7 | | 3.23 | 2.23 | 168.2 | |

In the accuracy test, the percentage of recovery, following **equation 3.6**, is 99%. Therefore, the method has been demonstrated to be accurate enough for the intended purpose of cholesterol quantification and adequate for routine analysis.

Table 3.15: Data results of the accuracy test of DPPC.

| Sample | Peak area | RSD % | log area | log concentration | Concentration (ppm) | Average |
|-----------------|-----------|-------|----------|-------------------|---------------------|---------|
| Sample 1 (S) | 3461 | | 3.54 | 2.54 | 345.5 | |
| Sample 2 (S) | 3481 | 0.34 | 3.54 | 2.54 | 346.6 | 345.87 |
| Sample 3 (S) | 3460.3 | | 3.54 | 2.54 | 345.5 | |
| Standard (P) | 992.8 | | 3.00 | 2.24 | 171.9 | |
| Standard (P) | 934.6 | 4.10 | 2.97 | 2.22 | 166.2 | 167.61 |
| Standard (P) | 918.9 | | 2.96 | 2.22 | 164.7 | |
| S + P | 6091 | | 3.78 | 2.68 | 473.9 | |
| S + P | 6556.9 | 5.00 | 3.82 | 2.69 | 493.8 | 489.32 |
| S + P | 6711.3 | | 3.83 | 2.70 | 500.3 | |

In the accuracy test, the percentage of recovery, following **equation 3.6**, is 86%, the result is near the acceptance limit of 90%, thus, the method has been demonstrated to be accurate enough for DPPC quantification.

3.2.2.4.6. Precision

The precision of an analytical procedure expresses the closeness of agreement (degree of scatter) between a series of measurements obtained from multiple sampling of the same homogeneous real sample under the prescribed conditions. The precision was assessed by the analysis of three freeze-dried aliquots coming from the same sample. The RSD of the triplicates must be inferior to 10%.

Table 3.16: Precision of cholesterol_PEG200_RGDether, cholesterol and DPPC

| Sample | % Recovery | RSD % |
|-----------------------------|------------|-------|
| | 31.77 | |
| Cholesterol_PEG200_RGDether | 38.81 | 9.98 |
| | 36.07 | |
| | 67.67 | |
| Cholesterol | 76.50 | 7.74 |
| | 78.46 | |
| | 66.12 | |
| DPPC | 75.91 | 8.41 |
| | 77.48 | |

All the determinations during the validation have an RSD ≤ 10 %. All the precision values are accepted for the quality criteria.

3.2.2.4.7. Quality criteria

To consider the methods validated, the obtained data must meet the quality criteria. Thus, the calibration curves must be linear with a correlation coefficient (R^2) higher than 0.99. The calculated percentage of recovery of each analyzed sample must be in the ranges specified above.

For the systematic analysis of sample, a Quality Control (QC) test was developed in order to evaluate the change over time of ELSD response. For this, a standard is injected systematically prior, during, and after the injection sequence to verify the stability of the performance. For instance, if the logarithm of the peak area changes more than a 10%, the response is non-stable and recalibration is needed before re-injecting the samples.

Once the method has been validated, the recovery of each analyzed sample is calculated using the **Equation 3.7**.

$$\% \text{ Recovery} = \frac{\text{Experimental concentration of DELOS-susp}}{\text{Theoretical concentration of DELOS-susp}} \times 100 \quad \text{(Equation 3.7)}$$

The method has been validated so it can be applied to determine the real concentration of cholesterol_PEG200_RGDether, cholesterol and DPPC in liposomes.

3.2.2.5. Sample analysis: quantification of lipids in liposomal formulations

Three different batches of liposomes-RGD_ether were prepared, lyophilized and analyzed following the methodologies described (Experimental Section 7.2.1.2).

The **Table 3.17** shows the percentage of recovery calculated for each component of membrane. The results are the average between three different lyophilized vials. As it is shown, the incorporation of DPPC and cholesterol is around 70%, and the cholesterol_PEG200_RGDether around 30%. The low recovery of the cholesterol_PEG200_RGDether can be expected from the DELOS-SUSP procedure: since the cholesterol_PEG200_RGDether is barely soluble in ethanol, an ethanolic suspension of the three membrane components (DPPC, cholesterol and cholesterol_PEG200_RGDether) was put inside the reactor to be pressurized with compressed CO₂. It is reasonable to expect loss of material during the process (pipettes, vials and finally the reactor) which can explain the results obtained. Further work developed in next Chapter 4 was done in order to ameliorate the incorporation of the membrane components in the final liposomal formulation.

Table 3.17: Recoveries achieved for the membrane components of liposomes-RGD.

| Batch | %Recovery | | |
|-------|-----------------------------|-------------|----------|
| | Cholesterol_PEG200_RGDether | Cholesterol | DPPC |
| #1 | 31±4 | 71±4 | 71±4 |
| #2 | 30±2 | 67±2 | 69±3 |
| #3 | 31±1 | 71.2±0.3 | 72.1±0.5 |

3.3. Summary and conclusions

- A HPLC-ELSD methodology for the quantification of DPPC, cholesterol and cholesterol_PEG200_RGDether has been successfully developed.
- The validation of HPLC-ELSD method has been performed in terms of linearity, goodness of fit, limit of detection, limit of quantification, precision and accuracy.
- The low concentration and recovery of cholesterol_PEG200_RGDether in real samples of liposomes-RGD_ether, in comparison to the recovery of the other membrane components cholesterol and DPPC, may be due to the low solubility of this membrane component in ethanol during the preparation of the liposomes-RGD_ether by DELOS-SUSP.

4. Optimization of the preparation method of liposomes-RGD and their chemical composition

4.1. Introduction

For an optimal preparation of vesicular systems using DELOS-SUSP technology is necessary the dissolution of the lipophilic components in an organic solvent, like ethanol. While the cholesterol and the phospholipid DPPC are well dissolved in ethanol, the cholesterol_PEG200_RGDether is barely soluble in this solvent. In previous studies, for the preparation of liposomes-RGD_ether a suspension of the three membrane components, with non-completely solubilized cholesterol_PEG200_RGDether, was added to the reactor as described in Experimental Section 7.2.1.2. However, this implies some problems, mainly the loss of cholesterol_PEG200_RGDether during the manipulation with pipettes, vials and the reactor. Indeed, the results described in the previous Chapter 3 showed there is a low incorporation of cholesterol_PEG200_RGDether in the final liposomal formulation, indicating a higher loss of this membrane component in comparison to the other two.








On the other hand, it was observed that the liposomes-RGD_ether formulations prepared with DELOS-sup experience a pH change along time which impact in their stability.

In the present chapter, are described the experiments and studies performed for: 1) finding a good solvent for cholesterol_PEG200_RGDether that avoids the loss of this liposomal membrane component during the preparation of liposomes-RGD_ether by DELOS-susp, and 2) finding an appropriate membrane composition that reduces the impact of pH change on the stability of the liposomes-RGD_ether samples.

4.2. Solvents for dissolving cholesterol_PEG200_RGDether

In order to achieve higher concentrations of cholesterol_PEG200_RGDether in the liposomal membrane and more reproducible final formulation, a screening of organic solvents was carried out to find the best one able to dissolve the cholesterol_PEG200_RGDether. Several alternative solvents to ethanol, used so far for the preparation of the liposomes-RGD_ether were tested to accomplish this purpose (see **Table 4.1**).

Table 4.1: Capability of different solvents to completely dissolve the cholesterol_PEG200_RGDether

| Solvents | Capability to completely solubilize the cholesterol_PEG200_RGDether |
|---------------------------|--|
| Acetone |  |
| Hexane |  |
| Acetonitrile |  |
| Methanol |  |
| Chloroform |  |
| Dimethylformamide (DMF) |  |
| Dimethyl sulfoxide (DMSO) |  |

Chloroform, DMF and DMSO were able to completely solubilize the cholesterol_PEG200_RGD. However, we knew from the results described in the previous Chapter 3 about HPLC that the recoveries of cholesterol_PEG200_RGDether in chloroform were not acceptable. Besides, chloroform is not miscible in water, which

makes it incompatible with the DELOS-SUSP process. Interestingly, although used in the mobile phase of the HPLC-ELSD methodology, methanol was not an adequate solvent to solubilize this membrane component at the concentrations used for DELOS-SUSP.

Since DPPC is not soluble in DMSO and DMF, we needed to use mixtures of these solvents and ethanol. Due to toxicity concerns regarding the final biological application of the nanovesicles, a low quantity of dimethyl sulfoxide, DMSO (1% of the final formulation) was selected to dissolve the cholesterol_PEG200_RGDether. According to ICH TrQ3C (R6) Impurities: Guideline for Residual Solvents, both ethanol and DMSO belong to Class 3, which means they are solvents with low toxic potential. In contrast, DMF belongs to Class 2, where the solvents must be limited.

Therefore, in this thesis, a mixture of ethanol and DMSO was used to prepare the liposomes-RGD_ether: the ethanolic solution of cholesterol and DPPC was slowly added to the solution of cholesterol_PEG200_RGDether in DMSO. The final mixture, completely transparent, was put inside the reactor. The system was maintained at 308 K and 10 MPa during approximately 1 hour, and then depressurized over 24 mL of Milli-Q water.

As can be observed with the DLS measurements gathered in **Table 4.2**, the liposomes-RGD_ether prepared with the ethanolic-DMSO solution have a reduced size and polydispersity index when compared with the liposomes-RGD_ether prepared with the ethanolic suspension. Cryo-TEM images of **Figure 4.1** showed very similar liposomes, mostly small unilamellar vesicles.

Table 4.2: Physicochemical characteristics of liposomes-RGD_ether prepared either with an ethanolic suspension of the three membrane components, or an ethanolic-DMSO solution of the membrane components.

| Liposomal systems | Size | | Z potential (mV) |
|---|------------------------|------------------|------------------|
| | Mean ^a (nm) | Pdl ^b | |
| LP-RGDe prepared with ethanolic suspension | 160±1 | 0.38±0.02 | 30±2 |
| LP-RGDe prepared with ethanolic-DMSO solution | 146±2 | 0.221±0.009 | 24±1 |

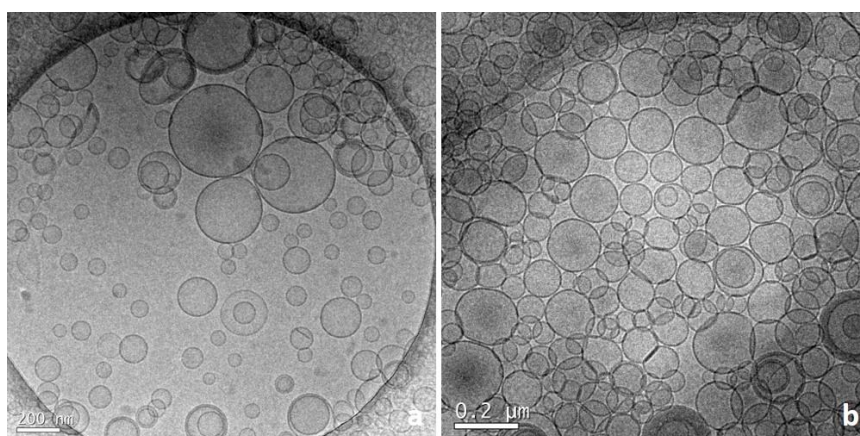


Figure 4.1: cryo-TEM images of a) liposomes-RGD_ether prepared with a suspension of the three membrane components in ethanol, and b) liposomes-RGD_ether prepared with an ethanolic-DMSO solution of the membrane components. Scale bars are 200 nm.

4.3. pH monitoring

We have observed a possible influence of the pH in the stability of the liposomes. Due to the use of the CO₂ during the DELOS-SUSP procedure, we knew that the formulations obtained from the reactor are slightly acidic. However, the management of the sample (opening of the vial and diafiltration process) involves a release of the CO₂ and this might influence on the pH of the sample and on its stability. Therefore,

we decided to do a systematic stability and pH monitoring of different liposome-RGD samples.

The liposomes-RGD_ether obtained from the reactor (from the ethanolic-DMSO solution of the three membrane components) presented appropriate macroscopic appearance, mean vesicle size, polydispersity index and Z-potential. One week after production, the liposomes were diafiltrated as it is explained in Experimental Section 7.4.1. After diafiltration, the good physicochemical characteristics of the systems were lost resulting in the sedimentation of the sample in two distinctly phases: organic material and aqueous transparent phase (see **Figure 4.1**). The main change during the diafiltration is the substitution of the medium (Milli-Q water with 4% ethanol and 1% DMSO) for Milli-Q water alone. In order to discard the influence of the ethanol and DMSO in the sample destabilization, samples were diafiltrated in the same composition medium obtained from the reactor. They were also destabilized. Besides, diluting the systems in both water and medium resulted in the aggregation of the samples.

The sedimentation of the samples also happened when the vials were opened repeatedly, since the presence of CO₂ in the sample, coming from the DELOS-SUSP is reduced with the escaping of this gas. Therefore, although samples obtained from DELOS-SUSP are slightly acidic, after diafiltrating the samples both with pure Milli-Q water and with Milli-Q water with 4% ethanol and 1% DMSO, the pH of the sample becomes near neutral suggesting the loss of the CO₂ from the sample.

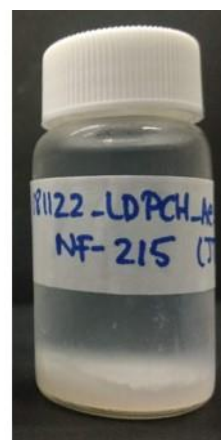
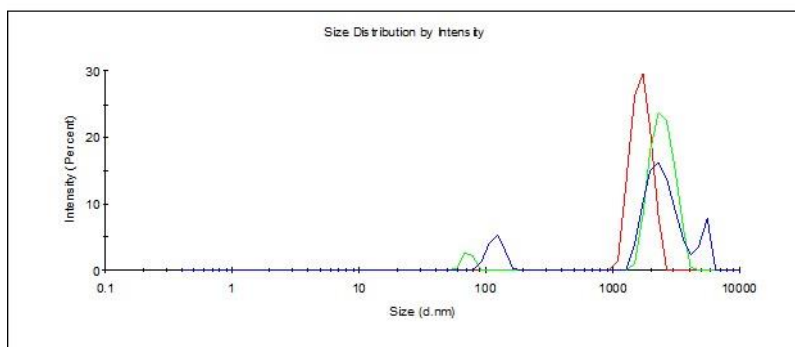


Figure 4.2: Sedimentation of liposomes-RGD_ether sample. DLS measurements not meeting quality criteria, and macroscopic appearance.

In order to confirm the relationship between the presence of CO₂ and the pH of the sample, and to study the impact of pH variation on liposomal stability, the samples described in **Figure 4.3** and **Table 4.3** were produced using DELOS-susp technology, and their pH and stability were monitored along time, since their preparation.

The pH monitoring was performed over plain liposomes without RGD, and over two different types of liposomes functionalized with RGD differing only in the conjugation bond between the cholesterol and the PEG200 linker (see **Figure 4.3**). We decided also to include in these experiments liposome-hybrid systems, which contain myristalkonium chloride (MKC) as stabilizer (see **Figure 4.3**). In these new liposomal systems, MKC represents the 2.2% molar ratio of the total membrane components. This new component is a quaternary ammonium surfactant, which provides cationic charge to the lipid bilayer enhancing the electrostatic interaction with e.g. the negatively charged GLA protein and stabilizing the system. The GLA is negatively charged at the pH in which the nanovesicles are self-assembled since the isoelectric point of the enzyme is around 5.6.

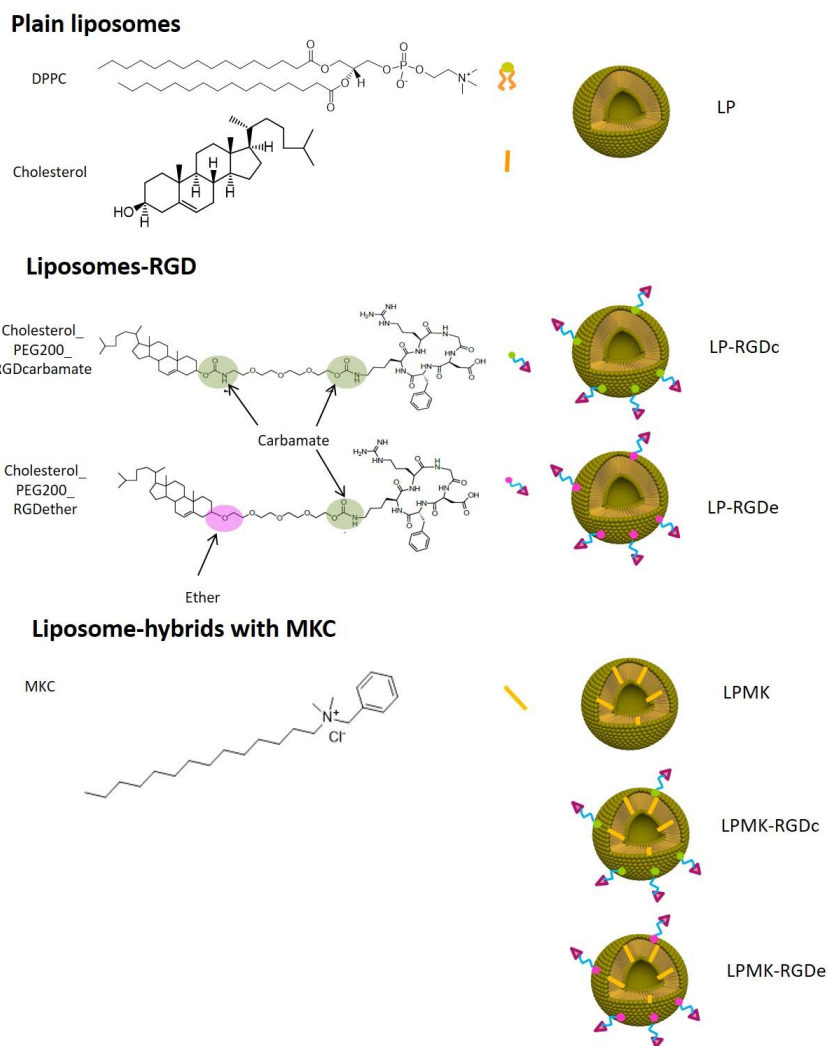


Figure 4.3: Schematic representation of the six types of liposomes included in the pH monitoring study

Table 4.3: Compositions and ratios used for the preparation of liposomes by DELOS-SUSP using CO₂-expanded ethanolic solutions at 10MPa, 308K and X_{CO₂} = 0.85.

| Liposomal systems [number of batches] | Theoretical composition | Organic phase | Aqueous phase | Lipidic concentration ^a (µg mL ⁻¹) |
|---|--|-------------------------------|---------------|--|
| Plain liposomes (without MKC) LP [2] | Cholesterol (19 mM) + DPPC (27 mM) | Ethanol | Water | 1.4 |
| Liposomes- RGD_ether (without MKC) LP-RGDe [2] | Cholesterol (17 mM) + DPPC (27 mM) + Chol-PEG ₂₀₀ -RGD (2.8 mM) | Ethanol (83%) + DMSO (17%) | Water | 1.6 |
| Liposomes- RGD_carbamate (without MKC) LP-RGDc [2] | Cholesterol (17 mM) + DPPC (27 mM) + Chol-PEG ₂₀₀ -RGD (2.8 mM) | Ethanol (83%) + DMSO (17%) | Water | 1.6 |
| Plain liposomes (with MKC) LPMK [2] | Cholesterol (19 mM) + DPPC (27 mM) + MKC (0.001 mM) | Ethanol | Water | 1.4 |
| Liposomes- RGD_ether (with MKC) LPMK-RGDe [2] | Cholesterol (17 mM) + DPPC (27 mM) + Chol-PEG ₂₀₀ -RGD_ether (2.8 mM) + MKC (0.001 mM) | Ethanol (83%) + DMSO (17%) | Water | 1.6 |
| Liposomes- RGD_carbamate (with MKC) LPMK-RGDc [2] | Cholesterol (17 mM) + DPPC (27 mM) + Chol-PEG ₂₀₀ - RGD_carbamate (2.8 mM) + MKC (0.001 mM) | Ethanol (83%) + DMSO (17%) | Water | 1.6 |

In **Table 4.3**, are summarized the operational parameters for the preparation of nanoliposomes using DELOS-SUSP procedure (see Experimental Section 7.2.1.2).

Physicochemical characterization of all samples of **Table 4.3** was performed on the same day of their preparation in terms of size, polydispersity index, surface charge and

pH. The progress of these physicochemical characteristics along time was studied also by DLS and pH measurements.

As expected because the acidic pH was related with the presence of CO₂ in the sample, the pH monitoring revealed an increment in the value towards neutral pH values when the vial of the sample was opened repeatedly. In addition, when the sample was diafiltrated, the pH raised to the value of the used Milli-Q water (**Figure 4.4**).

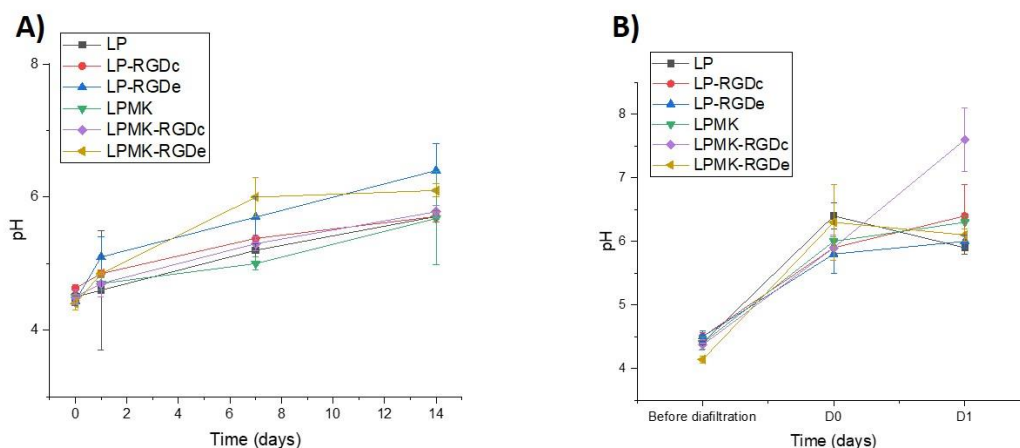


Figure 4.4: Evolution of pH vs time (A) and diafiltration process (B). D0 refers to time 0 days after diafiltration and D1 refers to time 1 day after diafiltration. Each value is the mean of two different batches.

We systematically observed that when the pH increases, whether by diafiltration or by repeated opening of the vial to perform the measurements, the systems with RGD and without MKC tend to sediment at 7 days after production and 1 day after diafiltration while plain systems and RGD systems with MKC remain stable. Remarkably, in some cases of plain liposomes without RGD and MKC, a little sediment easily resuspended is formed at the bottom of the vial.

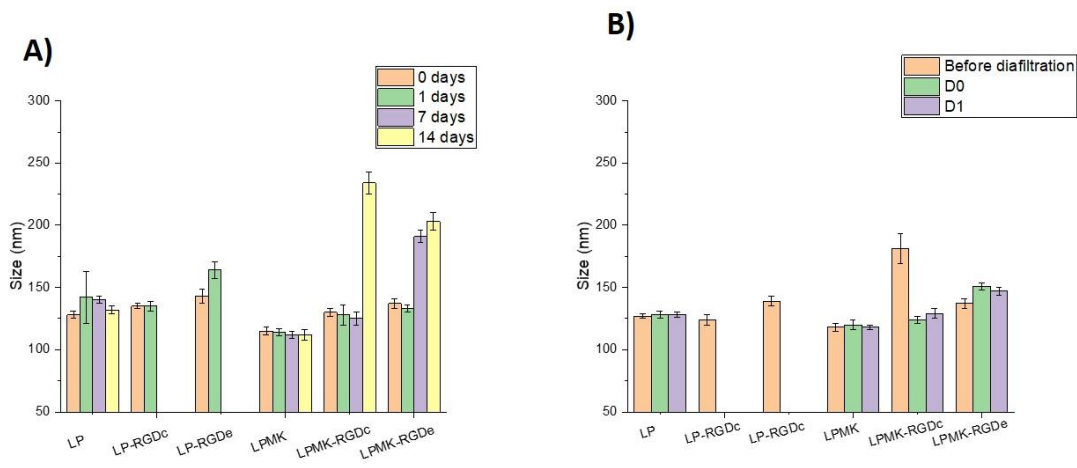


Figure 4.5: Evolution of size vs time (A) and diafiltration process (B). Systems ether and carbamate sediment at 7 days after production and 1 day after diafiltration not meeting quality criteria for the determination of the size. Plain systems and systems with RGD and with MKC remain stable in both cases. D0 refers to time 0 days after diafiltration and D1 refers to time 1 day after diafiltration. Each value is the mean of two different batches.

The expected results regarding the polydispersity index are an increment in the PDI of the systems with RGD and without MKC, as it is shown in the case of the liposomes-RGD_{ether}. However, there is not the data obtained for the liposomes-RGD_{carbamate}. The plain systems and the systems with MKC (plain, RGD_{ether} and RGD_{carbamate}) were expected to have a similar PDI not varying with the time after production and diafiltration.

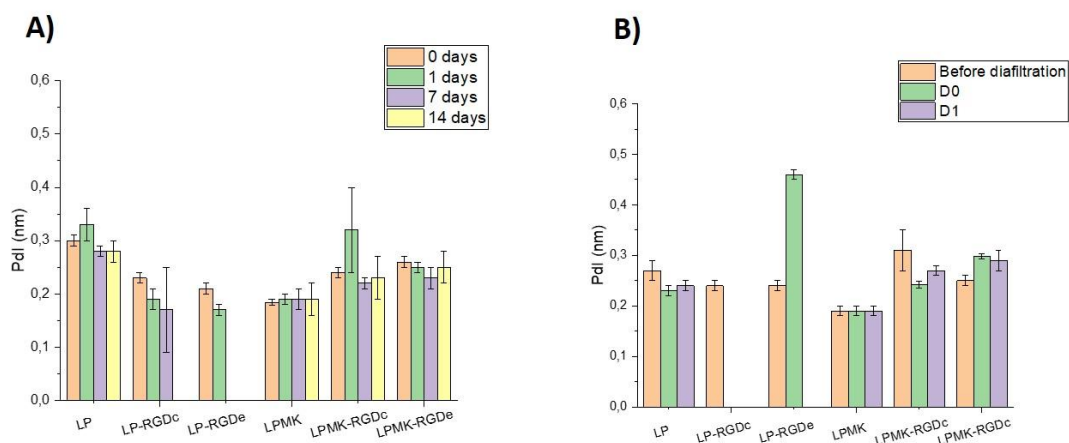


Figure 4.6: Evolution of Pdl vs time (A) and diafiltration process (B). The Pdl was expected to increase in the case of liposomes-RGD either ether or carbamate, whereas remained stable for plain and RGD systems with MKC. Systems without MKC, sedimented, not meeting the quality criteria for the DLS measurements, therefore they are nor represented in the Figure. D0 refers to time 0 days after diafiltration and D1 refers to time 1 day after diafiltration. Each value is the mean of two different batches.

The Z potential decreases in systems with RGD (ether or carbamate) and without MKC upon sedimentation. In the case of plain liposomes, the Z potential is near zero. As was explained before, this can be the cause of the apparition of a small sediment in the vial, easily resuspended. The liposomes with MKC have a high Z potential, which is in accordance with the presence of this positively charged surfactant. This high Z potential is the probable cause of the stability of systems with MKC.

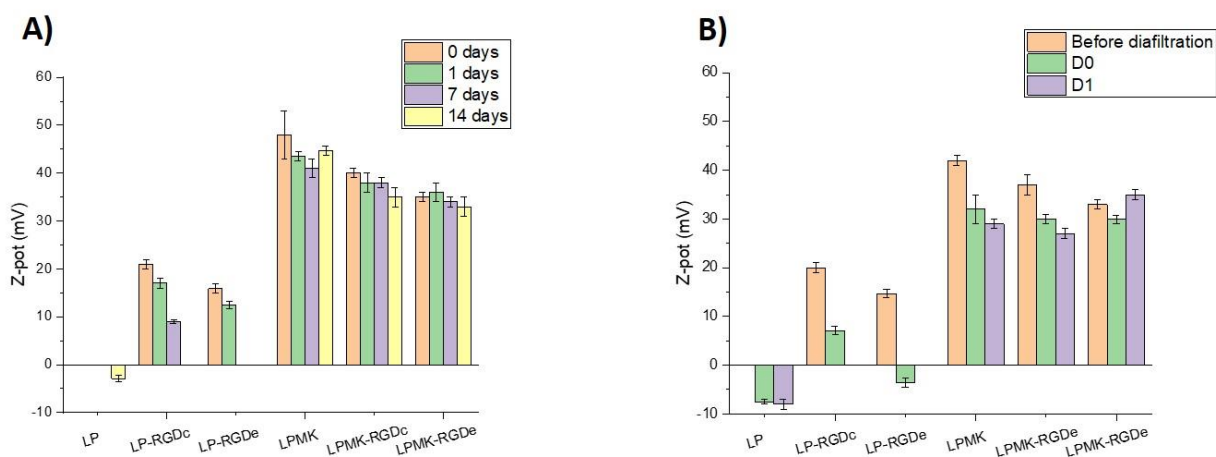


Figure 4.7: Evolution of *Z* potential (*Z*-pot) vs time (A) and diafiltration process (B). The *Z* potential decreases in liposomes-RGD upon sedimentation. *Z* potential of plain systems is low (near 0) and for the systems with MKC is very high, explaining the stability of these liposomes. D0 refers to time 0 days after diafiltration and D1 refers to time 1 day after diafiltration. Each value is the mean of two different batches.

It is true that pH has an impact in DPPC liposomes¹¹³ and films¹¹⁴, and in liposomes¹¹⁵ or monolayers¹¹⁶ composed of DPPC and cholesterol, but it is notorious at high changes in pH, whereas in our case we moved around 4.5-6 of pH. Furthermore, in our case the destabilization of the systems is more remarkable when they are functionalized with cholesterol_PEG200_RGD. However, in literature it seems that cRGDfK is not very sensitive to pH changes, being used with other pH-responsive peptides^{117,118} for stimuli-responsive liposomes¹¹⁹. There is probably some cumulative effect among the three membrane components (DPPC, cholesterol and cholesterol_PEG200_RGD) that change their interaction between pH 4.5-6. In any case, MKC gives a highly positively charge that seems to stabilize the liposome systems.

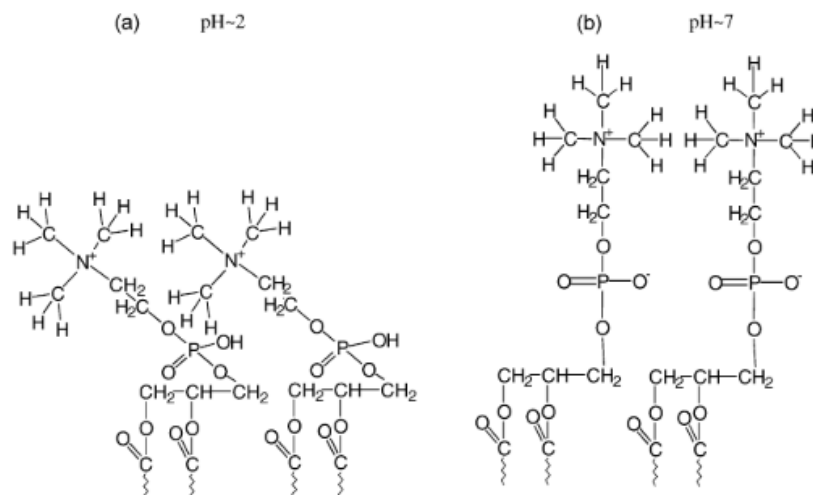


Figure 4.8: The phospholipids conformations depending on pH applied for liposome preparation. Phosphate group protonation in acid environment and the formation of hydrogen bonds between DPPC molecules could explain the differences in the properties of liposome membranes with pH. Adapted from Sułkowski, 2005¹¹⁵

Since the samples without MKC are not stable with the changes in pH derived from the evaporation of the CO₂ from the formulation obtained from the reactor, we proceeded to prepare the same systems but adding MKC to the formulation.

4.4. Summary and conclusions

- The preparation of liposomes-RGD has been improved achieving the complete dissolution of cholesterol_PEG200_RGD molecule in the organic phase by adding DMSO. Therefore, a higher incorporation of the cholesterol_PEG200_RGD is expected.
- The decrease of CO₂ content in the liposomes-RGD_ether, after their preparation by DELOS-SUSP, induces a pH increase which is the cause of the loss of their colloidal stability.
- The presence of MKC avoids the destabilization of the liposomes-RGD due to pH changes provoked by the CO₂ evaporation over time, in addition to enhancing the physicochemical properties of the liposomal formulations

5. Impact of RGD peptide functionalization mode of nanoliposomes on their cellular internalization

5.1. Introduction

One of the advantages of drug delivery systems is the ability to target specific sites¹²⁰, through passive and/or active targeting. The objective is to obtain a high local concentration of the drug in the target site, while avoiding the toxicity in healthy tissues¹²¹. Whereas conventional drug agents distribute non-specifically in the body, the specific targeting of nanocarriers improves the pharmacokinetics and pharmacodynamics of the drugs and reduces the side effects of the systemic toxicity^{122,123}.

The physicochemical features of nanoparticles like their chemical composition, particle size distribution profile, morphology, rigidity/deformability, surface chemistry, etc. modulate these targeting properties. There is a complex association of interrelated physicochemical and biological factors (drug loading, encapsulation efficiency, interaction mode with biological media and biological membranes, drug release profile or the pharmacokinetics)^{124,125}.

However, in contact with biological fluids, the nanoparticles are covered by the protein corona, which usually masks their original physicochemical features. The protein

corona refers to the absorption of biomolecules in the nanoparticles due to their high surface free energy, impacting on the physicochemical characteristics of nanoparticles and affecting their stability, particle solubility and sometimes inducing nanoparticle aggregation¹²⁶. Protein corona can promote the deposition in the nanoparticle surface of opsonins (proteins that facilitate recognition and clearance from the blood by phagocytes and macrophages) or dysopsonins (proteins that provide a prolonged blood circulation time)^{127,128}. Even though protein corona gives a new identity to nanoparticles, this corona is highly dependent on the physicochemical properties of the pristine nanoparticle (size, surface charge, composition, surface chemistry, curvature, hydrophobicity) but also on the biological fluid (relative ratio of the fluid to the nanoparticle dispersion) and environmental factors (exposure time, temperature)^{125,126,129,130,131}.

Traditionally, most of the drug delivery systems reach its targets by passive targeting which means the diffusion of the nanomedicine in the body and through the different biological membranes from the site of administration to the target tissue⁵², mainly skin mucosae epithelium, blood vessels and tissue barriers¹³². For example, cancer therapy using liposomal drug delivery is based on the enhanced permeation and retention (EPR) effect¹²⁹, typical of tumors but also of inflamed tissues like the ones of infarcts or other pathologies. Due to the anatomical and pathophysiological differences from normal tissues, tumor vasculature have several abnormalities, which include irregular architecture, poor lymphatic drainage and paracellular permeability¹³³. This ensures the sufficient supply of nutrients and oxygen to tumors for their rapid growth. The consequence is the selective extravasation and retention of macromolecular drugs larger than 40 kDa¹³⁴, with a cut-off from 200 nm to 1.2 μ m depending on the tumor type¹³⁵. The accumulation of these macromolecules inside the interstitial space was more than 10-200 times higher than in normal tissues because of the defects in the lymphatic drainage¹³⁶. Other small low-molecular-weight pharmaceutical agents are not retained in tumors since they return to the circulation by diffusion¹³³. However, not only size or molecular weight impacts on the EPR effect but also other factors like the surface charge and the in vivo surveillance system of macrophages and

phagocytes¹³⁴. Thus, passive targeting can be controlled modifying the size, shape or the surface dimensions of these nanoparticles¹³⁷.

In contrast, active targeting is based on the immobilization of targeting molecules on the nanoparticle surface with the objective of reaching specific cell types to perform their targeting action¹²⁷. Thus, a strong interaction of molecular recognition is exploited for a more specificity in the drug delivery system¹³⁷ along with multivalent interactions. Multivalent interactions refer to the simultaneous binding of multiple copies of a ligand in the nanocarriers' surfaces to various receptors in the cells. This increases the targeting since the binding of the first ligand to its receptor causes the subsequent binding of another ligand-receptor pairs^{138,139,140}. Thus, the binding to target cells can be modulated not only using the affinity of the targeting ligand but also the density of the targeting moiety in the nanocarriers' surfaces. Indeed, the density of the targeting ligand can result in higher internalization despite the low affinities of a given ligand¹⁴¹.

Targeting agents can be generally classified in proteins (mainly antibodies and their fragments), nucleic acids (aptamers), or other receptor ligands such as peptides, vitamins and carbohydrates¹³⁶.

Antibodies were the first agents employed for active targeting due to the surface antigens they present¹⁴². They can be used in their native state or as engineered fragments. There has been a great effort in the rational design of antibodies¹³⁶.

Aptamers are short single-stranded DNA or RNA oligonucleotides selected in vitro from random sequences¹³⁶. They are folded into secondary and tertiary structures with the ability of binding to specific biological targets, especially proteins. Because of their specificity, they are considered equivalent to antibodies. They present also some advantages compared with antibodies. For example, they are chemically synthesized without the need of biological systems, making the process easier to scale-up and with a lower cost¹⁴².

Other strategies are based in growth factor or vitamin interactions, taking advantage of the overexpression of receptors in cancer cells for nutrition. Common target units

employed for this objective are epidermal growth factor (EGF), the vitamin folic acid (folate) and transferrin^{136,137,142}.

The use of peptides as targeting unit results in an increased drug delivery since they promote selective binding to receptors overexpressed in cells. Compared to other ligands like antibodies, targeting peptides have a smaller size, easy chemical synthesis and modification, and more stability. Some examples are Tau peptide, NGR and RGD, among others^{143,144}.

As explained in Chapter 2, RGD-peptide is very well known to increase cellular penetration via RGD/integrin recognition. Using DELOS-SUSP process, in our group we have prepared new RGD functionalized nanoliposomes¹⁴⁵ with improved characteristics as nanocarriers for intracellular delivery¹⁴⁶. In previous works, these liposomes-RGD_ether have demonstrated a 30-fold higher cellular internalization than plain liposomes (without RGD)⁴⁹. This increased internalization was also observed when the liposomes-RGD_ether are loaded with GLA⁸⁵.

Our strategy to achieve RGD-functionalization on nanoliposomes, consist of inserting cholesterol covalently conjugated to RGD through a PEG linker (**Figure 5.1**) in the liposomal membrane.

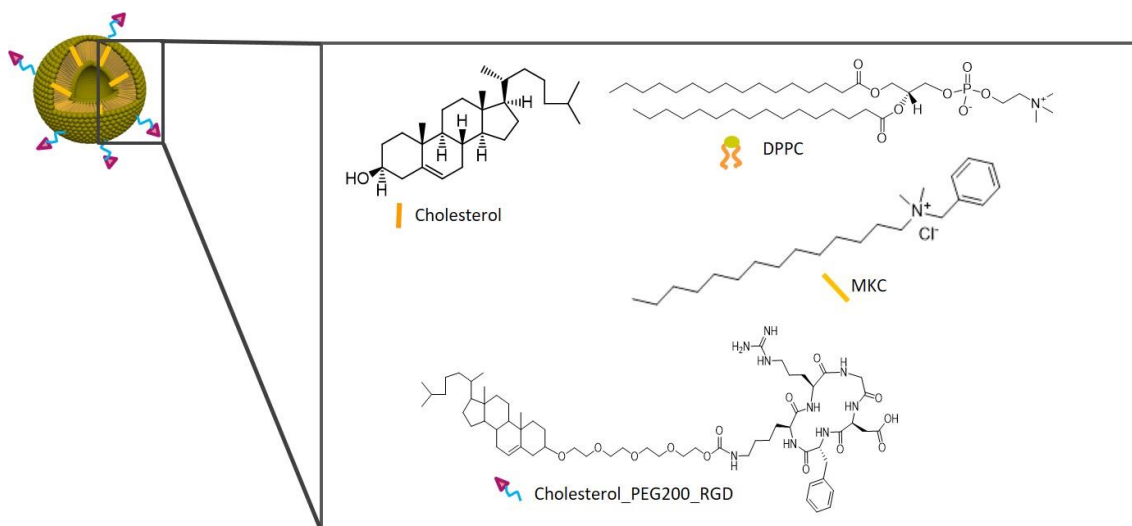


Figure 5.1: Schematic composition of liposomes composed of cholesterol, DPPC, MKC and cholesterol_PEG200_RGD.

The objective of the work described in this Chapter is to determine the impact of the conjugation mode between cholesterol and the PEG linker bounded to RGD, on the nanoliposome internalization. Two different types of conjugation were explored: ether and carbamate bond. While in the literature is commonly reported the binding of cholesterol and the PEG_RGD unit by a carbamate or ester bonds¹⁴⁷, using ether bond is a novelty introduced by our group.

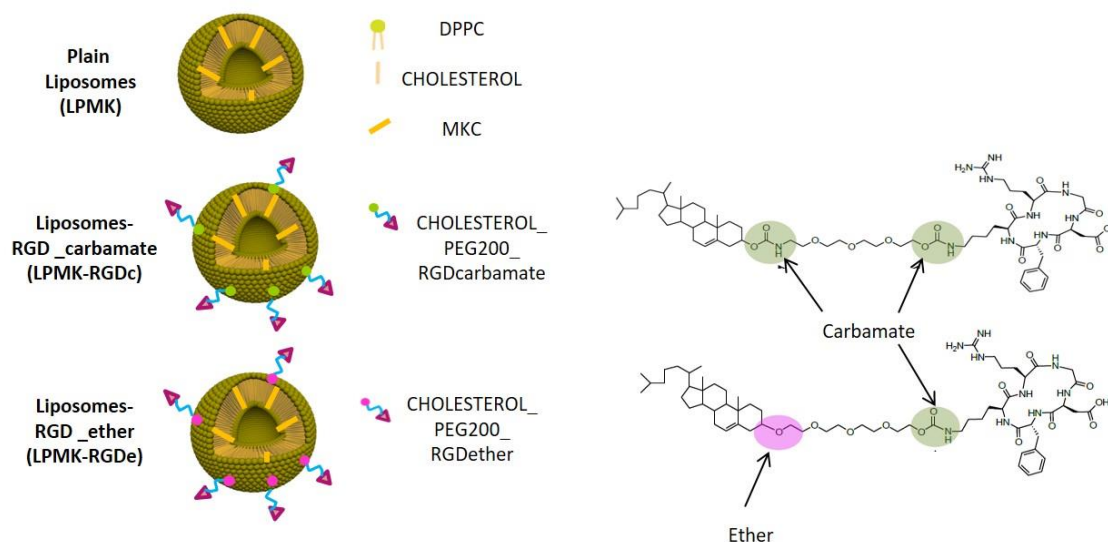


Figure 5.2: Schematic representation of the systems studied in this Chapter: plain liposomes, and liposomes-RGD_ether and carbamate, with MKC.

5.2. Preparation of liposomes by DELOS-SUSP

Following the DELOS-SUSP procedure, DPPC phospholipid, cholesterol and MKC surfactant were dissolved in ethanol, whereas cholesterol_PEG200_RGD, both ether and carbamate, were dissolved in DMSO. The ethanolic-DMSO solution was then added to the reactor. The density of RGD peptide units in the membrane of the liposomes can be tuned by the molar ratio between cholesterol_PEG200_RGD and the rest of molecular components of the nanoliposomal membrane. In this thesis, the molar ratio between DPPC, cholesterol and cholesterol_PEG200_RGD is 10:6:1 and MKC represents a 2.2% molar of the total components. The theoretical chemical compositions of the systems are shown in **Table 5.1**.

From previous works by Dr. Antonio Ardizzone, it was established that the incorporation of DiD dye in vesicular systems is enhanced when the dye is added during the process of DELOS-SUSP (in the ethanolic solution) in comparison to the incubation post-DELOS-SUSP¹⁴⁸ that was employed in Chapter 2. Thence, the three types of liposomes (plain, RGD_ether and RGD_carbamate) with DiD were prepared by DELOS-SUSP for the in vitro experiments.

We prepared three different batches of each type of liposomes (plain, liposomes-RGD ether and carbamate) without DiD, and two different batches for each system with DiD. Samples without DiD were prepared for the analysis by cryo-TEM and SAXS, with the idea that the dye does not interfere with the characterization. The samples were diafiltrated one week after production, following the procedure explained in Experimental Section 7.4.1. The DiD samples were used for the internalization studies by confocal and flow cytometry.

Table 5.1: Compositions and ratios used for the preparation of liposomes by DELOS-SUSP using CO₂-expanded ethanolic solutions at 10MPa, 308K and X_{CO₂} = 0.85.

| Liposomal systems (GLA concentration) [number of batches] | Theoretical composition | Organic phase | Aqueous phase | Lipidic concentration ^a (µg mL ⁻¹) |
|---|---|----------------------------|---------------|---|
| Plain liposomes (LPMK) [3] | Cholesterol (19 mM) + DPPC (27 mM) + MKC (0.001 mM) | Ethanol | Water | 1.4 |
| Liposomes-RGD_ether (LPMK-RGDe) [3] | Cholesterol (17 mM) + DPPC (27 mM) + Chol-PEG ₂₀₀ -RGD_ether (2.8 mM) + MKC (0.001 mM) | Ethanol (83%) + DMSO (17%) | Water | 1.6 |
| Liposomes-RGD_carbamate (LPMK-RGDc) [3] | Cholesterol (17 mM) + DPPC (27 mM) + Chol-PEG ₂₀₀ -RGD_carbamate (2.8 mM) + MKC (0.001 mM) | Ethanol (83%) + DMSO (17%) | Water | 1.6 |
| Plain liposomes with DiD (LPMK + DiD) [2] | Cholesterol (19 mM) + DPPC (27 mM) + MKC (0.001 mM) + DiD (50 nM) | Ethanol | Water | 1.4 |
| Liposomes-RGD_ether with DiD (LPMK-RGDe + DiD) [2] | Cholesterol (17 mM) + DPPC (27 mM) + Chol-PEG ₂₀₀ -RGD_ether (2.8 mM) + MKC (0.001 mM) + DiD (50 nM) | Ethanol (83%) + DMSO (17%) | Water | 1.6 |
| Liposomes-RGD_carbamate with DiD (LPMK-RGDc + DiD) [2] | Cholesterol (17 mM) + DPPC (27 mM) + Chol-PEG ₂₀₀ -RGD_carbamate (2.8 mM) + MKC (0.001 mM) + DiD (50 nM) | Ethanol (83%) + DMSO (17%) | Water | 1.6 |

5.3. Physicochemical characterization

5.3.1. Determination of size, polydispersity index and Z potential

The size, polydispersity index and Z potential was determined at time 0 (freshly produced), 1 day, 1 week and after diafiltration at time 0 (D0) and 1 day (D1). In the case of systems without DiD these attributes were also checked at 14 (D14) and 21 (D21) days, prior to the observation of the systems by cryo-TEM. Liposomes with DiD were checked at 42 (D42), 43 (D43) and 53 (D53) days by our collaborators who performed the cellular internalization. The results are the average between the replicates of each type of sample (three in the case of systems without DiD, two for the systems with DiD).

As shown in **Figure 5.3**, the size remains stable, increasing a little bit with diafiltration. The plain liposomes are smaller than the RGD ones (either ether or carbamate), which can be explained by the presence of the RGD in the membrane. This is corroborated by SAXS (**Figure 5.7**) using two parameters: Z_{head} is the position of the head-group contributions relative to the centre of the membrane and D is the distance between the bilayers. According to SAXS, plain liposomes have the smaller values of these parameters $\sim 32.2 \text{ \AA}$ and $\sim 67.9 \text{ \AA}$, respectively); whereas liposomes-RGD_ether are around $\sim 34.3 \text{ \AA}$ and $\sim 76.6 \text{ \AA}$, and liposomes-RGD_carbamate have $\sim 35.8 \text{ \AA}$ and $\sim 77.5 \text{ \AA}$. The measurements by DLS revealed no significant differences in size between RGD_ether and RGD_carbamate systems.

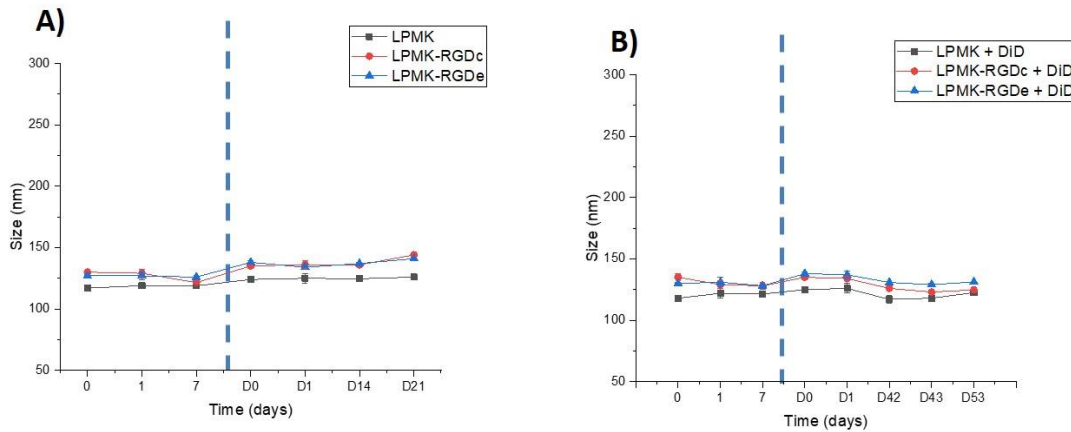


Figure 5.3: Evolution of size with time since production and diafiltration: **A)** Systems without DiD. The values are the mean of three different liposomes' batches. **B)** Systems with DiD. Each value corresponds to the mean of two different batches.

Regarding the polydispersity index (Pdl), it seems that it is lower for the liposomes-RGD_carbamate in comparison with liposomes-RGD_ether (**Figure 5.4**), but the difference is small.

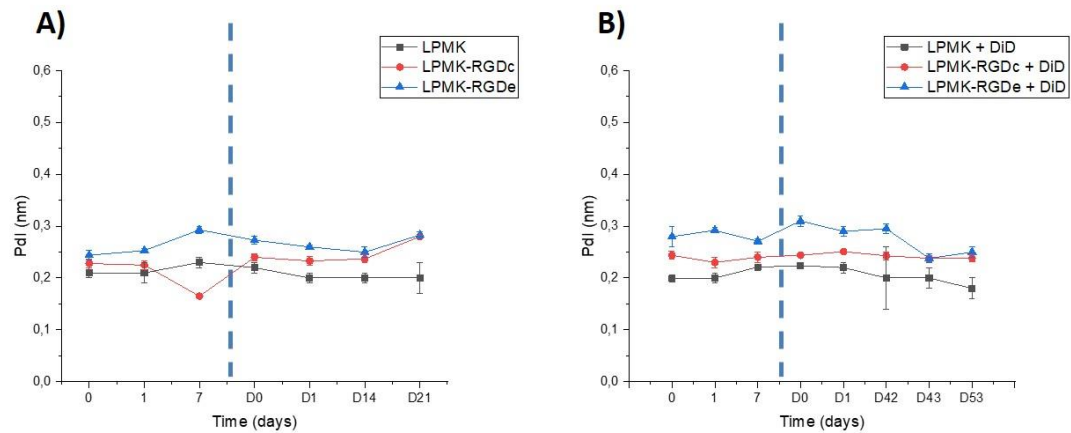


Figure 5.4: Evolution of Pdl with time since production and diafiltration: **A)** Systems without DiD. The values are the mean of three different liposomes' batches. **B)** Systems with DiD. Each value corresponds to the mean of two different batches.

The highest Z-potentials values correspond to plain systems, followed by the liposomes-RGD_carbamate, that are very similar to the values of liposomes-RGD_ether.

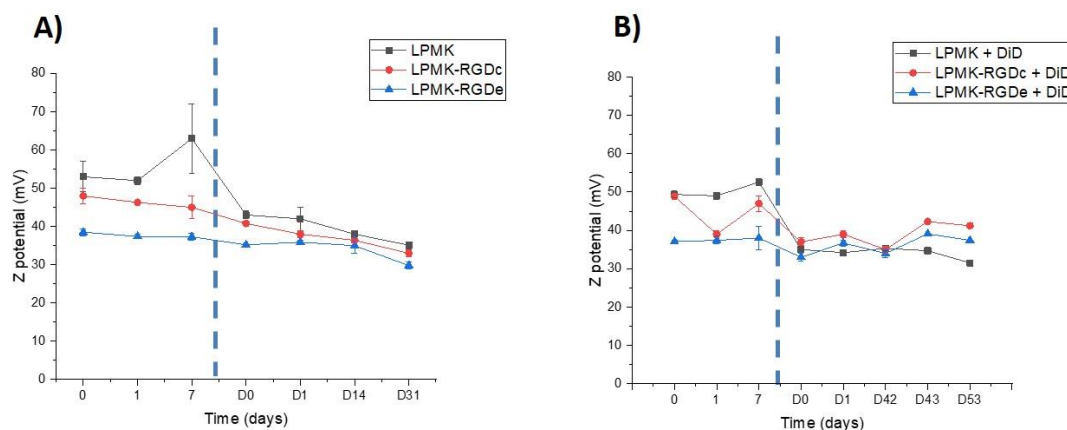


Figure 5.5: Evolution of Z potential with time since production and diafiltration: **A)** Systems without DiD. The values are the mean of three different liposomes' batches. **B)** Systems with DiD. Each value corresponds to the mean of two different batches.

5.3.2. Sample analysis: quantification of lipids in liposomal formulations

The HPLC-ELSD method developed in Chapter 3 was successfully tested, in addition to liposomes-RGD_ether matrixes, for the matrixes of plain and liposomes-RGD_carbamate with MKC for the accurate quantification of the membrane components: cholesterol and DPPC for the plain systems, and cholesterol, DPPC and cholesterol_PEG200_RGDcarbamate for the liposomes-RGD_carbamate

The **Table 5.2** shows the percentage of calculated recovery. The results are the average among three different lyophilized vials corresponding to the samples without DiD. As it is shown, the incorporation of DPPC and cholesterol is similar for the three types of liposomes, around 90%, which is significantly higher than the obtained in Chapter 3. The incorporation of cholesterol_PEG200_RGDcarbamate is slightly higher ($90\pm 12\%$) than the cholesterol_PEG200_RGDether ($78\pm 3\%$), but they are in the same order of magnitude. Compared with Chapter 3, the incorporation of cholesterol_PEG200_RGD both ether and carbamate is considerably increased, probably related with the achievement of the complete dissolution of this molecule in the organic phase previous DELOS-SUSP, thanks to the addition of DMSO, and because of the presence

of little quantity of MKC in liposomes-RGD composition, which possesses emulsifying properties.

Table 5.2: Recoveries of membrane components of plain liposomes, liposomes-RGD_ether and liposomes-RGD_carbamate.

| Sample | Batch | %Recovery | | |
|-----------|-------|------------------------|-------------|----------|
| | | Cholesterol_PEG200_RGD | Cholesterol | DPPC |
| LPMK | #1 | 0 | 92±4 | 89±13 |
| | #2 | 0 | 89±2 | 90±3 |
| | #3 | 0 | 76±2 | 79.9±0.8 |
| LPMK-RGDc | #1 | 92±11 | 89±2 | 88±4 |
| | #2 | 94±7 | 95±6 | 94±4 |
| | #3 | 85±8 | 87±2 | 86.4±0.3 |
| LPMK-RGDe | #1 | 70±2 | 79±3 | 76±7 |
| | #2 | 80±6 | 84±2 | 81±12 |
| | #3 | 85±5 | 90.75±0.07 | 86±13 |

5.3.3. Morphological analysis

Cryo-TEM images were performed in the group of Prof. Dganit Danino in Technion (Israel Institute of Technology, Israel). Three different batches of each type of sample without DiD were observed. Images showed mainly unilamellar vesicles, although in samples with RGD_carbamate, there is presence of stick-like structures, as can be seen in the selected images of **Figure 5.6** (white arrows). This may be related to the SAXS calculations (**Figure 5.7**) that found that liposomes-RGD_carbamate were bi-lamellar in contrast with plain and liposomes-RGD_ether which resulted unilamellar.

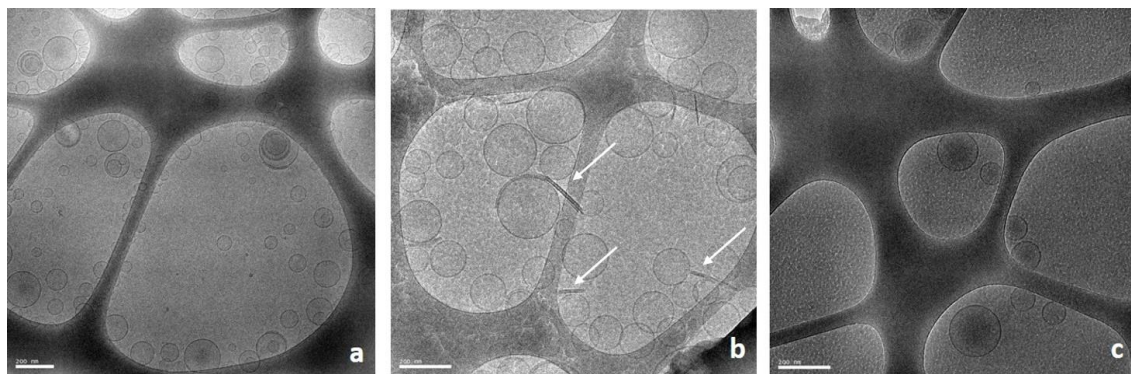


Figure 5.6: Cryo-TEM pictures showing the morphology of the nanoconjugates: a) Plain liposomes, b) liposomes-RGD_carbamate, c) liposomes-RGD_ether. Scale bars are 200 nm. The white arrows point to the stick-like structures.

5.3.4. Lamellarity determination

SAXS measurements were conducted by Prof. Jan Skov Pedersen group, from Aarhus University in Denmark. Samples analyzed by SAXS were the three replicates of each type of liposomal formulation without DiD. By applying the liposome model with and without an added polymer contribution, it was possible to successfully fit the data from all nine samples. The plain samples were fitted with the classical liposome model (without a polymer contribution). The RGD_ether and RGD_carbamate were fitted with the liposome model including a polymer contribution to properly fit the raised minima in these data due to the polymer scattering from the exterior PEG_RGD chains coating the liposomes.

There is good agreement between the fitting results from each subset of samples (plain, ether, and carbamate) and distinct differences between the sample types (**Figure 5.7**). Plain systems show an average low multilamellarity (1.2-1.3). In the liposomes-RGD_carbamate, a large decrease in the amount of unilamellar particles is observed and the average multilamellarity estimate yields liposomes that are approximately bi-lamellar (1.7-2.0). Liposomes-RGD_ether are very similar to plain systems, with a similar low average multilamellarity to a level of nearly unilamellar liposomes (1.2-1.3). As was explained in section 5.3.1, the size increased with the addition in the membrane of the cholesterol_PEG200_RGD both ether and carbamate.

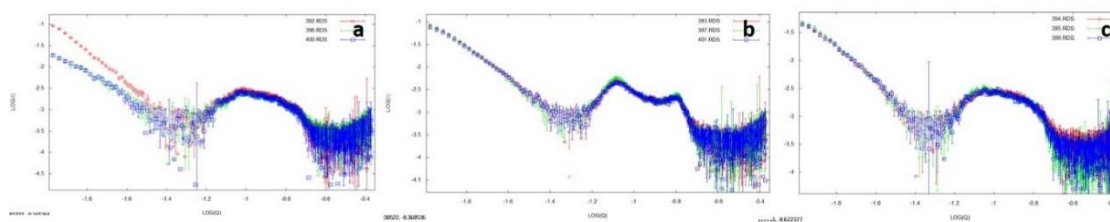


Figure 5.7: SAXS intensity profile versus the scattering vector modulus (q) recorded from: a) LPMK, b) LPMK-RGDc and c) LPMK-RGDe at 298K.

5.3.5. Quantification of DiD in the liposomal formulations

In order to perform and understand the cellular internalization studies, we decided to quantify the DiD present in the samples assessing the absorbance by UV-Vis spectrophotometer. Both flow cytometry and laser scanning confocal microscopy techniques measured the intensity of fluorescence of the nanoliposomes labelled with the dye. It is of extreme importance to discriminate if more fluorescence corresponds to more internalization or if it just that a specific type of liposome incorporates more DiD in its membrane.

Since the theoretical concentration of DiD is low (50 nM), we could not trust in the results considering the error inherent to the technique of quantification. Thence, to perform the measurements we concentrated the samples to a theoretical concentration of 250 nM (x5) using the freeze-drying procedure: we lyophilized 2.5 mL of each sample without any lyo-protectant in order to remove the water and then the lyophilized cake was dissolved in 0.5 mL of ethanol. Afterwards we analyzed the samples by UV-vis spectrophotometer.

Table 5.3: Quantification of DiD dye in the liposomes, measured by UV-vis

| Sample | Batch | DiD concentration (nM) |
|-----------|-------|------------------------|
| LPMK | #1 | 28.6 |
| LPMK-RGDc | #1 | 29.9 |
| | #2 | 26.0 |
| LPMK-RGDe | #1 | 31.3 |
| | #2 | 30.0 |

As it is shown in **Table 5.3** the concentration of DiD is around 30 nM with no big differences between batches and between each type of liposomes.

Indeed, we checked the fluorescence of the samples in water and we obtained similar values between the samples (**Figure 5.9**). We can then deduce that more intensity of fluorescence corresponds to more cellular internalization.

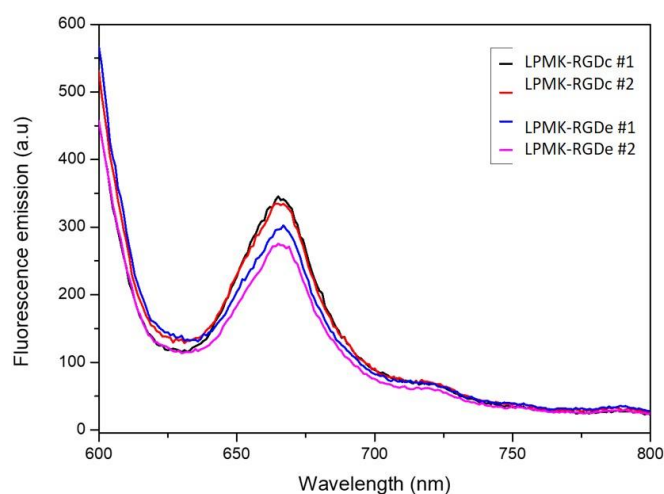


Figure 5.9: Similar fluorescence of two different batches of liposomes-RGD_ether and carbamate in water.

5.4. Biological Characterization of liposomes

5.4.1. Flow cytometry

For the flow cytometry assays, the cells were incubated during 30 and 180 min at 37 °C with 0.3 mg mL⁻¹ of liposomes labelled with DiD, at CIBBIM facilities by Dr. Ibane Abasolo team. These conditions were selected from the ones employed in Chapter 2, since the internalization is promoted at this temperature. As can be seen in **Figure 5.10**, RGD significantly accelerates the uptake in comparison to plain liposomes, especially in the case of liposomes-RGD_ether. From these results, liposomes-RGD_ether internalized more than liposomes-RGD_carbamate at the tested times and temperatures, which is also in agreement with previous studies performed in the

group⁸⁰. Following the logic displayed in Chapter 2, we can hypothesize that RGD in the surface is less available in the case of liposomes-RGD_carbamate since they are bilamellar. This can result in the higher internalization of liposomes-RGD_ether.

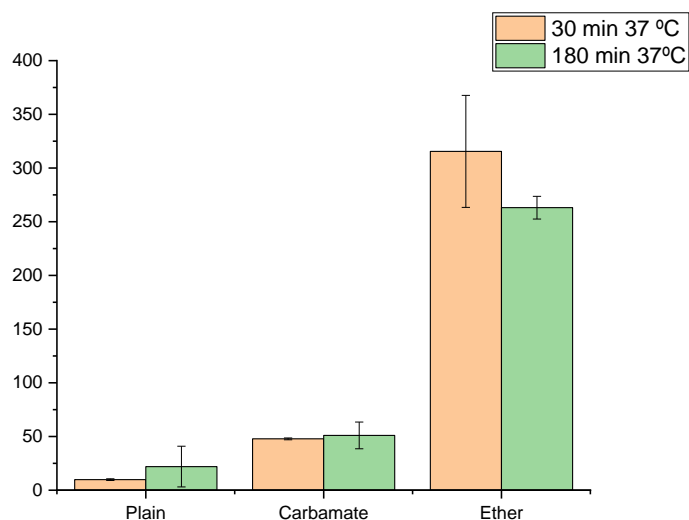


Figure 5.10 : Internalization of nanovesicles on endothelial cells assessed by flow cytometry after 30 and 180 min of incubation at 37 °C. Mean fluorescence intensity (MFI) of DiD in the cells normalized to the minimum fluorescence intensity.

5.4.2. Laser confocal scanning microscopy

Ruixue Xu, from Dr. Pilar Rivera team at UPF, performed these confocal experiments.

For the laser scanning confocal microscopy, HMEC-1 cells were incubated for 180 min with DiD labeled liposomes at 37 °C, to promote internalization (Experimental Section 7.7.2.1.). Cells were also stained with LysoTracker green. The results were comparable to the ones by flow cytometry: plain liposomes internalized less in comparison with liposomes-RGD (**Figure 5.11**). Interestingly, there is few colocalization between the liposomes (in red) and the lysosomes (in green) in contrast with what was observed in the Chapter 2 dedicated to Fabry disease. Probably the presence of mannose 6-phosphate in the GLA protein promotes the endosomal internalization assuring the final colocalization of the liposomes within the lysosomes. When the systems are unloaded, this colocalization is not observed.

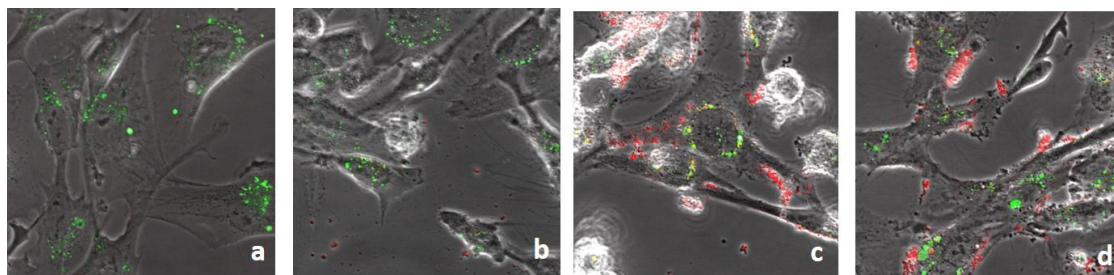


Figure 5.11: Confocal images of the cellular uptake of b) plain liposomes, c) liposomes-RGD_carbamate, d) liposomes-RGD_ether after 3 h incubation at 37 °C. In a) is the cellular control with Lysotracker.

5.5. Summary and conclusions

- Liposomes-RGD, both ether and carbamate, presented a higher size in comparison with plain liposomes, related with the added contribution of the polymer PEG_RGD in the surface, which was also observed by SAXS.
- The complete dissolution of cholesterol_PEG200_RGD, both ether and carbamate in the organic solution added to the reactor for the DELOS-SUSP procedure, enabled higher incorporation of this molecule in the membrane, with values around 80-90%.
- Plain and liposomes-RGD_ether are unilamellar systems, while liposomes-RGD_carbamate are bi-lamellar. By cryo-TEM, stick-like structures in liposomes-RGD_carbamate were also observed, indicating a more heterogeneity in the sample.
- The incorporation of DiD is very similar in all the prepared batches, around 30 nM, indicating that DiD can be incorporated by DELOS-SUSP procedure with a high reproducibility among batches. This allows a better interpretation of the flow cytometry studies.
- Liposomes-RGD_ether are the ones showing a larger cellular uptake, in comparison to liposomes-RGD_carbamate. This is probably due to its unilamellarity, which favours the complete exposition of the RGD to interact with the cell receptors, whereas the bi-lamellar vesicles compromise the availability of RGD in liposomes-RGD_carbamate.

6. Conclusions

From the work accomplished in the present PhD thesis, the following conclusions can be withdrawn:

1. New GLA loaded liposomes-RGD_ether have been developed using DELOS-SUSP and a diafiltration and concentration procedure, with the appropriate GLA concentration (around $300 \mu\text{g mL}^{-1}$), physico-chemical properties (size $\leq 160 \text{ nm}$ and polydispersity index ≤ 0.3), and colloidal stability, to be considered for their in vitro and in vivo testing and generate a solid experimental proof of concept.
2. The enhanced in vitro enzymatic activity, the in vivo efficacy comparable to commercial Replagal, and the increased plasma half-life in comparison to free Replagal have opened the door to the pre-clinical pharmaceutical development of this new GLA nanoformulation for the treatment of Fabry disease, in the frame of the European project Smart-4-Fabry.
3. A new HPLC methodology, using an evaporative light scattering detector, has been developed for the quantification of the membrane components of the liposomes-RGD in order to ensure the quality of the nanovesicles.
4. The decrease of CO_2 content in the RGD functionalized nanoliposomal formulations, after their preparation by DELOS-SUSP, induces a pH increase and the loss of their colloidal stability. The addition of a small percentage of cationic surfactant, MKC, on the membrane of RGD liposomes, avoids the loss of colloidal stability upon elimination of the CO_2 and pH increase.
5. The covalent attachment between cholesterol and PEG linker in cholesterol_PEG200_RGD molecules through an ether bond induces a larger

uptake of nanoliposomes-RGD by endothelial cells (HMEC), than when the attachment between them is through a carbamate bond.

Based on these general conclusions, we can considered that this PhD thesis contributes to demonstrate the potential of liposomes-RGD to formulate the GLA enzyme, in an attempt to develop a future nanomedicine for the treatment of Fabry disease.

7. Experimental Section

7.1. Materials

Cholesten-3 β -ol (cholesterol, 95% of purity) was supplied by Panreac (Barcelona, Spain), 1,2-Dipalmitoyl-sn-glycerol-3-phosphocholine by Corden Pharma (Massachusetts, USA). Myristalkonium chloride (MKC) was obtained from US Biological Science (Salem, USA). 1,1'-dioctadecyl-3,3',3'-tetramethyl-indodicarbocyanine perchlorate (DiD oil) was purchased from Invitrogen (Barcelona, Spain), LysoTracker Green DND-26 was obtained from Molecular probes (Eugene, Oregon), and Hoechst 33342 dye from Sigma-Aldrich. PBS and growth medium Dulbecco's Modified Eagle Medium (DMEM) were purchased from Gibco (Life Technologies).

The cholesterol_PEG200_peptide derivative molecules were specially designed and synthesized by Dr. Miriam Royo group from the Institut de Química Avançada de Catalunya (IQAC-CSIC) for the preparation of liposome nanoconjugates.

Chemical details of cholesterol_PEG200_RGDether: **HPLC-MS:** (Symmetry 300 C₄, 5-100% B, 30 min (A: ACN 0.07% HCOOH B: H₂O 0.1% HCOOH), 1mL/min, λ =210nm) RT: 17.31min, m/z= 1192,8 [M+H]⁺ (Calc.: 1192,53) **HPLC-PDA:** (C₄, 5-100% B, 30min (A: ACN 0.1% TFA B: H₂O 0.1% TFA), 1mL/min, λ =210nm) RT: 20.1 min. AMINO ACID ANALYSIS: Asp: 0.93, Gly: 1.11, Arg: 1., Lys: 0.87, Phe: 0.99.

Chemical details of cholesterol_PEG200_RGDcarbamate: **HPLC-MS:** (Symmetry 300 C₄, 5-100% B, 30 min (A: ACN 0.07% HCOOH B: H₂O 0.1% HCOOH), 1mL/min, λ =210nm) RT: 17.28 min, m/z= 1235.89 [M+H]⁺ **HPLC-PDA:** (C₄, 5-100% B, 30min (A: ACN 0.1% TFA B: H₂O 0.1% TFA), 1mL/min, λ =210nm) RT: 17.62 min.

Chemical details of cholesterol_PEG200_Transferrin: **HPLC-MS** (ESI, elution condition 6): RT: 13.50 min, calculated mass for $C_{89}H_{140}O_{18}N_{19}S^+$ $[M+2H]^{2+}$: 897.5; found: 898.2, $C_{89}H_{141}O_{18}N_{19}S^+$ $[M+3H]^{3+}$: 598.6; found: 599.3, chemical purity: 99%. HRMS (ESI): calculated mass for $C_{89}H_{139}O_{18}N_{19}S^+$ $[M+H]^+$: 1794.02662; found: 1794.02218.

Chemical details of cholesterol_PEG200_glutathione: **HPLC-MS** (ESI, elution condition 6): RT: 18.43 min, calculated mass for $C_{55}H_{91}O_{15}N_6S^+$ $[M+H]^+$: 1107.62; found: 1107.6, chemical purity: 98%. HRMS (ESI): calculated mass for $C_{55}H_{91}O_{15}N_6S^+$ $[M+H]^+$: 1107.62576; found: 1107.62330.

Ethanol HPLC grade and DMSO (Teknokroma Sant Cugat del Vallès, Spain) were purchased with high purity and used without further purifications. Formic acid is supplied by Merck, whereas isopropyl alcohol and methanol are LC-MS grade and supplied by Fisher Scientific S.L. like the acetonitrile, glacial acetic acid and ammonium acetate.

Carbon dioxide (purity 99.9%) was supplied by Carbueros Metálicos S.A. (Barcelona, Spain). All chemicals were used without further purification. The water employed was pre-treated with the Milli-Q Advantage A10 water purification system (Millipore Ibérica, Madrid, Spain).

7.2. Preparation of nanovesicle-bioactive conjugates. Equipments and procedures.

7.2.1. Preparation of nanovesicle-bioactive conjugation by DELOS-SUSP

7.2.1.1. Equipment

The equipment used for the preparation of nanoconjugates is schematized in **Figure 7.5**. The configuration includes a 7.5 mL reactor (*R*), whose temperature is controlled by an external heating jacket; a thermostated syringe pump (model 260D, ISCO Inc., Lincoln, US) (*P*) to introduce CO₂ inside *R* through valve *V1*; a depressurization valve (*V3*), from which the expanded liquid solution is depressurized into the aqueous phase placed in a collector (*C*) located after *V3*. N₂ can be introduced through *V2* directly

from a pressurized reservoir. Two one-way valves are located before *V1* and *V2* to prevent contamination in the CO₂ and N₂ lines. There is also a pressure indicator (*PI*) and another one-way valve before the reactor.

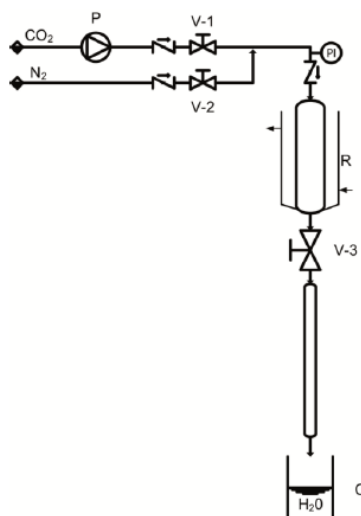


Figure 7.5: Equipment configuration of the 7.5 mL reactor.

7.2.1.2. Procedure

The DELOS-SUSP procedure (see **Figure 1.4**) involves as a first step the loading into a high-pressure autoclave of the membrane lipid components in solution.

For the preparation of the nanoliposomes described in **Tables 7.1, 7.2** and **7.5**, belonging to Chapters 2, 3 and the Annex, the preparation starts with a 1.2 mL ethanolic suspension of 4 mg of cholesterol_PEG200_RGDether, 8 mg of cholesterol and 24 mg of DPPC. This suspension was then loaded in the reactor (R).

The nanoliposomes described in **Tables 7.3** and **7.4**, belonging to Chapters 4 and 5, were prepared dissolving 4 mg of cholesterol_PEG200_RGD in DMSO (0.2 mL), whereas 8 mg of cholesterol and 24 mg of DPPC were dissolved in ethanol (1 mL). This 1.2 mL ethanolic-DMSO solution was then introduced into the high-pressure reactor (R) at atmospheric pressure and working temperature ($T_w = 308$ K).

Systems with MKC, described in **Tables 7.3** and **7.4**, from Chapters 4 and 5 were prepared using 0.5 mL of a 1 mg mL⁻¹ ethanolic solution of MKC (therefore, the mass

added corresponds to 0.5 mg), plus the 24 mg of DPPC and the 8 mg of cholesterol. This ethanolic solution was then slowly added to 0.2 mL of a DMSO solution containing the 4 mg of cholesterol_PEG200_RGD either ether or carbamate, to achieve a final 1.2 mL of an ethanolic-DMSO solution, which was introduced in the reactor (R).

Systems with DiD prepared by DELOS-SUSP (Chapter 5) involved the addition of the desired quantity of DiD (in order to have a final theoretical concentration of 50 nM) in the ethanol with the 8 mg of cholesterol, 24 mg of DPPC and 0.5 mg of MKC.

Once accomplished this first step of the DELOS-SUSP, the rest of the process (see **Figure 1.4**) was the same for all the samples described in Chapters 2, 3, 4, 5 and the Annex: the solution in the reactor was volumetrically expanded with compressed CO₂ until filling the entire reactor at a T of 308 K. The CO₂ molar fraction (X_{CO_2}) in all experiments performed in this thesis was of 0.85, and is determined by the volume of the initial solution loaded in the Reactor (1.2 mL). All experiments were performed at a working pressure (P_w) of 10 MPa. The system was maintained at 308 K and 10 MPa during approximately 1 hour, to achieve a complete homogenization and the thermal equilibration. Afterwards the depressurization of the volumetric expanded organic phase was performed over 24 mL of Milli-Q water. In this step, a flow of N₂ at the working pressure was used as a plunger to push down the CO₂-expanded solution from the reactor and to keep a constant P_w inside the vessel during this step. Average time per experiment was around 2 hours and the nanoconjugates prepared were stored at 277 K until characterization.

However, in the case of samples prepared in the Annex, the depressurization Milli-Q water volume was reduced from 24 to 6 mL, in order to increase the gold nanoparticles concentration.

7.2.1.3. Types of liposomes prepared

In the following Tables are collected the main theoretical parameters of the liposomes prepared for each Chapter.

Table 7.1: Compositions and ratios used for the preparation of the liposomes of Chapter 2, by DELOS-SUSP using CO₂-expanded ethanolic solutions at 10MPa, 308K and $X_{CO_2} = 0.85$. The theoretical molar ratio was always 10:6:1 of DPPC, cholesterol and cholesterol_PEG200_RGDether in liposomes-RGD_ether, and 10:7 of DPPC and cholesterol in plain liposomes (without RGD). The solvent of the organic phase was ethanol in all cases.

| Liposomal systems | Theoretical composition of the initial solution of membrane components | Aqueous phase | Expected protein conc. ($\mu\text{g mL}^{-1}$) | Membrane components conc. (mg mL^{-1}) in the final liposomal system |
|--|---|---|--|---|
| Liposomes-RGD_ether [LP-RGDe] | Chol (17 mM) + DPPC (27 mM) + Chol_RGDe (2.8 mM) | Water | 0 | 1.4 |
| GLA liposomes-RGD_ether total [GLA@LP-RGDe (T)] ($20 \mu\text{g mL}^{-1}$) | Chol (17 mM) + DPPC (27 mM) + Chol_RGDe (2.8 mM) | GLA ($20 \mu\text{g mL}^{-1}$) in water | 20 | 1.4 |
| GLA loaded liposomes-RGD_ether [GLA@LP-RGDe (L)] ($20 \mu\text{g mL}^{-1}$) | Chol (17 mM) + DPPC (27 mM) + Chol_RGDe (2.8 mM) | GLA ($20 \mu\text{g mL}^{-1}$) in water | 7 | 1.4 |
| GLA loaded liposomes-RGD_ether adsorbed [GLA@LP-RGDe (A)] ($20 \mu\text{g mL}^{-1}$) | Chol (17 mM) + DPPC (27 mM) + Chol_RGDe (2.8 mM) | Water | 7 | 1.4 |
| GLA loaded liposomes-RGD_ether [GLA@LP-RGDe (L)] ($8.5 \mu\text{g mL}^{-1}$) | Chol (17 mM) + DPPC (27 mM) + Chol_RGDe (2.8 mM) | GLA ($8.5 \mu\text{g mL}^{-1}$) in water | 2 | 1.4 |
| GLA loaded liposomes-RGD_ether [GLA@LP-RGDe (L)] ($42.5 \mu\text{g mL}^{-1}$) | Chol (17 mM) + DPPC (27 mM) + Chol_RGDe (2.8 mM) | GLA ($42.5 \mu\text{g mL}^{-1}$) in water | 11 | 1.4 |
| Plain liposomes [LP] | Chol (19 mM) + DPPC (27 mM) | Water | 0 | 1.3 |
| GLA loaded plain liposomes [GLA@LP (L)] | Chol (19 mM) + DPPC (27 mM) | GLA ($20 \mu\text{g mL}^{-1}$) | 7 | 1.3 |

| | | | | |
|--|---|---|-----|-----|
| (20 $\mu\text{g mL}^{-1}$) | | in water | | |
| GLA loaded liposomes- RGD_ether with DiD [GLA@LP-RGDe (L) + DiD] (20 $\mu\text{g mL}^{-1}$) | Chol (17 mM) + DPPC (27 mM) + Chol_RGDe (2.8 mM) | GLA (20 $\mu\text{g mL}^{-1}$) in water | 7 | 1.4 |
| GLA loaded plain liposomes [GLA@LP (L) + DiD] (20 $\mu\text{g mL}^{-1}$) | Chol (19 mM) + DPPC (27 mM) | GLA (20 $\mu\text{g mL}^{-1}$) in water | 7 | 1.3 |
| Replagal loaded liposomes-RGD_ether [Replagal@LP-RGDe (L)] (20 $\mu\text{g mL}^{-1}$) | Chol (17 mM) + DPPC (27 mM) + Chol_RGDe (2.8 mM) | Replagal (20 μg mL^{-1}) in water | 7 | 1.4 |
| Replagal loaded liposomes-RGD_ether concentrated x2 [Replagal@LP-RGDe (x2)] | Chol (17 mM) + DPPC (27 mM) + Chol_RGDe (2.8 mM) | Replagal (20 μg mL^{-1}) in water | 14 | 2.8 |
| Replagal loaded liposomes-RGD_ether concentrated x3 [Replagal@LP-RGDe (x3)] | Chol (17 mM) + DPPC (27 mM) + Chol_RGDe (2.8 mM) | Replagal (20 μg mL^{-1}) in water | 21 | 7.2 |
| Replagal loaded liposomes-RGD_ether concentrated x15 [Replagal@LP-RGDe (x15)] | Chol (17 mM) + DPPC (27 mM) + Chol_RGDe (2.8 mM) | Replagal (20 μg mL^{-1}) in water | 105 | 17 |
| Replagal loaded liposomes-RGD_ether concentrated x20 [Replagal@LP-RGDe (x20)] | Chol (17 mM) + DPPC (27 mM) + Chol_RGDe (2.8 mM) | Replagal (20 μg mL^{-1}) in water | 140 | 24 |
| Replagal loaded liposomes-RGD_ether concentrated x30 [Replagal@LP-RGDe (x30)] | Chol (17 mM) + DPPC (27 mM) + Chol_RGDe (2.8 mM) | Replagal (20 μg mL^{-1}) in water | 210 | 36 |
| Replagal loaded liposomes-RGD_ether in PBS [Replagal@LP-RGDe | Chol (17 mM) + DPPC (27 mM) + Chol_RGDe (2.8 | Replagal (20 μg mL^{-1}) in | 7 | 1.4 |

| | | | | |
|--|--|--|---|-----|
| (L) in PBS] (20 $\mu\text{g mL}^{-1}$) | mM) | water | | |
| Replagal loaded liposomes-RGD_ether in NaCl [Replagal@LP-RGDe (L) in NaCl] (20 $\mu\text{g mL}^{-1}$) | Chol (17 mM) + DPPC (27 mM) + Chol_RGDe (2.8 mM) | Replagal (20 $\mu\text{g mL}^{-1}$) in NaCl 0.9% | 7 | 1.4 |
| Dialyzed Replagal loaded liposomes-RGD_ether [dReplagal@LP-RGDe (L)] (20 $\mu\text{g mL}^{-1}$) | Chol (17 mM) + DPPC (27 mM) + Chol_RGDe (2.8 mM) | Dialysed Replagal (20 $\mu\text{g mL}^{-1}$) in water | 7 | 1.4 |
| DTPA loaded liposomes-RGD_ether (x30) [DTPA@LP-RGDe (x30)] | Chol (17 mM) + DPPC (27 mM) + Chol_RGDe (2.8 mM) | DTPA (54 mM) in water | 0 | 36 |
| Liposomes-pTf1_ether [LP-pTf1] | Chol (17 mM) + DPPC (27 mM) + Chol_pTf1 (2.7 mM) | Water | 0 | 1.6 |
| Liposomes-GSH_ether [LP-GSH] | Chol (17 mM) + DPPC (27 mM) + Chol_GSH (2.7 mM) | Water | 0 | 1.4 |

Abbreviations: Chol is cholesterol; Chol_RGDe is Cholesterol_PEG200_RGDether; GLA is His-GLA, dReplagal is dialyzed Replagal; Chol_pTf1 is Cholesterol_PEG200_pTf1ether; Chol_GSH is Cholesterol_PEG200_GSHether.

Table 7.2: Compositions and ratios used for the preparation of the liposomes of Chapter 3, by DELOS-SUSP using CO_2 -expanded ethanolic solutions at 10MPa, 308K and $X_{\text{CO}_2} = 0.85$. The theoretical molar ratio was always 10:6:1 of DPPC, cholesterol and cholesterol_PEG200_RGDether in liposomes-RGD_ether.

| Liposomal systems | Theoretical composition of the initial solution of membrane components | Membrane components conc. (mg mL^{-1}) in the final liposomal system |
|-------------------------------|--|---|
| Liposomes-RGD_ether [LP-RGDe] | Chol (17 mM) + DPPC (27 mM) + Chol_RGDe (2.8 mM) | 1.4 |

Abbreviations: Chol is cholesterol; Chol_RGDe is Cholesterol_PEG200_RGDether.

Table 7.3: Compositions and ratios used for the preparation of the liposomes of Chapter 4, by DELOS-SUSP using CO₂-expanded ethanolic solutions at 10MPa, 308K and $X_{CO_2} = 0.85$. The theoretical molar ratio was always 10:6:1 of DPPC, cholesterol and cholesterol_PEG200_RGD in liposomes-RGD_ether and liposomes-RGD_carbamate, and 10:7 of DPPC and cholesterol in plain liposomes (without RGD). The MKC molar ratio in samples with this surfactant was always 2.2% of the total formulation. The depressurization was performed over 24 mL of Milli-Q water in all cases.

| Liposomal systems | Theoretical composition of the initial solution of membrane components | Organic phase | Membrane components conc. (mg mL ⁻¹) in the final liposomal system |
|--|--|-------------------------|--|
| Plain liposomes [LP] | Chol (19 mM) + DPPC (27 mM) | EtOH | 1.3 |
| Liposomes-RGD_ether [LP-RGDe] | Chol (17 mM) + DPPC (27 mM) + Chol_RGDe (2.8 mM) | EtOH (83%) + DMSO (17%) | 1.4 |
| Liposomes-RGD_carbamate [LP-RGDc] | Chol (17 mM) + DPPC (27 mM) + Chol_RGDC (2.8 mM) | EtOH (83%) + DMSO (17%) | 1.4 |
| Plain liposomes with MKC [LPMK] | Chol (19 mM) + DPPC (27 mM) + MKC (0.001 mM) | EtOH | 1.3 |
| Liposomes-RGD_ether with MKC [LPMK-RGDe] | Chol (17 mM) + DPPC (27 mM) + Chol_RGDe (2.8 mM) + MKC (0.001 mM) | EtOH (83%) + DMSO (17%) | 1.4 |
| Liposomes-RGD_carbamate with MKC [LPMK-RGDc] | Chol (17 mM) + DPPC (27 mM) + Chol_RGDC (2.8 mM) + MKC (0.001 mM) | EtOH (83%) + DMSO (17%) | 1.4 |

Abbreviations: EtOH is ethanol; Chol is cholesterol; Chol_RGDe is Cholesterol_PEG200_RGDether; Chol_RGDC is Cholesterol_PEG200_RGDcarbamate.

Table 7.4: Compositions and ratios used for the preparation of the liposomes of Chapter 5, by DELOS-SUSP using CO₂-expanded ethanolic solutions at 10MPa, 308K and $X_{CO_2} = 0.85$. The theoretical molar ratio was always 10:6:1 of DPPC, cholesterol and cholesterol_PEG200_RGD in liposomes-RGD_ether and in liposomes-RGD_carbamate, and 10:7 of DPPC and cholesterol in plain liposomes (without RGD). The MKC molar ratio was always 2.2% of the total formulation. The depressurization was performed over 24 mL of Milli-Q water in all cases.

| Liposomal systems | Theoretical composition of the initial solution of membrane components | Organic phase | Membrane components conc. (mg mL ⁻¹) in the final liposomal system |
|---|---|-------------------------|--|
| Plain liposomes with MKC [LPMK] | Chol (19 mM) + DPPC (27 mM) + MKC (0.001 mM) | EtOH | 1.3 |
| Liposomes-RGD_ether with MKC [LPMK-RGDe] | Chol (17 mM) + DPPC (27 mM) + Chol_RGDe (2.8 mM) + MKC (0.001 mM) | EtOH (83%) + DMSO (17%) | 1.4 |
| Liposomes-RGD_carbamate with MKC [LPMK-RGDc] | Chol (17 mM) + DPPC (27 mM) + Chol_RGDc (2.8 mM) + MKC (0.001 mM) | EtOH (83%) + DMSO (17%) | 1.4 |
| Plain liposomes with MKC and DiD [LPMK + DiD] | Chol (19 mM) + DPPC (27 mM) + MKC (0.001 mM) + DiD (50 nM) | EtOH | 1.3 |
| Liposomes-RGD_ether with MKC and DiD [LPMK-RGDe + DiD] | Chol (17 mM) + DPPC (27 mM) + Chol_RGDe (2.8 mM) + MKC (0.001 mM) + DiD (50 nM) | EtOH (83%) + DMSO (17%) | 1.4 |
| Liposomes-RGD_carbamate with MKC and DiD [LPMK-RGDc + DiD] | Chol (17 mM) + DPPC (27 mM) + Chol_RGDc (2.8 mM) + MKC (0.001 mM) + DiD (50 nM) | EtOH (83%) + DMSO (17%) | 1.4 |

Abbreviations: EtOH is ethanol; Chol is cholesterol; Chol_RGDe is Cholesterol_PEG200_RGDether; Chol_RGDc is Cholesterol_PEG200_RGDcarbamate.

Table 7.5: Compositions and ratios used for the preparation of the liposomes of the Annex, by DELOS-SUSP using CO₂-expanded ethanolic solutions at 10MPa, 308K and X_{CO2} = 0.85. The theoretical molar ratio was always 10:6:1 of DPPC, cholesterol and cholesterol_PEG200_RGDether in liposomes-RGD_ether, and 10:7 of DPPC and cholesterol in plain liposomes (without RGD).

| Liposomal systems | Theoretical composition of the initial solution of membrane components in ethanol | Aqueous phase | Membrane components conc. (mg mL⁻¹) in the final liposomal system |
|--|--|--|---|
| Gold functionalized liposomes-RGD_ether [Au@LP-RGDe] (15 nm) | Chol (17 mM) + DPPC (27 mM) + Chol_RGDe (2.8 mM) | Au-15 nm-citrate (0.33 mM) in 24 mL of water | 1.4 |
| Gold functionalized liposomes-RGD_ether [Au@LP-RGDe] (15 nm) | Chol (17 mM) + DPPC (27 mM) + Chol_RGDe (2.8 mM) | Au-15 nm-citrate (1.17 mM) in 6 mL of water | 5 |
| Gold functionalized liposomes-RGD_ether [Au@LP-RGDe] (25 nm) | Chol (17 mM) + DPPC (27 mM) + Chol_RGDe (2.8 mM) | Au-25 nm-citrate (1.17 mM) in 6 mL of water | 5 |
| Gold functionalized liposomes-RGD_ether [Au@LP-RGDe] (5 nm) | Chol (17 mM) + DPPC (27 mM) + Chol_RGDe (2.8 mM) | Au-5 nm-citrate (1.17 mM) in 6 mL of water | 5 |
| Gold functionalized plain liposomes [Au@LP] (5 nm) | Chol (19 mM) + DPPC (27 mM) | Au-5 nm-citrate (1.17 mM) in 6 mL of water | 5 |

Abbreviations: EtOH is ethanol; Chol is cholesterol; Chol_RGDe is Cholesterol_PEG200_RGDether.

7.2.2. Preparation of liposomes functionalized with gold nanoparticles by thin film hydration (TFH)

7.2.2.1. Procedure

For the preparation of liposomes functionalized with gold nanoparticles by TFH, we followed the procedure described in Rasch et al¹⁴⁹. Gold dodecanethiol capped nanoparticles were supplied by Dr. Andreu Cabot group.

Briefly, DOPC was dissolved in 1 mL of a suspension of the gold dodecanethiol capped nanoparticles in chloroform. Then, we evaporated the chloroform using a rotary evaporator to form the thin film. After that, the annealing step was performed according to **Figure 7.6**. One hour later, the thin film was hydrated with 1 mL of water and sonicated to form the vesicles. Once finished, it was necessary to centrifuge for purification, at 2000 rpm for 10 min, and the supernatant was collected. The centrifugation process was repeated two times. After centrifugation, an extrusion step was performed 11 times (**Figure 7.7**) through a polycarbonate filter with a pore size of 100 nm. A commercially available manual extruder (Avanti® Mini-Extruder, Avanti Polar Lipids, Alabaster, AL, USA), was used for that purpose. The obtained vesicles were stored at 277 K until characterization.

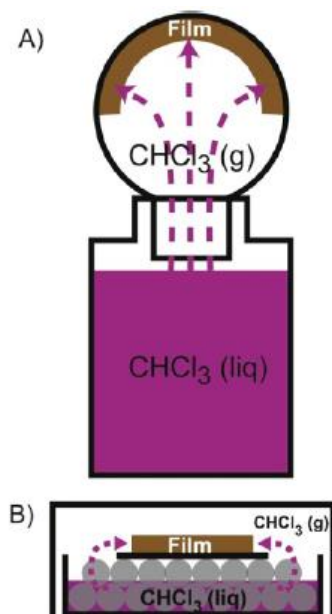


Figure 7.6: Annealing step, extracted from Rasch et al¹⁴⁹.

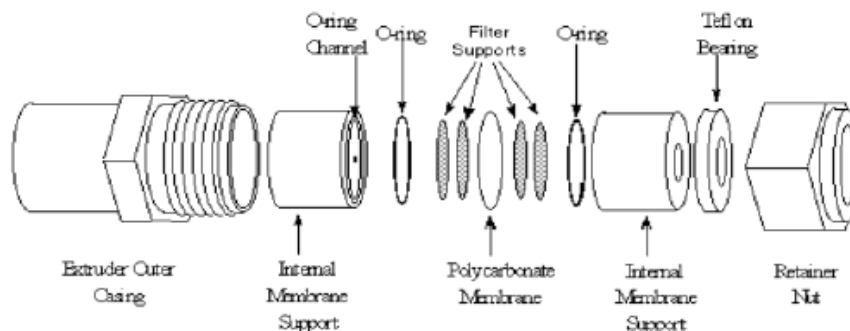


Figure 7.7: Extrusion setup

7.2.2.2. Types of liposomes prepared

In the following **Table 7.6** are gathered the main theoretical parameters for the preparation of gold functionalized liposomes using thin film hydration (THF).

Table 7.6: Compositions and ratios used for the preparation of the liposomes of the Annex, by THF and extrusion. The theoretical molar ratio was always 10:6:1 of DPPC, cholesterol and cholesterol_PEG200_RGDether in liposomes-RGD_ether. The gold nanoparticles were in chloroform in all cases, where the membrane components were also dissolved. After the evaporation, the thin film was hydrated with 1 mL of water

| Liposomal systems | Theoretical composition of the initial solution of membrane components in CHCl_3 | Membrane components conc. (mg mL^{-1}) in the final liposomal system |
|---|---|---|
| DOPC liposomes [DOPC] | DOPC (30 mM) | 23 |
| Gold functionalized DOPC liposomes [Au@DOPC] | DOPC (30 mM) + Au-2 nm-dodecanethiol (3 mg mL^{-1}) | 23 |
| Gold functionalized liposomes-RGD_ether [Au@LP-RGDe] | Chol (17 mM) + DPPC (27 mM) + Chol_RGDe (2.8 mM) + Au-2 nm-dodecanethiol (3 mg mL^{-1}) | 36 |

Abbreviations: EtOH is ethanol; CHCl_3 is chloroform, Chol is cholesterol; Chol_RGDe is Cholesterol_PEG200_RGDether; LP is plain liposomes; LP-RGDe is liposomes-RGD_ether.

7.3. Physicochemical characterization of the nanovesicle-bioactive conjugates. Instruments, techniques and procedures

7.3.1. Determination of size, polydispersity index and Z potential

The size, the polydispersity index (PDI) and the Z-potentials of all the vesicular systems produced were measured using a dynamic light scattering analyzer combined with non-invasive backscatter technology (NIBS) (Malvern Zetasizer Nanoseries, Malvern Instruments, U.K). Samples were analyzed without any previous modification or dilution (except when is indicated otherwise). All reported values were the average result of 3 consecutive measurements on the same sample. Size and polydispersity index were measured putting 1 mL of sample in the DLS equipment cell. Z-potentials were measured putting 1 mL of sample in the specific cell for measuring Z-potential.

7.3.2. Determination of pH

The determination of pH was measured with the equipment HANNA Instruments HI5221-02, which is calibrated once a week using the buffers 4.0, 7.0 and 10.0, and is verified with the 4.0 buffer before performing the measurements. The samples from the fridge are left 30 minutes before are measured to reach room temperature. Each sample is measured three times, cleaning the electrode between measurements. No stirring is used in order to not disturb the samples.

7.3.3. Quantification of membrane components (cholesterol, DPPC and cholesterol_PEG200_RGD)

7.3.3.1. Preliminary studies

Preliminary studies were done on an Alliance HPLC (Waters, Spain). Detection was performed with UV detector. For separation several columns were tested, gathered in

Table 7.1. All the solvents employed were HPLC grade, or Milli-Q water. The standard solutions tested were in ethanol and the concentrations were 32 ppm of cholesterol, 95 ppm of DPPC and 16 ppm of cholesterol_PEG200_RGDether, which are the theoretical concentrations present in the liposomal formulations divided by a factor of 10.

Table 7.1: Columns used for the development of a HPLC-UV methodology for the analysis of membrane components of liposomes-RGD_ether

| Column | Supplier | Phase | Inner diameter x length | Particle size |
|----------------|-----------------|-----------------|-------------------------|---------------|
| ALLTIMA | Hichrom limited | C ₁₈ | 4.6x150 mm | 3 µm |
| SunFire | Waters | C ₁₈ | 4.6x75 mm | 3.5 µm |
| Simmetry300 | Waters | C ₄ | 4.6x250 mm | 5 µm |
| XTerra | Waters | C ₈ | 2.1x50mm | 3.5µm |
| SimmetryShield | Waters | C ₈ | 2.1x150 mm | 3.5 µm |

7.3.3.2. Optimization and validation of HPLC-ELSD methodology

All analyses were done on a HPLC 1100 series (Agilent Technologies, Spain SL.). Detection was performed with a low evaporative light scattering detector, 1260 infinity ELSD (Agilent Technologies, Spain SL.). For separation of cholesterol_PEG200_RGD, cholesterol and DPPC a Teknokroma Symmetry C₁₈ column, 5 µm, 4.6x150 mm (Waters S.A.S.) was used following the elution gradient analysis displayed in **Table 7.2**. Mobile phase A consisted in methanol/water (95:5) and mobile phase B in 0.1% of formic acid in isopropanol. The injection volume is 20 µL. Column temperature was fixed at 25 °C, while the nebulization temperature is 40 °C and the evaporation temperature 80 °C. Detection was performed with a gain of 2.

Table 7.2: Gradient elution mode for quantitative analysis of cholesterol_PEG200_RGD, cholesterol and DPPC.

| Time (minutes) | Mobile phase A (%) | Mobile phase B (%) | Flow rate (mL/min.) |
|----------------|--------------------|--------------------|---------------------|
| 0 | 97 | 3 | 1 |
| 3.0 | 97 | 3 | 1 |
| 4.0 | 88 | 12 | 2 |
| 16.0 | 88 | 12 | 2 |
| 16.5 | 95 | 5 | 2 |
| 19.0 | 97 | 3 | 2 |
| 19.5 | 97 | 3 | 1 |

Standard solutions of cholesterol (25 to 125 ppm), DPPC (35 to 350 ppm), and cholesterol_PEG200_RGD (5 to 50 ppm) were prepared in methanol. Solutions were injected into the HPLC system preceding each measurement with the objective of establishing the calibration curves and as a reference check. It is important to verify that each component does not interfere in the quantification of the others.

The calibration curve of each compound is established by plotting the logarithm values of peak area against the logarithm values of analyte concentrations. Correlation (r^2) is determined for all curves by regression analysis.

The quantification and the validation were performed with real samples. The samples are lyophilized without any cryo/lyo-protectant. The freeze-drying of the samples has been done with the freeze-dryer LyoQuest, Telstar. 1 mL of the sample is freeze-dried during 4 days at -80 °C and 0.03 mbars of pressure. Once performed the freeze-drying, the samples are subsequently diluted in the solvent (methanol). All the samples were filtered with Millex-LG syringe filter (hydrophilic PTFE 0.2 μm) (Merk Millipore) before their injection in HPLC-ELSD.

The validation of the analytical method was determined analyzing the linearity, the precision, the stock dilution test, the samples dilution test, the accuracy test, the LOQ and LOD.

Here are presented the **Tables** of the calibration curves displayed in Chapter 3 (**Figures 3.9, 3.10** and **3.11**).

Table 7.3.: Calibration curve for cholesterol_PEG200_RGD in standard solutions of the three components (Figure 3.9)

| Theoretical concentration (ppm) | Experimental concentration (ppm) | log concentration | Peak area | log area |
|---------------------------------|----------------------------------|-------------------|-----------|----------|
| 5 | 5.0 | 0.70 | 5 | 0.70 |
| 10 | 10.0 | 1.00 | 17 | 1.23 |
| 20 | 19.9 | 1.30 | 64.7 | 1.81 |
| 35 | 34.9 | 1.54 | 175.9 | 2.25 |
| 40 | 49.8 | 1.70 | 334.3 | 2.52 |
| 100 | 99.6 | 2.00 | 874.9 | 2.94 |

Table 7.4.: Calibration curve for cholesterol in standard solutions of the three components (Figure 3.10)

| Theoretical concentration (ppm) | Experimental concentration (ppm) | log concentration | Peak area | log area |
|---------------------------------|----------------------------------|-------------------|-----------|----------|
| 12.5 | 12.4 | 1.09 | 17.5 | 1.24 |
| 25 | 24.8 | 1.40 | 53.8 | 1.73 |
| 50 | 49.7 | 1.70 | 182.3 | 2.26 |
| 87.5 | 86.9 | 1.94 | 542.9 | 2.73 |
| 125 | 124.2 | 2.09 | 1023.9 | 3.01 |
| 250 | 248.4 | 2.40 | 3389.8 | 3.53 |

Table 7.5.: Calibration curve of DPPC in standard solutions of the three components (Figure 3.11)

| Theoretical concentration (ppm) | Experimental concentration (ppm) | log concentration | Peak area | log area |
|---------------------------------|----------------------------------|-------------------|-----------|----------|
| 35 | 35.6 | 1.55 | 59.9 | 1.78 |
| 70 | 71.3 | 1.85 | 194.1 | 2.29 |
| 140 | 142.5 | 2.15 | 708.4 | 2.85 |
| 245 | 249.4 | 2.40 | 2052.8 | 3.31 |
| 350 | 356.3 | 2.55 | 3893.6 | 3.59 |
| 700 | 712.6 | 2.85 | 11738 | 4.07 |

7.3.4. Morphological analysis

The morphology of the vesicles was studied using cryogenic transmission electron microscopy (Cryo-TEM), in the Servei de Microscòpia Universitat Autònoma (UAB). The images were obtained with a JEOL JEM-2011 microscopy (JEOL LTD, Tokio, Japan) operating at 120 kV. The preparation of the frozen samples was performed in a vitrification system with controlled environment (CEVS) Leica, model EM-CPC (Leica Microsystems, Germany). A 4 μ l drop of sample was placed in a copper grid coated with a perforated polymer film. The sample excess was removed by blotting with filter paper to obtain a thin film. Right after this, the grid was plunged into liquid ethane held at a temperature just above its freezing point (94 K). The vitrified sample was transferred to the microscope for analysis. To prevent sample perturbation and the formation of crystals, the specimens were kept cool (77 K) during the transfer and the viewing procedure.

Samples of Chapter 5 were examined at Prof. Dganit Danino group in Technion (Israel Institute of Technology, Israel). The samples were stored at 277 K until their

vitrification in perforated Ted Pella grids, using a controlled specimen preparation chamber for this process. The examination of the samples was performed in a T12 G2 Tecnai (FEI) at cryogenic temperatures, always below 103 K. Images were recorded with a Gatan UltraScan 2kx2k CCD camera at low dose operation¹⁵⁰.

7.3.5. Lamellarity determination

Vesicle structure was probed by synchrotron Small Angle X-ray scattering (SWAXS) patterns measured in the Austrian SAXS beamline at Elettra synchrotron in Trieste (Italy), for the samples in Chapter 2. These samples were exposed to polarized monochromatic X-rays of wavelength $\lambda=1.5418 \text{ \AA}$ (8.05 keV) for 30 s. SAXS patterns were recorded using a Pilatus detector at a sample to detector distance of 1.0 m allowing for an observable q -range (nm^{-1}) from 0.1 to 6.6, where q is the scattering vector magnitude, $q=(4\pi \sin\theta)/\lambda$ (2θ is the scattering angle). Experimental parameters, e.g. beam center, sample-to-detector distance, detector tilt plane and rotation, were calibrated with a Fit2D1 analysis of silver behenate. The given scattering plots corresponds to an averaged over 4 identical sequences after verifying precise reproducibility. A background correction was accomplished by subtracting the integrated images of buffer in the solution cell, measured under the same conditions before and after the sample, from that of the sample¹⁵¹.

Chapter 5 samples were measured on an optimized NanoStar SAXS instrument from Bruker AXS set up at Aarhus University¹⁵² and equipped with a liquid Ga metal jet-X-ray source (Excillum) and scatterless slits¹⁵³. 1.5 mg mL^{-1} of each sample of liposomes in water were measured, the matching backgrounds subtracted and water was used for absolute scale calibration. Plain liposomes were fitted with the classical liposome model with no GLA enzyme component and without a polymer contribution. Liposomes-RGD both ether and carbamate were fitted with the liposome model including a polymer contribution to properly fit the raised minima in these data due to the polymer scattering from the exterior PEG-RGD chains coating the liposomes^{154,155}.

7.4. Determination of the degree of loading/functionalization of vesicles

7.4.1. Separation and concentration using a diafiltration equipment

We have separated the non-incorporated active using the KrossFlo® Research Ili TFF System (KR2i) (**Figure 7.8**). The diafiltration process can separate the non-encapsulated biomolecule, concentrate the sample and change the dispersant medium if desired. The columns were selected according to the size of the active, in the case of this thesis the separation of free GLA (100 kDa) was accomplished with a 300 kDa cutoff. The column retains the loaded vesicles diafiltrating the free enzyme through the membrane pores.

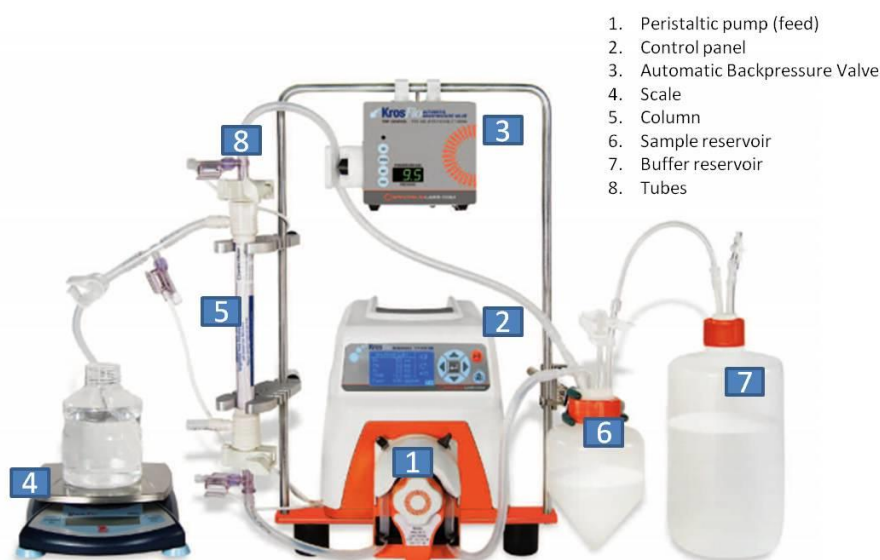


Figure 7.8: Configuration of the KrossFlo® Research Ili TFF System (KR2i)

In order to perform the diafiltration, a volume is added to the sample container, which is connected to the column and the buffer reservoir. Once the parameters have been set, the system can function automatically. Based on the experience, 6 cycles should be performed in order to eliminate the free biomolecules and the ethanol that is present in the sample. For instance, if the initial sample volume is 4 mL the process is considered finished when the diafiltrated water volume is 24 mL. The same initial

sample volume with the loaded vesicles and free of ethanol is collected from the sample reservoir. The process takes about 30 min.

To concentrate the sample, the connection with the buffer reservoir is closed in order to extract the dispersant medium through the diafiltration column while the liposomes remain in the circuit. One batch of 24 mL is enough to concentrate x2 and x3. The mix of different batches is needed to perform the concentration x15 (3-4 batches), x20 (4 batches) and x30 (6 batches).

7.4.2. Quantification of GLA in liposomes

The quantification of GLA was performed in *Instituto de Biotecnología y Biomedicina* (IBB-UAB) by Dr. Pepe Corchero. After the separation of non-encapsulated GLA from the loaded system, the amount of GLA in the different fractions was quantified. To estimate the incorporation of GLA into SUVs, samples from initial GLA in water, total sample (directly from the reactor) and loaded liposomes (after diafiltration process), were mixed with denaturing, loading buffer and analyzed by SDS-PAGE and further Western-blot developed with a rabbit polyclonal anti-GLA serum (Santa Cruz Biotechnology, a-gal A H-104: sc-25823) and a goat anti-rabbit IgG HRP-conjugate (Bio-Rad Laboratories, Inc., cat.# 170-6515) as secondary antibody. Amounts of GLA within each of the above-mentioned samples were estimated by comparison with known amounts (usually ranging from 25 to 125 ng) of GLA previously produced, purified, and quantified in IBB laboratories. Samples to be quantitatively compared were run in the same gel and processed as a set. Densitometric analyses of the bands were performed with the Quantity One software (Bio-Rad Laboratories, Inc). The errors are the standard deviation (SD) of three replicates. Percentage of encapsulated α -galactosidase was obtained by dividing the amounts of enzyme found in the loaded vesicles by the amount found in the total sample.

7.5. Synthesis and characterization of bioactive compounds

7.5.1. Production of GLA-HIS enzyme

The production of the protein was performed by the group of Dr. Antonio Villaverde in the IBB-UAB with the valuable collaboration of Dr. José Luis Corchero. The suspension-adapted cell line HEK (human embryonic kidney) FreeStyle™ 293-F (Gibco, Invitrogen Corporation) was used to produce a recombinant human GLA by means of polyethylenimine (PEI)-mediated transient gene expression. Details of GLA production and purification have been described elsewhere¹⁵⁶. Briefly, human GLA monomer was produced with a hexahistidine tag (GLA-HIS) fused to its C-terminus, allowing enzyme purification directly from the clarified supernatant, in a single affinity chromatography step, to a high degree of purity (>95% according to SDS-PAGE and Coomassie staining).

7.5.2. Dialysis of Replagal

The dialysis of Replagal was performed in the CIBBIM (Hospital Universitari Vall d'Hebron), group of Dr. Ibane Abasolo. Replagal was dialyzed against an acetic buffer in order to eliminate the excipients (namely sodium phosphate monobasic, monohydrate, polysorbate 20, sodium chloride and water). The process takes between 16-24 h at 4 °C with two changes of buffer. The buffer is in a proportion of 1:500 with respect to the volume of Replagal. Enzymatic activity was tested after the dialysation step according to procedure described in Experimental Section 7.8.1.

7.6. Labelling of nanovesicles with DiD dye

For the labelling of nanovesicles with DiD dye performed in Chapter 2, the first step is the preparation of a stock dilution of DiD dye in ethanol (1 mM). Then, a volume of stock solution was incubated with 500 µL of liposomes during 2 hours at 298 K, in order to have the desired final concentration. After the labelling, non-integrated DiD is separated from the loaded vesicles by size-exclusion chromatography using PD Spin Trap G-25. Prior to use, columns must be equilibrated to remove storage buffer, by

adding 400 μL of PBS and centrifuging 1 min to 1000 rpm. The resultant fraction was discarded, and the collection tube replaced. This procedure is done twice and after that, sample is added (100-180 μL) slowly in the middle of the packed bed and centrifuged 5 min at 1000 rpm. DiD-loaded samples are recovered in the collector tube. This was the procedure employed in Chapter 2.

As explained in section 7.2.1.2, for the preparation of DiD labelled samples of Chapter 5, DiD was incorporated in the ethanolic solution along with the membrane components (cholesterol, DPPC, cholesterol_PEG200_RGD and MKC) to the DELOS-SUSP reactor, then pressurized with compressed CO_2 and depressurized over water.

7.7. Cellular uptake assays

7.7.1. Protocol under clean conditions for the preparation of liposomal samples tested in cell and in vivo assays.

Despite the properties of DELOS-SUSP method to allow sterile operation conditions, a protocol to prepare liposomal samples to be tested in cell and in vivo assays was established. This protocol is explained in detail below and it was strictly followed in order to avoid contamination:

- The working lab should be clean and organized before starting the experiment
- All the lab material (micropipettes tips, eppendorf tubes, depressurization container, glass container to keep the sample, test tube, etc.) should be autoclaved
- Once the sterilization process has finished the clean material should be covered in aluminum paper until used. It is highly recommended to perform the autoclave process the day before the experiment
- The reactor should be cleaned three times with the proper organic solvent and CO_2 at 10 MPa and 308 K before starting the experiment
- The fume hood should be clean and the air extractor in on position (ideally the fume hood should have a laminar flux)

- The compounds to be processed should be weighted in a clean analytical balance where no other compounds considered possible contaminants are weighted.

7.7.2. Cell culture experiments

7.7.2.1. Cellular uptake of liposomes assessed by laser scanning confocal microscopy

Laser scanning confocal microscopy was performed by Dr. Pilar Rivera and Ruixue Xu, Universitat Pompeu Fabra (UPF, Barcelona). HMEC-1 cells were seeded onto Fluorodish culture plates (World Precision Instruments, Sarasota, FL) at a density of 2×10^5 cells per plate and allowed to grow for 36–48 h. 50 μL of DiD-labeled liposomes or DiD-labeled liposome-RGD conjugates (1.5 mg mL^{-1}) were mixed with 200 μL MCDB 131 medium, added into the cells and incubated for 180 min at 37 °C in a humidified atmosphere with 5% CO_2 . Subsequently, cells were washed with serum-free MCDB 131 and incubated at 37 °C for 5 min with LysoTracker Green DND-26 (50 nM, Molecular probes, Eugene, Oregon) to label the endosomal/lysosomal compartments. The nuclei in live cells were stained with Hoechst 33342 dye (Sigma). Cells were examined under an inverted Leica SP5 laser scanning confocal spectral microscope (Leica Microsystems Heidelberg GmbH, Mannheim, Germany) using a 60×1.42 NA oil immersion objective. To visualize two colors of fluorescence simultaneously, we used the 514 nm line from Argon laser for LysoTracker Green and the 630 nm line from a He–Ne laser for DiD.

7.7.2.2. Flow cytometry experiment

Flow cytometry experiments were performed at CIBBIM (Hospital Universitari Vall d'Hebron), under the supervision of Dr. Ibane Abasolo. For this, HMEC-1 cells were detached using trypsin and incubated with DiD-labeled liposomes (0.3 mg mL^{-1}) resuspended into MCDB 131 media supplemented with 10 mM L-glutamine for 30 and 180 min at 16 °C or 37 °C. Since no significant toxicity was observed after this short-term incubation, cells were washed twice with Dulbecco's phosphate buffered saline

(DPBS) solution and resuspended in cell culturing medium before subjecting to fluorescence-activated cell sorting analysis. Data acquisition and analysis was performed using FACScan (Beckton-Dickinson) and BD FACSDiva software. At least 10^4 viable cells were evaluated in each experiment.

7.8. Biological activity of GLA

The determination of biological activity in GLA conjugates was performed in CIBBIM (Hospital Universitari Vall d'Hebron) under the supervision of Dr. Ibane Abasolo.

7.8.1. Specific enzymatic activity

GLA enzymatic activity was assayed fluorometrically, as described by Desnick et al.¹⁵⁷, with the modifications of Mayes et al.¹⁵⁸ Basically, it was performed by using 4-methylumbelliferyl-d-galactoside (4- MUG, Sigma Chemical) as substrate, at a concentration of 2.46 mM in a buffer (0.01 M acetic acid, pH 4.5). A typical assay reaction mixture contains 100 μ L of substrate and 25 μ L of the sample. Enzymatic reactions took place in agitation (tubes placed in a rotator, set at a rotation speed of 25 rpm), at 37 °C for 1 h, and were stopped with 1.25 mL of 0.2 M glycine-NaOH buffer (pH 10.4). The released product (4- methylumbelliferone or 4-MU) was determined by fluorescence measurement at 365 and 450 nm as excitation and emission wavelengths, respectively. Samples of commercial product 4-MU (from Sigma Chemical) ranging from 5 to 500 ng/mL in 0.2 M glycine-NaOH buffer, pH 10.4, were used to obtain a calibration curve in order to transform fluorescence readings into product 4-MU concentration. Enzymatic activity and specific activities are expressed as “ng 4-MU/mL/h” and “ μ mol 4-MU/mg GLA/h”, respectively. The error is the standard error of the mean (SEM) of the three replicates.

7.8.2. In vitro enzymatic efficacy

Primary cultures of mouse aortic endothelial cells (MAEC) of GLA deficient KO mice (Gla^{tmKul1}) were isolated following procedures previously described¹⁵⁹. Endothelial origin of isolated cells was confirmed by CD105 staining. For activity assays, cells in passages 2 to 5 were seeded in 24 well plates and maintained at 37 °C and 5% of CO₂.

Twenty-four hours after seeding 8 μM of NBD-Gb3 (Matreya) was added to the cultures along with the specified concentrations of tested compounds (free enzyme, enzyme-vesicle conjugates or empty vesicles). After 48 h incubation, cells were trypsinized and Gb3-NBD fluorescent signal was analyzed by flow cytometry (FacsCalibur, Beckton Dickinson). To calculate the percentage of Gb3-NBD signal, fluorescent signal in control cells (without treatment) was established as 100% and the rest of the values were normalized accordingly. Since alpha-galactosidase activity reduces those Gb3 deposits, the percentage of Gb3 loss ($\% \text{ Gb3 loss} = 100 - \% \text{ Gb3-NBD signal}$) was used to plot the results.

7.9. In vivo experiments

Dr. Ibane Abasolo's team of CIBBIM (Hospital Universitari Vall d'Hebron) with the valuable support of Natalia García performed in vivo experiments.

7.9.1. Pharmacokinetics

A preliminary pharmacokinetic study was developed by means of evaluating the presence of enzymatic activity in plasma of Replagal® and Replagal loaded systems at three time points: 1, 5, and 60 min. For this, a mouse model of Fabry disease, which is GLA KO mice (GlatmKul), was employed, using three animals per time point. The Replagal and Replagal loaded systems were administered as a single dose intravenously. The animals were euthanized in each time point (1, 5 and 60 min) and the enzymatic activity in plasma was measured, as explained in 7.8.1.

7.9.2. Toxicity

Preliminary toxicity assays were performed with the administration of the maximum feasible dose (MFD) which in this case was of 300 mg kg^{-1} in lipid content, equivalent to 1.5 mg kg^{-1} of Replagal. This MFD was the Replagal@LP-RGDe (x30) in Milli-Q water, without any dilution. Fabry mice were monitored for 21 days post-administration and then euthanized in order to do gross necropsy.

7.9.3. Efficacy

In the experiment, 40 Fabry mice were injected with five different samples: the vehicle which is PBS, free Replagal at 3 mg kg⁻¹ and 1.5 mg kg⁻¹, Replagal@LP-RGDe (x30) at 1.5 mg kg⁻¹ and 0.5 mg kg⁻¹ (8 animals for each sample). In the study were also included 10 wild type mice, which are healthy mice without Fabry disease. Three weeks after administration, they were euthanized, and the RT-PCR was performed.

Annex:

Functionalization of liposomes with different gold nanoparticles

A.1. Introduction

Vesicles are attractive carriers for dispersing metallic nanoparticles, since they have lipid membranes that can host hydrophobic species, and aqueous cavities for incorporating hydrophilic material¹⁴⁹. In addition, nanoparticles can be physically or chemically adsorbed onto the liposome surface¹⁶⁰. These hybrid therapeutic systems combining both organic and inorganic materials not only possess properties of each type of carrier individually but also offer complementary advantages¹⁶¹. For example, liposomes are biocompatible and allow drug loading while inorganic materials have optical, electrical, magnetic and catalytic properties. Thus, liposomes avoid the metallic nanoparticles toxicity and side effects, making their hybrids excellent candidates for drug delivery, imaging, and biosensor development^{162,163}. The incorporation of inorganic nanoparticles in liposomes can enable the remote release of the cargo using external stimuli like magnetic fields, laser irradiation or electromagnetic radiation^{160,164}.

The interactions between the liposomes and the metallic nanoparticles depend on the composition, size, and surface chemistry of both liposomes and inorganic surfaces¹⁶³. For instance, electrostatic, Van der Waals and/or a combination of both of them¹⁶⁵.

Among all the types of metallic nanoparticles, gold nanoparticles are very important in nanotechnology given their color, high stability, tunable surface chemistry and low toxicity¹⁶³. The study of vesicle-nanoparticle hybrids could help in the determination of the fate of nanomaterials inside the cells and organisms¹⁶⁶.

During Dr. Lidia Ferrer-Tasies thesis, she achieved the incorporation of silicon nanocrystals in vesicular systems called quatsomes¹⁶⁷ using sonication, but this incorporation was not possible in liposomal formulations since they sedimented after three days¹⁶⁸. As part of this thesis, the functionalization with gold nanoparticles was tried in order to use these systems for cryotomography in the water window using an X-ray microscope at beamline Mistral (ALBA synchrotron).

The aim of this emerging technique, with a resolution between confocal and electron microscopies, is to locate subcellular structures at the time of key cellular events. An interesting property of these soft X-rays is the water window spectral range, between the inner-shell absorption edges of carbon (284 eV) and oxygen (543 eV). In this water window, water (oxygen) is relatively transparent in the X-ray range while protein (carbon) absorb much more. Therefore, organic cell structures can be visualized with good absorption contrast. Soft X-ray cryo tomography (cryo-SXT) is the only imaging technique that allows the 3D study of vitrified whole cell-samples avoiding modifications like chemical treatment or sectioning, since only requires the vitrification of the water via a cryo-fixation process^{169,170,171}.

Cryo-SXT has been successfully employed for the visualization of vaccinia virus and their inner compartments¹⁷², and also of cells infected with these vaccinia virus¹⁷³. Of particular interest is the study of the cellular ultrastructural alterations induced by Hepatitis C virus infection. Cryo-SXT enabled the observation of modifications in the cell organelles, mainly the endoplasmic reticulum and the mitochondria. Interestingly, the administration of antivirals achieved the complete reversion of these ultrastructural changes¹⁷¹.

We were granted with beam time in ALBA synchrotron with the first objective being to locate the liposomes-RGD inside HeLa/HMEC cells. In order to distinguish our liposomes from other vesicles naturally produced by the cell, we needed to mark them

with metallic nanoparticles that give a strong contrast, for example, gold. Synchrotron data is not presented in this thesis, since its treatment is still on going, but the great effort to obtain gold functionalized liposomes is described in this Annex.

A.2. Preparation of Au-nanoliposomes

The goal was to functionalize with gold nanoparticles plain liposomes and liposomes-RGD_ether for cryo-SXT studies.

All the different types of gold nanoparticles (AuNPs) were provided by Dr. Andreu Cabot group in Catalonia Institute for Energy Research (IREC).

We were aware of the works of Rasch et al. with dodecanethiol capped gold nanoparticles and dioleoylphosphatidylcholine (DOPC) liposomes using chloroform-enhanced thin film hydration¹⁴⁹. As a starting point, we began trying to apply their methodology to the liposomes-RGD_ether. Since it was not possible to adapt the procedure to DELOS-SUSP (chloroform is not miscible in the depressurization water), we decided to try thin film hydration (TFH). Therefore, we dissolved DPPC, cholesterol and cholesterol_PEG200_RGDether in the chloroform containing the AuNPs and proceeded following the procedure described in detail in Experimental Section 7.2.2. When observed by cryo-TEM it resulted a heterogeneous sample with vesicles but also stick-like structures (**Figure A.1a**). It seemed that the AuNPs incorporated preferably in the stick structures. As a control we prepared the vesicles with the same composition that is reported in Rasch et al., 2012¹⁴⁹, DOPC at 30 mM. DOPC liposomes were also formed without AuNPs. The composition of the three systems are gathered in **Table A.1**.

Table A.1: Compositions and ratios used for the preparation of AuNPs functionalized liposomes by TFH using annealing with chloroform.

| Liposomal systems [number of batches] | Theoretical composition of the initial solution of membrane components in CHCl ₃ | Membrane components conc. (mg mL ⁻¹) in the final liposomal system |
|--|--|--|
| Au liposomes- RGD_ether [1] (Au@LP-RGDe) | Cholesterol (17 mM) + DPPC (27 mM) + Chol-PEG ₂₀₀ -RGD (2.8 mM) + AuNPs (3 mg mL ⁻¹) | 36 |
| Au liposomes DOPC [7] (Au@DOPC) | DOPC (30 mM) + AuNPs (3 mg mL ⁻¹) | 24 |
| Liposomes DOPC [1] | DOPC (30 mM) | 22 |

The size, polydispersity index and Z-potential are given in **Table A.2**. In comparison with Au liposomes-RGD_ether which were more polydisperse, the liposomes with DOPC showed a size around 110 nm and a Pdl lower than 0.1. By cryo-TEM we observed very homogenous samples with multivesicular systems probably formed by the extrusion step in the procedure (**Figure A.1b** and **c**). Au plain liposomes of DOPC showed incorporation of AuNPs (**Figure A.1b**).

Table A.2: Physicochemical characteristics of the systems prepared by TFH.

| Liposomal systems | Size | | Z potential (mV) |
|-------------------|------------------------|------------------|------------------|
| | Mean ^a (nm) | Pdl ^b | |
| Au@LP-RGDe | 144±2 | 0.259±0.004 | 10.7±0.9 |
| Au@DOPC | 109.40±0.05 | 0.09±0.01 | 30±2 |
| Liposomes DOPC | 104.4±0.2 | 0.08±0.01 | -6.6±0.5 |

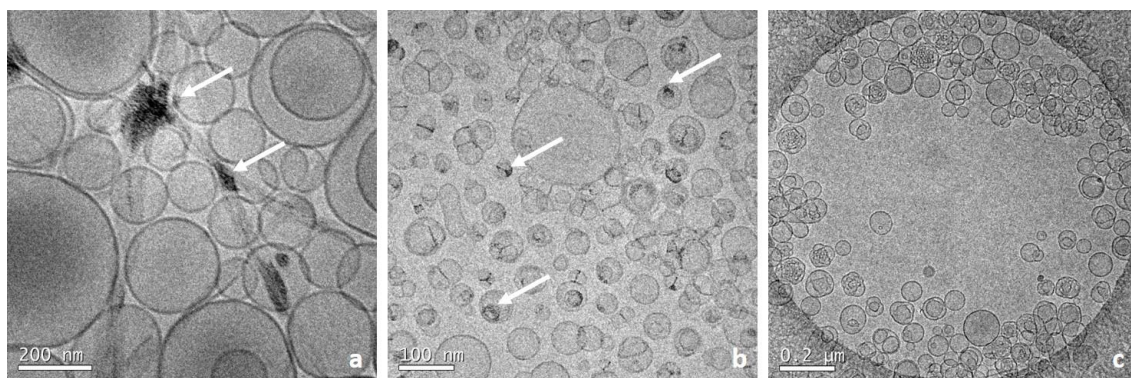


Figure A.1: Cryo-TEM pictures showing the morphology of the nanoconjugates: a) Au@LP-RGDe b) Au@DOPC, c) liposomes DOPC. Scale bars are 200 nm, except in b that is 100 nm. White arrows mark the presence of AuNPs.

We performed other trials with TFH e.g. substituting the DOPC for DPPC and adding cholesterol to prepare plain liposomes without RGD. However, in these cases extrusion was not possible since the liposomal formulation was too viscous.

In order to take advantage of the DELOS-SUSP technology and maintain the liposome's composition used in other Chapters of this thesis, another approach was tried. Instead of using hydrophobic gold nanoparticles like the ones capped with dodecanethiol, we changed to hydrophilic nanoparticles with citrate as ligand. The organic phase was composed of cholesterol (17 mM), cholesterol_PEG200_RGDether (2.8 mM) and DPPC (27 mM), while the AuNPs were dispersed in the water of depressurization. In order to increase the 15 nm-AuNPs concentration (from 0.33 nM up to 1.17 nM) the volume of Milli-Q water was reduced from 24 mL to 6 mL, obtaining a final lipid concentration of 5 mg mL⁻¹. After the DELOS-SUSP process, diafiltration and centrifugation (following the conditions reported in Rasch et al., 2012¹⁴⁹) were tried to separate the non-incorporated AuNPs. Comparison between the two methodologies is shown in **Table A.3** and **Figure A.2**.

Table A.3: Physicochemical characteristics of the liposomes-RGD_ether fractions: total samples (obtained from the reactor), loaded samples after diafiltration process to separate free AuNPs and loaded samples after centrifugation.

| Liposomes-RGD_ether systems | Size | | Z potential (mV) |
|-----------------------------|------------------------|------------------|------------------|
| | Mean ^a (nm) | Pdl ^b | |
| Total | 246±2 | 0.548±0.005 | 4.7±0.5 |
| Loaded (diafiltration) | 199.3±0.3 | 0.39±0.01 | 14±1 |
| Loaded (centrifugation) | 158±1 | 0.21±0.01 | -6.2±0.8 |

Systems obtained from the reactor (total) have a high polydispersity index, more than 0.5, which makes the size measure not reliable. Moreover, upon time a little sediment of AuNPs was observed in the vial. On the other hand, diafiltration improves the samples slightly reducing the polydispersity index to around 0.4, and the hydrodynamic size decreases. In addition, Z-potential increases pointing to a more stable system. Nevertheless, they seem more homogenous when systems are centrifuged since the size is around 160 nm and the polydispersity index is 0.2. Besides, Z-potential changes from positive to negative values. Considering the absolute value of the Z-potential, the centrifuged samples seemed less stable than the diafiltrated. However, both centrifuged and diafiltrated Au liposomes-RGD_ether presented no sediment of AuNPs upon time.

The observation by cryo-TEM corroborates the DLS measurements. Total samples are heterogeneous in sizes and morphologies having tubular structures. Diafiltrated systems have also diversity of size and morphology with big and not spherical vesicles.

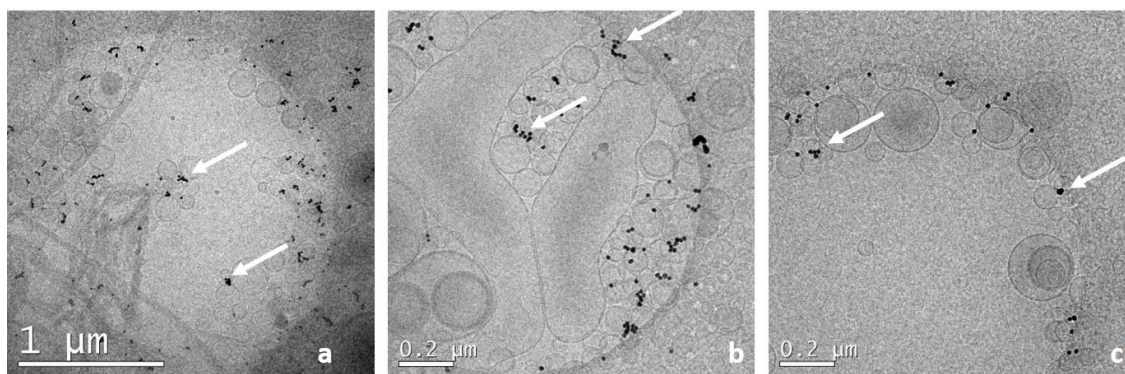


Figure A.2: Cryo-TEM pictures showing the morphology of the nanoconjugates: a) Total liposomes-RGD_ether, b) loaded liposomes-RGD_ether by diafiltration, c) loaded liposomes-RGD_ether by centrifugation. Scale bars are 200 nm, except in a) that is 1 μm . White arrows mark the presence of AuNPs.

Given the results, centrifugation was selected as the best method to eliminate the free AuNPs. Then, different sizes of nanoparticles were evaluated (25, 15 and 5 nm) for the preparation of liposomes-RGD_ether. Although the vesicle size is very similar for all the liposomes-RGD_ether, around 140 nm, the Pdl decreases with the size of the AuNPs and the Z-potential also changes from positive values (for the 25 nm-AuNPs) to negative values in the other cases.

Table A.4: Physicochemical characteristics of the liposomes-RGD_ether with different AuNPs size prepared by DELOS-SUSP using CO_2 -expanded ethanolic solutions at 10MPa, 308K and $X_{\text{CO}_2} = 0.85$.

| AuNPs size | Size Au@LP-RGDe | | Au@LP-RGDe |
|------------|------------------------|-------------------|------------------|
| | Mean ^a (nm) | Pdl ^b | Z potential (mV) |
| 25 nm | 135.6 \pm 0.8 | 0.12 \pm 0.03 | 9 \pm 1 |
| 15 nm | 143 \pm 1 | 0.095 \pm 0.007 | -5.3 \pm 0.1 |
| 5 nm | 138 \pm 1 | 0.08 \pm 0.01 | -8 \pm 2 |

By cryo-TEM, we observed that the AuNPs are incorporated in the outer or inner surface of the membrane probably adsorbed. It seems that reducing the size of the AuNPs, the particles tend to increase their incorporation in the liposomes-RGD_ether. Therefore, we selected the 5 nm-AuNPs for the next experiments.

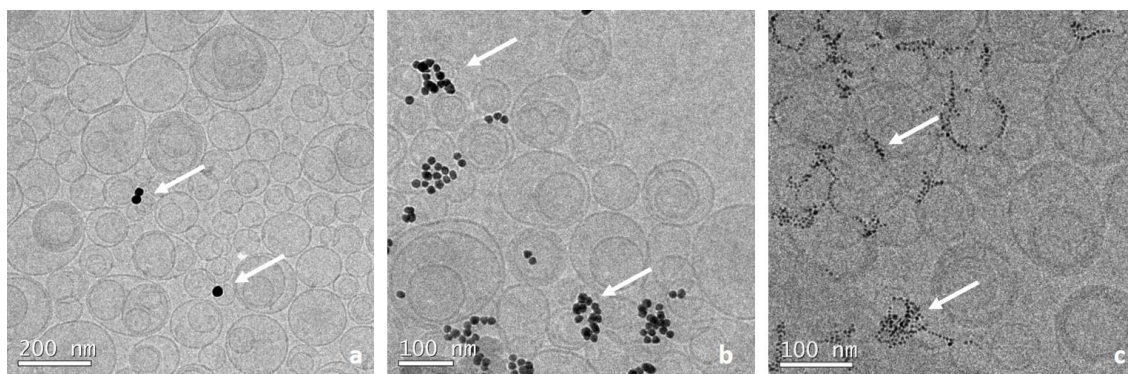


Figure A.3: Cryo-TEM pictures showing the morphology of the nanoconjugates: a) Au@LP-RGDe with 25 nm-AuNPs, b) Au@LP-RGDe with 15 nm-AuNPs, c) Au@LP-RGDe with 5 nm-AuNPs. Scale bars are 100 nm, except in a) that is 200 nm. White arrows mark the presence of AuNPs.

According to these obtained results, we produced plain liposomes and liposomes-RGD_ether with 5 nm-AuNPs.

Table A.5: Physicochemical characteristics of the two types of liposomes prepared by DELOS-SUSP using CO₂-expanded ethanolic solutions at 10MPa, 308K and X_{CO2} = 0.85, with 5 nm-AuNPs.

| Liposomal systems | Size | | Z potential (mV) |
|-------------------|------------------------|------------------|------------------|
| | Mean ^a (nm) | Pdl ^b | |
| Au@LP | 127.2±0.7 | 0.08±0.02 | -23±2 |
| Au@LP-RGDe | 159±1 | 0.08±0.02 | -29.2±0.8 |

The sizes of the liposomes range from 130-160 nm, while the polydispersity indexes remain very low (0.08-0.09) and the Z-potential is quite high with a negative charge, indicating good stability. In cryo-TEM images, plain liposomes seem less loaded with AuNPs than liposomes-RGD either ether or carbamate.

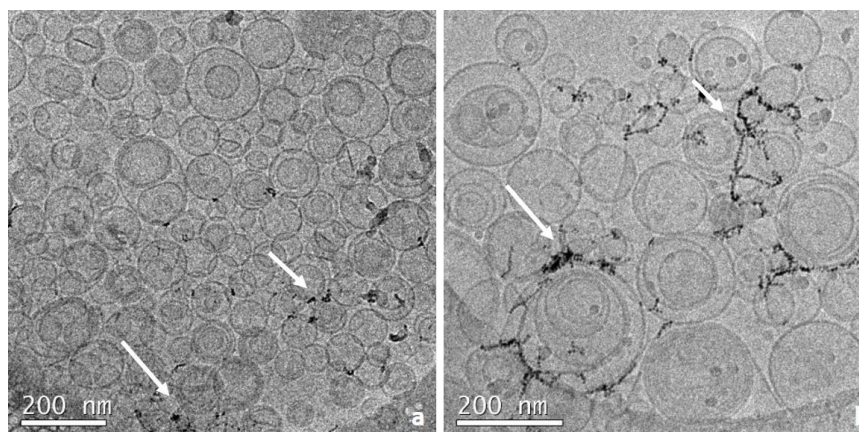


Figure A.4: Cryo-TEM pictures showing the morphology of the nanoconjugates: a) Au@LP, b) Au@LP-RGD. Scale bars are 200 nm.

We can conclude that the incorporation of AuNPs using DELOS-SUSP is possible which opens the door to the cryo-SXT studies, in order to locate plain liposomes and liposomes-RGD_ether inside MAEC cells.

A.3. Summary and conclusions

- The incorporation of 2-nm AuNPs capped with dodecanethiol in plain liposomes and liposomes-RGD_ether was not possible using TFH methodology since no small unilamellar vesicles marked with AuNPs was obtained.
- The incorporation of AuNPs of different sizes (5, 15, 25 nm) capped with citrate in liposomes-RGD_ether with a lipid composition of 5 mg mL⁻¹ and a concentration of 1.17 nM of AuNPs, was achieved using DELOS-SUSP procedure.
- 5 nm-AuNPs capped with citrate seemed to accomplish a higher incorporation, at the same time that maintain good physicochemical characteristics. Therefore, they were selected to prepare plain and liposomes-RGD_ether for the cryo-SXT experiments.

Bibliography

1. Bobo, D., Robinson, K. J., Islam, J., Thurecht, K. J. & Corrie, S. R. Nanoparticle-Based Medicines: A Review of FDA-Approved Materials and Clinical Trials to Date. *Pharm. Res.* **33**, 2373–2387 (2016).
2. Feynman, R. P. There's Plenty of Room at the Bottom: An Invitation to Enter a New Field of Physics. *Engineering and Science (Caltech)* (1960). Available at: <https://authors.library.caltech.edu/53057/>. (Accessed: 28th November 2019)
3. Krukemeyer, M., Krenn, V., Huebner, F., Wagner W & R, R. History and Possible Uses of Nanomedicine Based on Nanoparticles and Nanotechnological Progress. *J Nanomed Nanotechnol* **6**, 336 (2015).
4. Soares, S., Sousa, J., Pais, A. & Vitorino, C. Nanomedicine: Principles, properties, and regulatory issues. *Front. Chem.* **6**, 1–15 (2018).
5. Freeman, R. *et al.* Reversible self-assembly of superstructured networks. *Science* **362**, 808–813 (2018).
6. Mostafavi, E. & Soltantabar, P. Nanotechnology and picotechnology: A new arena for translational medicine. *Biomater. Transl. Med.* 191–212 (2019). doi:10.1016/B978-0-12-813477-1.00009-8
7. Kreuter, J. Nanoparticles-a historical perspective. *International Journal of Pharmaceutics* **331**, 1–10 (2007).
8. Molina, A. A., Angel Méndez-Rojas, M., Angulo-Molina, A. & Aguilera-Portillo, G. Nanomedicine: Small Steps, Big Effects. in *CRC Concise Encyclopedia of Nanotechnology* (eds. Khariso, B. I., Kharissova, O. V. & Ortiz-Mendez, U.) (CRC press, 2016).
9. Liu, D., Yang, F., Xiong, F. & Gu, N. The Smart Drug Delivery System and Its Clinical Potential. *Theranostics* **6**, 1306–23 (2016).

10. Youn, Y. S. & Bae, Y. H. Perspectives on the past, present, and future of cancer nanomedicine. *Adv. Drug Deliv. Rev.* **130**, 3–11 (2018).
11. Jafarizadeh-Malmiri, H., Sayyar, Z., Anarjan, N. & Berenjian, A. Nano-encapsulation for Nutrition Delivery. in *Nanobiotechnology in Food: Concepts, Applications and Perspectives* 95–114 (Springer International Publishing, 2019). doi:10.1007/978-3-030-05846-3_7
12. Riley, R. S., June, C. H., Langer, R. & Mitchell, M. J. Delivery technologies for cancer immunotherapy. *Nat. Rev. Drug Discov.* doi:10.1038/s41573-018-0006-z
13. Deb, P. K., Al-Attraqchi, O., Chandrasekaran, B. & Paradkar, A. Protein/Peptide Drug Delivery Systems: Practical Considerations in Pharmaceutical Product Development. *Basic Fundam. Drug Deliv.* 651–684 (2019). doi:10.1016/B978-0-12-817909-3.00016-9
14. Duro-Castano, A., Talelli, M., Rodríguez-Escalona, G. & Vicent, M. J. Smart Polymeric Nanocarriers for Drug Delivery. *Smart Polym. their Appl.* 439–479 (2019). doi:10.1016/B978-0-08-102416-4.00013-2
15. Kauscher, U., Holme, M. N., Björnmalm, M. & Stevens, M. M. Physical stimuli-responsive vesicles in drug delivery: Beyond liposomes and polymersomes. *Adv. Drug Deliv. Rev.* **138**, 259–275 (2019).
16. Yoshioka, Y. & Ochiya, T. Extracellular Vesicles as Novel Nanocarriers for Therapeutic Delivery. *Nucleic Acid Nanotheranostics* 391–407 (2019). doi:10.1016/B978-0-12-814470-1.00012-5
17. Shen, J. *et al.* Self-assembled vesicles formed by C18 unsaturated fatty acids and sodium dodecyl sulfate as a drug delivery system. *Colloids Surfaces A Physicochem. Eng. Asp.* **568**, 66–74 (2019).
18. Soltani, F., Parhiz, H., Mokhtarzadeh, A. & Ramezani, M. Synthetic and Biological Vesicular Nano-Carriers Designed for Gene Delivery. *Curr. Pharm. Des.* **21**, 6214–6235 (2015).
19. Tambe, V., Maheshwari, R., Chourasiya, Y., Choudhury, H. & Gorain, B. Clinical

- Aspects and Regulatory Requirements for Nanomedicines. *Basic Fundam. Drug Deliv.* 733–752 (2019). doi:10.1016/B978-0-12-817909-3.00018-2
20. Bremer-Hoffmann, S., Halamoda-Kenzaoui, B. & Borgos, S. E. Identification of regulatory needs for nanomedicines. *J. Interdiscip. Nanomedicine* **3**, 4–15 (2018).
 21. Flühmann, B., Ntai, I., Borchard, G., Simoens, S. & Mühlebach, S. Nanomedicines: The magic bullets reaching their target? *Eur. J. Pharm. Sci.* **128**, 73–80 (2019).
 22. Islam Shishir, M. R., Karim, N., Gowd, V., Zheng, X. & Chen, W. Liposomal delivery of natural product: A promising approach in health research. *Trends Food Sci. Technol.* **85**, 177–200 (2019).
 23. Doktorova, M. *et al.* Preparation of asymmetric phospholipid vesicles for use as cell membrane models. *Nat. Protoc.* **13**, 2086–2101 (2018).
 24. Hindley, J. W. *et al.* Light-triggered enzymatic reactions in nested vesicle reactors. *Nat. Commun.* **9**, 1093 (2018).
 25. Cui, W., Li, J. & Decher, G. Self-Assembled Smart Nanocarriers for Targeted Drug Delivery. *Adv. Mater.* **28**, 1302–1311 (2016).
 26. Milani, D., Athiyah, U., Hariyadi, D. M. & Pathak, Y. V. Surface Modification of Nanocarriers for Specific Cell Targeting for Better Therapeutic Effect. in *Surface Modification of Nanoparticles for Targeted Drug Delivery* 355–368 (Springer International Publishing, 2019). doi:10.1007/978-3-030-06115-9_18
 27. Zhang, Y., Ng, W., Feng, X., Cao, F. & Xu, H. Lipid vesicular nanocarrier: Quick encapsulation efficiency determination and transcutaneous application. *Int. J. Pharm.* **516**, 225–230 (2017).
 28. Bangham, A. D., Standish, M. M. & Watkins, J. C. *Diffusion of Univalent Ions across the Lamellae of Swollen Phospholipids.* *Journal of Molecular Biology* **13**, (1965).
 29. Gregoriadis, G., Leathwood, P. D. & Ryman, B. E. Enzyme entrapment in

- liposomes. *FEBS Lett.* **14**, 95–99 (1971).
30. Gregoriadis, G. Drug entrapment in liposomes. *FEBS Lett.* **36**, 292–296 (1973).
 31. Pattni, B. S., Chupin, V. V. & Torchilin, V. P. New Developments in Liposomal Drug Delivery. *Chem. Rev.* **115**, 10938–10966 (2015).
 32. Aryasomayajula, B., Salzano, G. & Torchilin, V. P. Multifunctional Liposomes. in *Cancer Nanotechnology: Methods and Protocols* (ed. Zeineldin, R.) 41–61 (Springer, 2017). doi:10.1007/978-1-4939-6646-2_3
 33. Bozzuto, G. & Molinari, A. Liposomes as nanomedical devices. *Int. J. Nanomedicine* **10**, 975–99 (2015).
 34. Zylberberg, C. & Matosevic, S. Drug Delivery Pharmaceutical liposomal drug delivery: a review of new delivery systems and a look at the regulatory landscape. *Drug Deliv.* **23**, 3319–3329 (2016).
 35. Bulbake, U., Doppalapudi, S., Kommineni, N. & Khan, W. Liposomal formulations in clinical use: An updated review. *Pharmaceutics* **9**, 1–33 (2017).
 36. Haleem, R. M., Salem, M. Y., Fatahallah, F. A. & Abdelfattah, L. E. Quality in the pharmaceutical industry – A literature review. *Saudi Pharm. J.* **23**, 463–469 (2015).
 37. Teasdale, A., Elder, D. & Nims, R. W. *ICH Quality Guidelines An Implementation Guide*. (2018).
 38. Soh, S. H., Lee, L. Y., Soh, S. H. & Lee, L. Y. Microencapsulation and Nanoencapsulation Using Supercritical Fluid (SCF) Techniques. *Pharmaceutics* **11**, 21 (2019).
 39. Elizondo, E., Veciana, J. & Ventosa, N. Nanostructuring molecular materials as particles and vesicles for drug delivery, using compressed and supercritical fluids. *Nanomedicine* **7**, 1391–1408 (2012).
 40. Campardelli, R., Baldino, L. & Reverchon, E. Supercritical fluids applications in nanomedicine. *J. Supercrit. Fluids* **101**, 193–214 (2015).

41. Madan, V. K. Supercritical Carbon Dioxide as Greener Solvent of 21 st Century. *Asian J. Chem.* (2018).
42. Tsai, W.-C. & Rizvi, S. S. H. Liposomal microencapsulation using the conventional methods and novel supercritical fluid processes. *Trends Food Sci. Technol.* **55**, 61–71 (2016).
43. Sala, S. *et al.* Crystallization of Microparticulate Pure Polymorphs of Active Pharmaceutical Ingredients Using CO₂-Expanded Solvents. *Cryst. Growth Des.* **12**, 1717–1726 (2012).
44. Sala, S. *et al.* Kinetically Driven Crystallization of a Pure Polymorphic Phase of Stearic Acid from CO₂-Expanded Solutions. *Cryst. Growth Des.* **10**, 1226–1232 (2010).
45. Ventosa, N., Sala, S., Veciana, J., Torres, J. & Llibre, J. Depressurization of an Expanded Liquid Organic Solution (DELOS): A New Procedure for Obtaining Submicron- Or Micron-Sized Crystalline Particles. *Cryst. Growth Des.* **1**, 299–303 (2001).
46. Ventosa, N., Sala, S. & Veciana, J. DELOS process: A crystallization technique using compressed fluids - 1. Comparison to the GAS crystallization method. *J. Supercrit. Fluids* **26**, 33–45 (2003).
47. Cano-Sarabia, M. *et al.* Preparation of uniform rich cholesterol unilamellar nanovesicles using CO₂-expanded solvents. *Langmuir* **24**, 2433–2437 (2008).
48. Elizondo, E. *et al.* Influence of the preparation route on the supramolecular organization of lipids in a vesicular system. *J. Am. Chem. Soc.* **134**, 1918–1921 (2012).
49. Cabrera, I. *et al.* Multifunctional Nanovesicle-Bioactive Conjugates Prepared by a One-Step Scalable Method Using CO₂-Expanded Solvents. *Nano Lett.* **13**, 3766–3774 (2013).
50. Solomon, M. & Muro, S. Lysosomal enzyme replacement therapies: Historical development, clinical outcomes, and future perspectives. *Adv. Drug Deliv. Rev.*

- 118**, 109–134 (2017).
51. Kishnani, P. S. *et al.* Immune response to enzyme replacement therapies in lysosomal storage diseases and the role of immune tolerance induction. *Mol. Genet. Metab.* **117**, 66–83 (2016).
 52. Ma, X., Gong, N., Zhong, L., Sun, J. & Liang, X. J. Future of nanotherapeutics: Targeting the cellular sub-organelles. *Biomaterials* **97**, 10–21 (2016).
 53. Platt, F. M., Boland, B. & van der Spoel, A. C. Lysosomal storage disorders: The cellular impact of lysosomal dysfunction. *J. Cell Biol.* **199**, 723–734 (2012).
 54. Luzio, J. P., Pryor, P. R. & Bright, N. A. Lysosomes: Fusion and function. *Nat. Rev. Mol. Cell Biol.* **8**, 622–632 (2007).
 55. Futerman, A. H. & Van Meer, G. The cell biology of lysosomal storage disorders. *Nat. Rev. Mol. Cell Biol.* **5**, 554–565 (2004).
 56. Kornfeld, S. Trafficking of lysosomal enzymes in normal and disease states. *J Clin Invest* **77**:1_6, 1986. 1–6 (1986).
 57. Giannotti, M. I. *et al.* Highly Versatile Polyelectrolyte Complexes for Improving the Enzyme Replacement Therapy of Lysosomal Storage Disorders. *ACS Appl. Mater. Interfaces* **8**, 25741–25752 (2016).
 58. Lee, H. J. *et al.* α -Galactosidase delivery using 30Kc19-human serum albumin nanoparticles for effective treatment of Fabry disease. *Appl. Microbiol. Biotechnol.* **100**, 10395–10402 (2016).
 59. Lenders, M., Schmitz, B., Brand, S. M., Foell, D. & Brand, E. Characterization of drug-neutralizing antibodies in patients with Fabry disease during infusion. *J. Allergy Clin. Immunol.* **141**, (2018).
 60. Lenders, M. *et al.* Serum-Mediated Inhibition of Enzyme Replacement Therapy in Fabry Disease. *J. Am. Soc. Nephrol.* **27**, 256–264 (2016).
 61. Rombach, S. M. *et al.* Long-Term Effect of Antibodies against Infused Alpha-Galactosidase A in Fabry Disease on Plasma and Urinary (lyso)Gb3 Reduction and Treatment Outcome. *PLoS One* **7**, 1–7 (2012).

62. Safary, A., Khiavi, M. A., Mousavi, R., Barar, J. & Rafi, M. A. Enzyme replacement therapies: What is the best option? *BiolImpacts* **8**, 153–157 (2018).
63. Muro, S. New biotechnological and nanomedicine strategies for treatment of lysosomal storage disorders. *Wiley Interdiscip. Rev. Nanomedicine Nanobiotechnology* **2**, 189–204 (2010).
64. Ortiz, A. *et al.* Fabry disease revisited: Management and treatment recommendations for adult patients. *Mol. Genet. Metab.* **123**, 416–427 (2018).
65. Beck, M. Treatment strategies for lysosomal storage disorders. *Dev. Med. Child Neurol.* **60**, 13–18 (2018).
66. del Pozo-Rodríguez, A., Solinís, M. Á. & Rodríguez-Gascón, A. Applications of lipid nanoparticles in gene therapy. *Eur. J. Pharm. Biopharm.* **109**, 184–193 (2016).
67. De Garibay, A. P. R., Solinís, M. Á. & Rodríguez-Gascón, A. Gene therapy for Fabry disease: A review of the literature. *BioDrugs* **27**, 237–246 (2013).
68. Sharma, A., Vaghasiya, K., Ray, E. & Verma, R. K. Lysosomal targeting strategies for design and delivery of bioactive for therapeutic interventions. *J. Drug Target.* **26**, 208–221 (2018).
69. Hollak, C. E. M. & Linthorst, G. E. Immune response to enzyme replacement therapy in Fabry disease: Impact on clinical outcome? *Mol. Genet. Metab.* **96**, 1–3 (2009).
70. Sunder-Plassmann, G., Schiffmann, R. & Nicholls, K. Migalastat for the treatment of Fabry disease. *Expert Opin. Orphan Drugs* **6**, 301–309 (2018).
71. Hsu, J. *et al.* Enhanced endothelial delivery and biochemical effects of α -galactosidase by ICAM-1-targeted nanocarriers for Fabry disease. *J. Control. Release* **149**, 323–331 (2011).
72. Wanner, C. *et al.* European expert consensus statement on therapeutic goals in Fabry disease. *Mol. Genet. Metab.* **124**, 189–203 (2018).
73. Wanner, C. *et al.* Therapeutic goals in Fabry disease: Recommendations of a

- European expert panel, based on current clinical evidence with enzyme replacement therapy. *Mol. Genet. Metab.* 0–1 (2018). doi:10.1016/j.ymgme.2018.04.004
74. Hughes, D. A. *et al.* Oral pharmacological chaperone migalastat compared with enzyme replacement therapy in Fabry disease: 18-month results from the randomised phase III ATTRACT study. *J. Med. Genet.* **54**, 288–296 (2017).
 75. Guérard, N. *et al.* Lucerastat, an Iminosugar for Substrate Reduction Therapy: Tolerability, Pharmacodynamics, and Pharmacokinetics in Patients With Fabry Disease on Enzyme Replacement. *Clin. Pharmacol. Ther.* **103**, 703–711 (2018).
 76. Beauvais, D. M., Ell, B. J., McWhorter, A. R. & Rapraeger, A. C. Syndecan-1 regulates $\alpha_v\beta_3$ and $\alpha_v\beta_5$ integrin activation during angiogenesis and is blocked by synstatin, a novel peptide inhibitor. *J. Exp. Med.* **206**, 691–705 (2009).
 77. Asati, S., Pandey, V. & Soni, V. RGD Peptide as a Targeting Moiety for Theranostic Purpose: An Update Study. *Int. J. Pept. Res. Ther.* **25**, 49–65 (2019).
 78. Bodary, P. F., Shayman, J. A. & Eitzman, D. T. α -Galactosidase A in Vascular Disease. *Trends in Cardiovascular Medicine* **17**, 129–133 (2007).
 79. Utsumi, K. *et al.* Urinary excretion of the vitronectin receptor (integrin $\alpha(V)\beta_3$) in patients with Fabry disease. *Clin. Chim. Acta* **279**, 55–68 (1999).
 80. Cabrera, I. Nanovesicle-bioactive conjugates to be used as nanomedicines, prepared by a one-step scalable method using CO₂-expanded solvents. (Universitat Autònoma de Barcelona, 2013).
 81. NANOFABRY: "Development of a nanomedicine for enzymatic replacement treatment of Fabry's disease. Financed by Marato TV3 Foundation; Coordinator: S. Schwartz (CIBBIM – Hospital Universitari Vall d'Hebron); 2011-2013.
 82. LIPOCELL: Functionalized nanoliposomes for the development of therapies for intracellular-based diseases. Application to Fabry disease. Financed by: PRAXIS BIOPHARMA RESEARCH INSTITUTE SL. & CIBER-BBN; Coordinator: N. Ventosa (CSIC/CIBER-BBN) 2014-2015.

83. TERARMET: Development of therapies for the treatment of rare congenital metabolic diseases RTC-2014-2207-1 MINECO. Collaboration Challenges from the National Program of R+D+i oriented to Societal Challenges. Coordinator: E. Gainza (Praxis Pharmaceutical);
84. Smart4Fabry: Smart multifunctional GLA-nanoformulation for Fabry disease. European Union H2020. Coordinator: N. Ventosa (CSIC/CIBER-BBN); 2017-2020.
85. Cabrera, I. *et al.* α -Galactosidase-A Loaded-Nanoliposomes with Enhanced Enzymatic Activity and Intracellular Penetration. *Adv. Healthc. Mater.* **5**, 829–840 (2016).
86. Bigdeli, A. *et al.* Exploring Cellular Interactions of Liposomes Using Protein Corona Fingerprints and Physicochemical Properties. *ACS Nano* **10**, 3723–3737 (2016).
87. Ma, T. G., Ling, Y. H., McClure, G. D. & Tseng, M. T. Effects of trifluoroacetic acid, a halothane metabolite, on C6 glioma cells. *J. Toxicol. Environ. Health* **31**, 147–158 (1990).
88. Cornish, J. *et al.* Trifluoroacetate, a contaminant in purified proteins, inhibits proliferation of osteoblasts and chondrocytes. *Am. J. Physiol.* (1999). doi:10.1152/ajpendo.1999.277.5.E779
89. Fan, J. & de Lannoy, I. A. M. Pharmacokinetics. *Biochem. Pharmacol.* **87**, 93–120 (2014).
90. Arms, L., Smith, D. W., Flynn, J. & Palmer, W. Advantages and Limitations of Current Techniques for Analyzing the Biodistribution of Nanoparticles. *Front. Pharmacol.* | www.frontiersin.org **1**, (2018).
91. Llop, J. & Gómez-Vallejo, V. *Isotopes in nanoparticles: fundamentals and applications.*
92. Moura, R. P., Martins, C., Pinto, S., Sousa, F. & Sarmiento, B. Blood-brain barrier receptors and transporters: an insight on their function and how to exploit them through nanotechnology. *Expert Opin. Drug Deliv.* **0**, 17425247.2019.1583205

- (2019).
93. Sharma, G. *et al.* Advances in nanocarriers enabled brain targeted drug delivery across blood brain barrier. *Int. J. Pharm.* **559**, 360–372 (2019).
 94. Sabir, A. M., Moloy, M. & Bhasin, P. S. Hplc Method Development and Validation: a Review. *Int. Res. J. Pharm.* **4**, 39–46 (2016).
 95. Moldoveanu S.C. & David V. *Sample Preparation in Chromatography, Volume 65.* (Elsevier Science, 2002).
 96. Almeling, S. The use of aerosol-based detection systems in the quality control of drug systems. (Julius-Maximilians-Universität Würzburg, 2011).
 97. Megoulas, N. C. & Koupparis, M. A. Twenty years of evaporative light scattering detection. *Crit. Rev. Anal. Chem.* **35**, 301–316 (2005).
 98. Roces, C. B., Kastner, E., Stone, P., Lowry, D. & Perrie, Y. Rapid quantification and validation of lipid concentrations within liposomes. *Pharmaceutics* **8**, 1–11 (2016).
 99. Oswald, M., Platscher, M., Geissler, S. & Goepferich, A. HPLC analysis as a tool for assessing targeted liposome composition. *Int. J. Pharm.* **497**, 293–300 (2016).
 100. Storm, G. & Crommelin, D. J. A. Liposomes : quo vadis ? **1**, 7–8 (1998).
 101. Kanášová, M. & Nesměrák, K. Systematic review of liposomes' characterization methods. *Monatshefte fur Chemie* **148**, 1581–1593 (2017).
 102. Edwards, K. A. & Baeumner, A. J. Analysis of liposomes. *Talanta* **68**, 1432–1441 (2006).
 103. Sas, B., Peys, E. & Helsen, M. Efficient method for (lyso)phospholipid class separation by high-performance liquid chromatography using an evaporative light-scattering detector. *J. Chromatogr. A* **864**, 179–182 (1999).
 104. Schweikart, F. & Hulthe, G. HPLC–UV–MS Analysis: A Source for Severe Oxidation Artifacts. (2019). doi:10.1021/acs.analchem.8b05845

105. Carelli, A. A., Brededan, M. I. V. & Crapiste, C. H. Quantitative determination of phospholipids in sunflower oil. *JAOCS, J. Am. Oil Chem. Soc.* **74**, 511–514 (1997).
106. Singleton, J. A. & Stikeleather, L. F. High-performance liquid chromatography analysis of peanut phospholipids. I. Injection system for simultaneous concentration and separation of phospholipids. *J. Am. Oil Chem. Soc.* **72**, 481–483 (1995).
107. Bernhard, W. *et al.* High-Performance Liquid Chromatographic Analysis of Phospholipids from Different Sources with Combined Fluorescence and Ultraviolet Detection. *Analytical Biochemistry* **220**, 172–180 (1994).
108. Singh, R., Ajagbe, M., Bhamidipati, S., Ahmad, Z. & Ahmad, I. A rapid isocratic high-performance liquid chromatography method for determination of cholesterol and 1,2-dioleoyl-sn-glycero-3-phosphocholine in liposome-based drug formulations. *J. Chromatogr. A* **1073**, 347–353 (2005).
109. Morales, J., Zanocco, A. L., Günther, G. & Lemp, E. A high-performance liquid chromatography method for determination 2-(n-(N,N,N-trimethyl)-n-alkyl)-5-alkylfuryl halides in dipalmitoylphosphatidylcholine liposome solutions. *J. Chromatogr. A* **1125**, 89–94 (2006).
110. Laouini, A. *et al.* Preparation, Characterization and Applications of Liposomes: State of the Art. *J. Colloid Sci. Biotechnol.* **1**, 147–168 (2012).
111. Lang, J. K. Quantitative determination of cholesterol in liposome drug products and raw materials by high-performance liquid chromatography. *J. Chromatogr.* **507**, 157–163 (1990).
112. ICH. Guidance for industry: Q2B validation of analytical procedures: methodology. *Int. Conf. Harmon. Tech. Requir. Regist. Tripart. Guidel.* 13 (1996). doi:62 FR 27464
113. Kaviratna, A. S. & Banerjee, R. The effect of acids on dipalmitoyl phosphatidylcholine (DPPC) monolayers and liposomes. *Colloids Surfaces A Physicochem. Eng. Asp.* **345**, 155–162 (2009).

114. Banik, S., Saha, M., Hussain, S. A. & Bhattacharjee, D. pH induced interaction of DPPC with a fluorescent dye in Langmuir and Langmuir Blodgett (LB) films. *Mol. Cryst. Liq. Cryst.* **643**, 255–265 (2017).
115. Sułkowski, W. W., Pentak, D., Nowak, K. & Sułkowska, a. The influence of temperature, cholesterol content and pH on liposome stability. *J. Mol. Struct.* **744–747**, 737–747 (2005).
116. Gong, K., Feng, S. S., Go, M. L. & Soew, P. H. Effects of pH on the stability and compressibility of DPPC/cholesterol monolayers at the air-water interface. *Colloids Surfaces A Physicochem. Eng. Asp.* **207**, 113–125 (2002).
117. Shi, K. *et al.* Liposomes Combined an Integrin $\alpha v \beta 3$ -Specific Vector with pH-Responsible Cell-Penetrating Property for Highly Effective Antiglioma Therapy through the Blood–Brain Barrier. (2015). doi:10.1021/acsami.5b06429
118. Shi, K. *et al.* A pH-responsive cell-penetrating peptide-modified liposomes with active recognizing of integrin $\alpha v \beta 3$ for the treatment of melanoma. *J. Control. Release* **217**, 138–150 (2015).
119. Lee, Y. & Thompson, D. H. Stimuli-Responsive Liposomes for Drug Delivery. doi:10.1002/wnan.1450
120. Xu, X., Ho, W., Zhang, X., Bertrand, N. & Farokhzad, O. Cancer nanomedicine: From targeted delivery to combination therapy. *Trends in Molecular Medicine* **21**, 223–232 (2015).
121. Hirsjärvi, S., Passirani, C. & Benoit, J. Passive and Active Tumour Targeting with Nanocarriers Normal tissue Tumour tissue Blood vessel. *Curr. Drug Discov. Technol.* **8**, 188–196 (2011).
122. Danhier, F., Feron, O. & Préat, V. To exploit the tumor microenvironment: Passive and active tumor targeting of nanocarriers for anti-cancer drug delivery. *Journal of Controlled Release* **148**, 135–146 (2010).
123. Lammers, T., Hennink, W. E. & Storm, G. Tumour-targeted nanomedicines: principles and practice. *Br. J. Cancer* **99**, 392–397 (2008).

124. Moghimi, S. M., Hunter, A. C. & Andresen, T. L. Factors Controlling Nanoparticle Pharmacokinetics: An Integrated Analysis and Perspective. *Annu. Rev. Pharmacol. Toxicol.* **52**, 481–503 (2012).
125. Lilia Barra, A. *et al.* Time Evolution of Nanoparticle–Protein Corona in Human Plasma: Relevance for Targeted Drug Delivery. *Langmuir* (2013). doi:10.1021/la401192x
126. Treuel, L., Docter, D., Maskos, M. & Stauber, R. H. Protein corona - from molecular adsorption to physiological complexity. *Beilstein J. Nanotechnol.* **6**, 857–73 (2015).
127. Verderio, P. *et al.* Delivering Colloidal Nanoparticles to Mammalian Cells: A Nano-Bio Interface Perspective. *Adv. Healthc. Mater.* **3**, 957–976 (2014).
128. Monopoli, M. P. *et al.* Physical-Chemical aspects of protein corona: Relevance to in vitro and in vivo biological impacts of nanoparticles. *J. Am. Chem. Soc.* **133**, 2525–2534 (2011).
129. Caracciolo, G. Clinically approved liposomal nanomedicines: lessons learned from the biomolecular corona. *Nanoscale* **10**, 4167–4172 (2018).
130. Docter, D. *et al.* The nanoparticle biomolecule corona: lessons learned – challenge accepted? *Chem. Soc. Rev.* **44**, 6094–6121 (2015).
131. Corbo, C. *et al.* The impact of nanoparticle protein corona on cytotoxicity, immunotoxicity and target drug delivery. *Nanomedicine* **11**, 81 (2016).
132. Couvreur, P. & Vauthier, C. *Nanotechnology: Intelligent design to treat complex disease. Pharmaceutical Research* **23**, (2006).
133. Torchilin, V. Tumor delivery of macromolecular drugs based on the EPR effect. *Advanced Drug Delivery Reviews* **63**, 131–135 (2011).
134. Fang, J., Nakamura, H. & Maeda, H. The EPR effect: Unique features of tumor blood vessels for drug delivery, factors involved, and limitations and augmentation of the effect. *Advanced Drug Delivery Reviews* (2011). doi:10.1016/j.addr.2010.04.009

135. Wong, A. D., Ye, M., Ulmschneider, M. B. & Searson, P. C. Quantitative Analysis of the Enhanced Permeation and Retention (EPR) Effect. (2015). doi:10.1371/journal.pone.0123461
136. Peer, D. *et al.* Nanocarriers as an emerging platform for cancer therapy. *Nat. Nanotechnol.* **2**, 751–760 (2007).
137. Wakaskar, R. R. Passive and Active Targeting in Tumor Microenvironment. *Int. J. Drug Dev. Res.* **9**, 37–41 (2017).
138. Arsiwala, A., Castro, A., Frey, S., Stathos, M. & Kane, R. S. Designing multivalent ligands to control biological interactions: From vaccines and cellular effectors to targeted drug delivery. *Chem. Asian J.* **78**, 244–255 (2019).
139. Li, M.-H., Zong, H., Leroueil, P. R., Ki Choi, S. & Baker, J. R. Ligand Characteristics Important to Avidity Interactions of Multivalent Nanoparticles. *Bioconjugate Chem* **28**, 1649–1657 (2017).
140. Hong, S. *et al.* The Binding Avidity of a Nanoparticle-Based Multivalent Targeted Drug Delivery Platform. *Chem. Biol.* **14**, 107–115 (2007).
141. Davis, M. E., Chen, Z. & Shin, D. M. Nanoparticle therapeutics: An emerging treatment modality for cancer. *Nat. Rev. Drug Discov.* **7**, 771–782 (2008).
142. Bazak, R., Houry, M., El Achy, S., Kamel, S. & Refaat, T. Cancer active targeting by nanoparticles: a comprehensive review of literature. *Journal of Cancer Research and Clinical Oncology* **141**, 769–784 (2015).
143. Dissanayake, S., Denny, W. A., Gamage, S. & Sarojini, V. Recent developments in anticancer drug delivery using cell penetrating and tumor targeting peptides. *Journal of Controlled Release* **250**, 62–76 (2017).
144. Mousavizadeh, A., Jabbari, A., Akrami, M. & Bardania, H. Cell targeting peptides as smart ligands for targeting of therapeutic or diagnostic agents: a systematic review. *Colloids Surfaces B Biointerfaces* **158**, 507–517 (2017).
145. Veciana J., Sala S. Cano M., V. N. METHOD FOR OBTAINING MICRO- AND NANO-DISPERSE SYSTEMS - Patent - Europe PMC. *Patent* (2006).

146. Ventosa N., Veciana J., Cabrera I., Elizondo E., Sala S., V. A. Functionalized liposomes useful for the delivery of bioactive compounds. (2014).
147. He, Z.-Y. *et al.* Recent development of poly(ethylene glycol)-cholesterol conjugates as drug delivery systems. *Int. J. Pharm.* **469**, 168–178 (2014).
148. Ardizzone, A. New Fluorescent Nanovesicles, by Self-assembly of Organic Fluorophores, Sterols and Surfactants, as Probes for Bioimaging. (2017).
149. Rasch, M. R., Yu, Y., Bosoy, C., Goodfellow, B. W. & Korgel, B. A. Chloroform-enhanced incorporation of hydrophobic gold nanocrystals into dioleoylphosphatidylcholine (DOPC) vesicle membranes. *Langmuir* **28**, 12971–12981 (2012).
150. Danino, D. Cryo-TEM of soft molecular assemblies. *Current Opinion in Colloid and Interface Science* **17**, 316–329 (2012).
151. Hammersley, A. P. *et al.* Calibration and correction of distortions in two-dimensional detector systems ^a. *Rev. Sci. Instrum.* **66**, 2729–2733 (1995).
152. Pedersen, J. S. A flux- and background-optimized version of the NanoSTAR small-angle X-ray scattering camera for solution scattering. *J. Appl. Crystallogr.* **37**, 369–380 (2004).
153. Li, Y., Beck, R., Huang, T., Choi, M. C. & Divinagracia, M. Scatterless hybrid metal-single-crystal slit for small-angle X-ray scattering and high-resolution X-ray diffraction. *J. Appl. Crystallogr.* **41**, 1134–1139 (2008).
154. Pabst, G., Rappolt, M., Amenitsch, H. & Laggner, P. *Structural information from multilamellar liposomes at full hydration: Full q-range fitting with high quality x-ray data.*
155. Pabst, G. *et al.* Structural analysis of weakly ordered membrane stacks. *J. Appl. Crystallogr.* **36**, 1378–1388 (2003).
156. Corchero, J. L. *et al.* Integrated approach to produce a recombinant, his-tagged human α -galactosidase a in mammalian cells. *Biotechnol. Prog.* **27**, 1206–1217 (2011).

157. Desnick, R. J. *et al.* Fabry's disease: Enzymatic diagnosis of hemizygotes and heterozygotes: α -Galactosidase activities in plasma, serum, urine, and leukocytes. *J. Lab. Clin. Med.* **81**, 157–171 (1973).
158. Mayes, J. S., Scheerer, J. B., Sifers, R. N. & Donaldson, M. L. Differential assay for lysosomal alpha-galactosidases in human tissues and its application to Fabry's disease. *Clin. Chim. Acta* **112**, 247–251 (1981).
159. Shu, L., Murphy, H. S., Cooling, L. & Shayman, J. A. An In Vitro Model of Fabry Disease. *J Am Soc Nephrol* **16**, 2636–2645 (2005).
160. Al-jamal, T. & Kostarelos, K. Liposomes: From a Clinically Established Drug Delivery System to a Nanoparticle Platform for Theranostic Nanomedicine. *Acc. Chem. Res.* **44**, 2 (2011).
161. Zhang, N. *et al.* Gold conjugate-based liposomes with hybrid cluster bomb structure for liver cancer therapy. *Biomaterials* **74**, 280–291 (2016).
162. Dichello, G. A. *et al.* Preparation of liposomes containing small gold nanoparticles using electrostatic interactions. *Eur. J. Pharm. Sci.* **105**, 55–63 (2017).
163. Liu, J. Interfacing Zwitterionic Liposomes with Inorganic Nanomaterials: Surface Forces, Membrane Integrity, and Applications. *Langmuir* 4393–4404 (2016). doi:10.1021/acs.langmuir.6b00493
164. Li, Z., Ye, E., David, Lakshminarayanan, R. & Loh, X. J. Recent Advances of Using Hybrid Nanocarriers in Remotely Controlled Therapeutic Delivery. *Small* **12**, 4782–4806 (2016).
165. Vargas, K. M. & Shon, Y. S. Hybrid lipid-nanoparticle complexes for biomedical applications. *J. Mater. Chem. B* **7**, 695–708 (2019).
166. Rasch, M. R. *et al.* Hydrophobic gold nanoparticle self-assembly with phosphatidylcholine lipid: Membrane-loaded and janus vesicles. *Nano Lett.* **10**, 3733–3739 (2010).
167. Ferrer-Tasies, L. *et al.* Quatsomes: Vesicles formed by self-assembly of sterols

- and quaternary ammonium surfactants. *Langmuir* **29**, 6519–6528 (2013).
168. Ferrer Tasies, L. P. Cholesterol and compressed CO₂: a smart molecular building block and advantageous solvent to prepare stable self-assembled colloidal nanostructures. *TDX (Tesis Doctorals en Xarxa)* (2016).
169. Pereiro, E., Nicolás, J., Ferrer, S. & Howells, M. R. A soft X-ray beamline for transmission X-ray microscopy at ALBA. *J. Synchrotron Radiat.* **16**, 505–512 (2009).
170. Oton, J. *et al.* Image formation in cellular X-ray microscopy. *J. Struct. Biol.* **178**, 29–37 (2012).
171. Pérez-Berná, A. *et al.* Structural Changes In Cells Imaged by Soft X-ray Cryo-Tomography During Hepatitis C Virus Infection. (2016). doi:10.1021/acsnano.6b01374
172. Carrascosa, J. L. *et al.* Cryo-X-ray tomography of vaccinia virus membranes and inner compartments. *J. Struct. Biol.* **168**, 234–239 (2009).
173. Chichón, F. J. *et al.* Cryo X-ray nano-tomography of vaccinia virus infected cells. *J. Struct. Biol.* **177**, 202–211 (2012).